

Seton Hall University

**eRepository @ Seton Hall**

---

Seton Hall University Dissertations and Theses  
(ETDs)

Seton Hall University Dissertations and Theses

---

Spring 4-29-2020

## Surface Chemistry and Surface Properties of Energetic Nitrocellulose (NC)

Henry Grau

henry.grau@student.shu.edu

Follow this and additional works at: <https://scholarship.shu.edu/dissertations>



Part of the [Analytical Chemistry Commons](#), [Materials Chemistry Commons](#), [Organic Chemistry Commons](#), and the [Physical Chemistry Commons](#)

---

### Recommended Citation

Grau, Henry, "Surface Chemistry and Surface Properties of Energetic Nitrocellulose (NC)" (2020). *Seton Hall University Dissertations and Theses (ETDs)*. 2762.  
<https://scholarship.shu.edu/dissertations/2762>

# **Surface Chemistry and Surface Properties of Energetic Nitrocellulose (NC)**

By: Henry Grau

Dissertation submitted to the Department of Chemistry and Biochemistry of Seton Hall  
University in partial fulfillment of the requirements for the degree of

**Doctor of Philosophy**

April 2020

Seton Hall University

South Orange, New Jersey


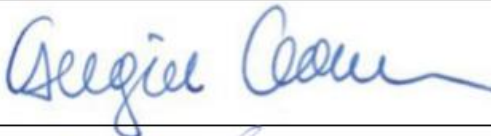
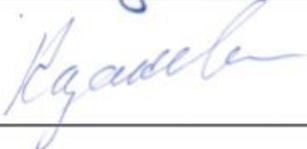

© 2020 (Henry Grau)

**Seton Hall University  
College of Arts and Sciences  
Department of Chemistry and Biochemistry**

**APPROVAL FOR SUCCESSFUL DEFENSE**

**Henry Grau** has successfully defended and made the required modifications to the text of the doctoral dissertation for the **Ph.D.** during this **Spring Semester 2020**.

**Dissertation Committee**  
(please sign and date beside your name)

Mentor: Dr. Alexander Y. Fadeev	 4-29-2020
Committee Member Dr. Sergiu M. Gorun	 4-29-2020
Committee Member Dr. Yuri Kazakevich	 4-29-2020
Department Chair Dr. Stephen P. Kelty	 4-29-2020

The mentor and any other committee members who wish to review revisions will sign and date this document only when revisions have been completed. Please return this form to the Office of Graduate Studies, where it will be placed in the candidate's file and submit a copy with your final dissertation.

Dedicated to my family:

My wife Sandy

My daughter Sadie

My son Trent

## Abstract

This research describes an investigation into the wettability of nitrocellulose (NC), most importantly to nitroglycerin (NG), which are key components of formulations used to propel military ammunition. NG demonstrates complete wetting of NC and, overtime, NG sweats on the NC surface and leaks out. The leaking out of NG from the solid formulation is a known cause of fires and explosions resulting from storage. The origin of this research is inspired by the need to engineer a solution to leakage problems of energetic plasticizer in NC based propellant. While searching for a viable material for a specific application, we journeyed into the very specific details of the properties of NC, and the chemical structures used for surface functionalization. In Chapter 1, we discuss the properties of nitrocellulose and the classes of propellant that contain NC and NG. We discuss the significance of the contact angle and how it's measured. Experimental data showing the surface tension of nitroglycerin and its use as a probe fluid is described.

In Chapter 2, silane surface chemistry and its applications are discussed. We described reactions from previous work involving cellulose that assisted us with work with NC. We discuss our results from reacting alpha cellulose and silyl isocyanate that provided conformation for further applications with NC. We explain experiments for functionalizing NC using acyl chlorides and isocyanate chemistry. We then proceed with our findings that allowed us to establish chemical designs described in the following chapter. We describe approaches for producing a 'tunable' NC surface that is derived from a two-step process using the reaction of 3-(triethoxysilyl-propyl) isocyanate followed by reactions with alkyl-, fluoroalkyl-, or phenyl-silane, producing NC surfaces ranging in lyophobicity. Each functional group allows various degrees of reduced wettability of NC with NG. We

demonstrate surface preparation using tetramethoxysilane and polydimethylsilane vapor reactions on solid state NC. We further functionalized the silanol rich solid state NC with alkyl and fluoroalkyl functionalities. In Chapter 3, the progress of reactions is demonstrated by chemical analysis. SEM analysis of modified NC materials suggests bulk properties of NC were not affected by silane. DSC demonstrated consistent decomposition of bare and treated NC. XPS provided evidence of chemically modified fibers. Increased lyophobicity of modified NC demonstrate thermal stability and equivalent energetic properties compared to bare NC. NC was characterized by dynamic contact angles using water, hexadecane, and NG as probe fluids. Wettability of modified NC demonstrated significant variations in surface energy in accordance with the nature of surface functionalities. In Chapter 4, we discuss the methods of measuring contact angles. The contact angles of modified NC demonstrated surfaces with “tunable” wetting. NC grafted with fluoroalkyl-groups showed the most NG-repelling properties ( $\theta_{Adv}/\theta_{Rec} \sim 90^\circ/50^\circ$ ). Estimation of contact angles on nitrocellulose treated fibers allowed insight of the surface properties showing an increase in curvature and reduced capillary effect. Surface energy was estimated using contact angle measurements. In Chapter 5, nitrogen gas adsorption gives insight on textural properties of bare and treated NC.

**Key words:** Wetting and contact angle, Nitrocellulose, Nitroglycerin, Surface functionalization, Silane coupling agents, Surface energy, Energetic materials, Fiber analysis, XPS, Adsorption.

## Acknowledgements

I would like to thank the following individuals for their support, teachings, and friendship.

**Dr. Alexander Y. Fadeev:** Thank you for taking me on and showing me a whole new world of chemistry. You do things the ‘old school way’. The way academics and research should be done. I remember a meeting we had before my matriculation exam, I could not answer what should have been a simple chemistry question and you let me ‘have it’ for a good hour. You may not realize how that woke me up and helped me excel in my work, but it did. Thank you for that. Thank you for allowing me to pursue the PhD degree on a part-time basis so I could work full time. I am forever thankful for your help.

**Matriculation committee:** Thank you Dr. Gorun, Dr. Sabatini, Dr Kazakevich, and Dr. Sabatini. You took the time to help me get through the matriculation process and agreed to read my dissertation.

**Seton Hall University Chemistry Department Staff and Students:** While at SHU I heard time and time again how everyone is so ‘nice’ and how everyone at SHU treats each other with respect. This holds true. The first day I visited SHU as a PhD student, I met Dr. Marzabadi. She really took the time to talk to me and answer my many questions. She was very gracious. I must say, to this day she is the nicest college professor I’ve ever met. Thank you to Dr. Maloy, who took the time out to help me with statistic questions as well as my matriculation exam.



**Picatinny Arsenal:** I would like to thank my employers and my management at Picatinny Arsenal for funding and allowing me to pursue my PhD. I would like to thank Bill DePiero for giving me a chance to advance my career. I would like to thank Ed Cooke who was always willing for me to pick his brain. Most of all, I would like to thank Alex Gandzelko. He was always willing to help me out with some tough problems. I will be forever grateful.

## Table of Contents

Chapter 1: Nitrocellulose, Nitroglycerin, Propellant, and the Importance to Understand their Surface Chemistry .....	1
1.1    Introduction .....	1
1.2    Nitrocellulose and its Properties .....	2
1.3    Nitrocellulose Double Base Propellants .....	4
1.4    Nitroglycerin Migration in Solid Propellant and Possible Solutions .....	6
1.4.1    Co-extruded Propellant and the Lyophobic Barrier .....	7
1.5    Nitroglycerin Wetting Properties & Surface Tension at Various Temperatures .....	10
1.5.1    The Young's Equation and the Contact Angle .....	10
1.5.2    Experimental .....	14
1.5.2.1    General Information .....	14
1.5.2.2    Nitroglycerin Purity .....	15
1.5.2.3    Wetting and Contact angles .....	15
1.5.2.4    Surface Tension of Nitroglycerin .....	16
1.6    Results and Discussion .....	16
1.7    Conclusions .....	20
Chapter 2: Approaches for Nitrocellulose Functionalization .....	22
2.1    Introduction .....	22
2.2    Cellulose: Its Role in Understanding Nitrocellulose Surface Functionalization .....	23
2.3    Silane Chemistry for Surface and Polymer Modification .....	24
2.4    Cellulose Surface Modification .....	26
2.4.1    Experimental (Cellulose Modification) .....	27
2.4.1.1    General Information .....	27
2.4.1.2    Cellulose Modification with 3-triethoxysilyl Propyl Isocyanate .....	27
2.4.1.3    Results and Discussion .....	28
2.5    Nitrocellulose Functionalization with Acyl Chloride and Isocyanate .....	30
2.5.1    Preconditioning of Nitrocellulose .....	30
2.5.2    General Information .....	31
2.5.3    Nitrocellulose Surface Functionalization with Acyl Chlorides .....	31
2.5.4    Nitrocellulose Surface Functionalization with Isocyanates .....	33
2.5.5    Discussion .....	34

2.6	Surface Chemistry Approach to Control Wetting of Nitrocellulose with Nitroglycerin .....	35
2.6.1	Organosiloxanes $R_{4-n}SiX_n$ .....	36
2.6.2	General Information.....	37
2.6.3	Experimental .....	37
2.6.3.1	Reaction of Nitrocellulose with 3-(Triethoxysilylpropyl) Isocyanate and other Silanes.....	37
2.6.3.2	Vapor Approach for Preparation of Organosilane Surfaces .....	38
2.6.3.2.1	Preparation of Tetramethoxysilane Surface .....	38
2.6.3.2.2	Preparation of Polydimethylsiloxane Surface .....	38
2.7	Results .....	39
2.8	Discussion .....	41
2.9	Conclusion.....	42
Chapter 3: Characterization of Nitrocellulose Reactions.....		46
3.1	Abstract .....	46
3.2	Introduction .....	46
3.2.1	General Information.....	47
3.3	Gel Permeation Characterization (GPC) of Nitrocellulose .....	48
3.4	Characterization of Acyl Chlorides and Isocyanate Modified Nitrocellulose .....	50
3.5	Characterizing the Reaction of Nitrocellulose Isocyanate and Organosilanes .....	54
3.6	SEM and DSC of Functionalized Nitrocellulose. ....	60
3.7	X-Ray Photoelectron Spectroscopy (XPS) .....	62
3.8	Conclusion.....	68
Chapter 4: Macroscopic and Microscopic Wetting .....		70
4.1	Abstract .....	70
4.2	Introduction .....	70
4.3	Macroscopic Contact Angles .....	73
4.3.1	General Information.....	73
4.3.2	Contact Angles on Nitrocellulose treated with Acyl Chlorides and Isocyanates.....	74
4.3.3	Wetting Properties of Functionalized Nitrocellulose.....	75
4.4	Discussion .....	83
4.5	Contact Angle on Fibers.....	84
4.5.1	Critical Surface Tension .....	91
4.5.2	Surface Energy on Treated Fibers .....	94

4.6	Discussion .....	100
4.7	Conclusions .....	100
Chapter 5: Porosity and Surface Characterization using Nitrogen Adsorption and Stability of Functionalized Nitrocellulose .....		103
5.1	Abstract .....	103
5.2	Introduction .....	104
5.3	Physical Adsorption of Vapor: Theoretical Overview .....	105
5.4	Adsorption Isotherms .....	106
5.5	Experimental .....	108
5.5.1	General Information.....	108
5.5.2	Nitrogen Adsorption .....	109
5.6	Nitrogen Adsorption Isotherm on Nitrocellulose.....	110
5.7	Nitrogen Adsorption Isotherm on Functionalized Nitrocellulose .....	111
5.8	BET Analysis .....	112
5.9	$\alpha_s$ Method for Nitrogen Adsorption .....	117
5.10	Pore Size Distribution PSD .....	119
5.11	Conditioning and Thermal Stability .....	122
5.11.1	General Information.....	122
5.11.2	Wetting Measurements .....	124
5.11.3	Elemental Nitrogen .....	127
5.12	Conclusions .....	129
APPENDIX A.....		131
APPENDIX B .....		134
References.....		141

## Figures

### Chapter 1

Figure 1- 1: Nitrocellulose: Crystalline Powder, Chemical Structure, and SEM Photo.....	2
Figure 1- 2: Chemical Structure of Nitrocellulose.....	4
Figure 1- 3: Propellant Types .....	5
Figure 1- 4: Bottled Nitroglycerin and Chemical Ctructure of Nitroglycerin. ....	6
Figure 1- 5: Nitroglycerin Exposure of Nitrocellulose Cartridge Casing.....	7
Figure 1- 6: Co-extruded Propellant Grain. <sup>141</sup> .....	8
Figure 1- 7: Proposed Outcome of Lyophobic Barrier .....	9
Figure 1- 8: Young’s Contact Angle.....	11
Figure 1- 9: Comparison of a Water Contact Angle on Polar and Non-polar Surface. ....	12
Figure 1- 10: Advancing and Receding ( $\theta_{Adv}/\theta_{Rec}$ ) Contact Angle.....	14
Figure 1- 11: Graphical representation of Temperature vs. Surface Tension of NG using Two Different Capillary Diameters.....	18

### Chapter 2

Figure 2- 1: Cellulose Chain. ....	24
Figure 2- 2: Silane Surface Chemistry Reactions. ....	25
Figure 2- 3: FTIR Comparison of Neat Alpha Cellulose.....	30
Figure 2- 4: Perfluoracylation of Ethyl Cellulose. <sup>44</sup> .....	32
Figure 2- 5: Reaction of Nitrocellulose with Perfluorinated Acyl Chloride.....	33
Figure 2- 6: Reaction of Nitrocellulose with 3-(triethoxysilyl propyl) Isocyanate. ....	34
Figure 2- 7: Reaction Schematic for the Covalent Functionalization of Nitrocellulose with Organosilanes.....	41

Figure 2- 8: Synthesis of 3-(triethoxysilylpropyl) Carbamate Linkage on Nitrocellulose .....	43
Figure 2- 9: Reaction of TMOS Vapor on Nitrocellulose .....	43
Figure 2- 10: Synthesis of Surface Silanol on Nitrocellulose.....	43

### Chapter 3

Figure 3- 1: FTIR spectra.....	55
Figure 3- 2: FTIR spectra.....	56
Figure 3- 3: FTIR spectra.....	58
Figure 3- 4: Kinetics of Water Adsorption .....	59
Figure 3- 5 Figure: 3-5: Representative SEM images of Nitrocellulose materials:.....	60
Figure 3- 6 Figure 3-6: DSC Thermograms of Unmodified and Modified Nitrocellulose Decomposition. ....	61
Figure 3- 7: XPS Survey Spectra .....	63
Figure 3- 8: Chemical states of Carbon Atoms in Nitrocellulose determined by XPS.....	64
Figure 3- 9: Results of Deconvolution of XPS High Resolution Spectra.....	66

### Chapter 4

Figure 4- 1:Treated Nitrocellulose.....	72
Figure 4- 2: Time Behavior of the NG Droplets.....	80
Figure 4- 3: Droplet Measurement.....	85
Figure 4- 4: Droplets on NC Fibers .....	88
Figure 4- 5: Contact Angles of n-alkanes on C <sub>6</sub> F <sub>13</sub> Treated Nitrocellulose Fibers. ....	92
Figure 4- 6: Zisman Plot from Nitrocellulose Fibers Treated with Perfluoroalkyl Silane. ....	94
Figure 4- 7: Barrel Droplets on NC Treated with C <sub>6</sub> F <sub>13</sub> used for Measuring Surface Energies. .....	95

Figure 4- 8: Wetting Control on Fibers.....	101
---	-----

## Chapter 5

Figure 5- 1: Types of Adsorption Isotherms (IUPAC 1985).....	107
Figure 5- 2: Classification of Hysteresis Loops (IUPAC 1985).....	109
Figure 5- 3: Nitrogen Adsorption Isotherm of Bare Nitrocellulose at 77K.....	111
Figure 5- 4: Nitrogen Adsorption Isotherms of Nitrocellulose.....	113
Figure 5- 5: BET plots .....	116
Figure 5- 6: $\alpha_s$ Plot .....	120
Figure 5- 7: Pore Size Distribution .....	121
Figure 5- 8: Dispensed Droplets .....	123
Figure 5- 9: Change of Water Contact Angle of NC-C <sub>6</sub> F <sub>13</sub> Aged at Room Temperature Over 21 days. ....	125
Figure 5- 10: Nitrocellulose Treated with C <sub>6</sub> F <sub>13</sub> at 50°C and 65°C for 21 days.....	126
Figure 5- 11: 5-11 Change of Nitrogen Content Over Time .....	128

## APPENDIX A

Figure A- 1:Nonafluoropentanoyl Acyl chloride	131
Figure A- 2: Pentafluorobenzoyl Acyl chloride	131
Figure A- 3: 3,3,3,-trifluoropropanionyl Acyl chloride	131
Figure A- 4: Pentadecafluorooctanoyl Acyl chloride	131
Figure A- 5: Phenyltrichlorosilane	131
Figure A- 6: Dimethyldichlorosilane	131
Figure A- 7: n-Octadecyldimethyl chlorosilane	1322
Figure A- 8: Tridecafluorotetramethoxyhydrooctyl trimethoxysilane	132

Figure A- 9: Pentafluorophenyl Isocyanate	132
Figure A- 10: 3-5 bis(trifluoromethyl)phenyl Isocyanate	132
Figure A- 11: Trimethylsilyl Isocyanate	132
Figure A- 12: 3-(Triethoxysilyl)propyl Isocyanate	132
Figure A- 13: Tetramethoxysilane	133
Figure A- 14: Hunig's Base	133

## APPENDIX B

Figure B- 1: Solvent Loss of Ethanol/NG Stock Solution for Purity. ....	135
Figure B- 2: GC-MS Chromatogram. ....	135
Figure B- 3: GC-MS Chromatogram .....	136
Figure B- 4: GC-MS Chromatogram .....	137
Figure B- 5: DSC thermogram of neat NC decomposition (exotherm down).....	138
Figure B- 6: DSC Thermogram of 3,3,3,-trifluoropropanionyl Acyl Chloride Treated Nitrocellulose showing decomposition. (Exotherm down) .....	138
Figure B- 7: DSC Thermogram of Nonafluoropentanoyl Acyl Chloride Treated Nitrocellulose showing Decomposition. (Exotherm down).....	139
Figure B- 8: Measured Parameters for Estimating Dimensionless Symmetric Contact Angles of NG droplet on a functionalized NC surface .....	139



## Tables

### Chapter 1

Table 1- 1: $\gamma_{LV}$ (mN/m) Measurements at Different Temperatures. ....	17
Table 1- 2: Dynamic contact angles ( $\theta_{Adv}/\theta_{Rec}$ , deg) for Nitroglycerin and Methylene Iodide .....	19

### Chapter 3

Table 3- 1: Molecular weight distribution (in thousands) for Timed Stirring of Nitrocellulose in THF. ....	50
Table 3- 2: Gel permeation Chromatography (GPC). ....	51
Table 3- 3: Elemental Analysis Data for Nitrocellulose Functionalized with Acylchlorides and Isocyanates. ....	52
Table 3- 4: DSC Decomposition Temperatures for Nitrocellulose .....	53
Table 3- 5: Chemical analysis data for Bare and Treated Nitrocellulose. ....	59
Table 3- 6: Onset and Peak Decomposition Temperatures of Bare and Treated Nitrocellulose. .....	62
Table 3- 7: XPS Atomic Compositions for Nitrocellulose Reacted with Organosilanes. ....	66
Table 3- 8: Thickness of Organosilanes Layers Grafted to Nitrocellulose. ....	68

### Chapter 4

Table 4- 1: Advancing/Receding Contact Angle Measurements of Perfluoro Acyl Chloride and Isocyanate Modified NC ( $^{\circ}$ ). ....	75
Table 4- 2: Dynamic Contact Angles ( $\theta_{Adv}/\theta_{Rec}$ , deg) of Water Hexadecane, and Nitroglycerine on Pellets of Functionalized Nitrocellulose and Selected Surfaces of Known Composition.* .....	76

Table 4- 3: Estimated Average Contact Angles and Surface Tension Values.....	89
Table 4- 4: Critical Surface Tension of Treated Nitrocellulose Fibers.....	93
Table 4- 5: Surface Energy Values of Treated Surfaces. ....	99

## **Chapter 5**

Table 5- 1: BET values for Bare and Treated Nitrocellulose .....	118
--	-----

## **APPENDIX B**

Table B- 1: Solvent Loss Over Time to Monitor Remaining Nitroglycerin for Purity Conformation. ....	134
Table B- 2: Standard data for Adsorption of N <sub>2</sub> at 77K on Nonporous Hydroxylated Silica. .....	140

# Equations

## Chapter 1

Eq. 1- 1 The Young's Equation .....	10
Eq. 1- 2 The Work of Cohesion .....	10
Eq. 1- 3 Surface Tension Based on Capillary Rise .....	17
Eq. 1- 4 Graphical Reporting of Nitroglycerin Surface Tension .....	17

## Chapter 3

Eq. 3- 1 Thickness of Grafted Layers .....	67
--	----

## Chapter 4

Eq. 4- 1 Israelachvilli Equation .....	77
Eq. 4- 2 Zisman Equation .....	93
Eq. 4- 3 Van Oss Good-Chaudhury Equation.....	96
Eq. 4- 4 Van Oss Good-Chaudhury Method of Components .....	96
Eq. 4- 5 Li-Neumann Equation of State.....	97

## Chapter 5

Eq. 5- 1 Brunauer Emmett Teller (BET) Method .....	114
Eq. 5- 2 $C_{\text{BET}}$ Constant.....	114
Eq. 5- 3 Brunauer Emmett Teller (BET) Model for Data Plotting .....	114

# **Chapter 1: Nitrocellulose, Nitroglycerin, Propellant, and the Importance to Understand their Surface Chemistry**

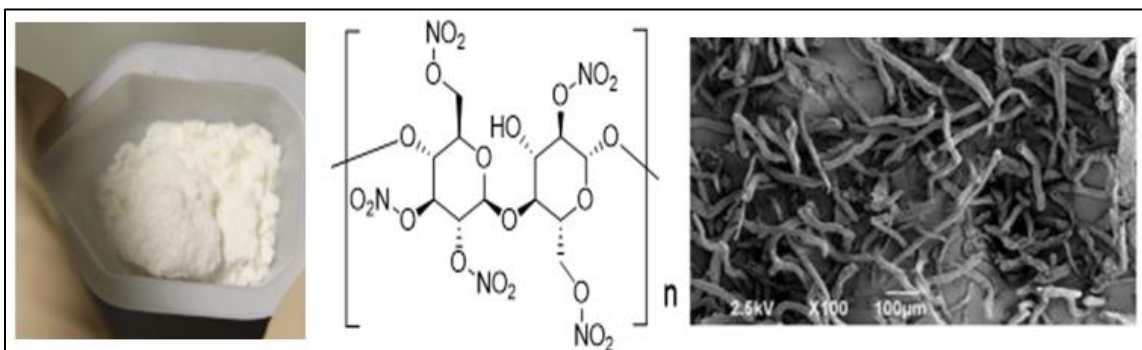
## **1.1 Introduction**

The focus of this work was to study the fundamental wetting of NC with liquid and how we can control the wetting of nitrocellulose by developing tunable interfaces. In Chapter 1, we begin the discussion with focusing on the properties of nitrocellulose, the nitration of cellulose, and how the properties of NC relate to its functionalization. A discussion pertaining to double based propellants will be addressed, since this type of propellant is formulated with both nitrocellulose and nitroglycerin (NG). We describe the issues associated with the movement of NG in solid propellant formulations and the potential applications to solve this problem by the means of using lyophobic nitrocellulose. We introduce the important parameters of the contact angle measurement and surface tension. We report the results of wetting properties and surface tension measurements of nitroglycerin (NG). In this chapter we report experiments that utilize NG as a probe fluid to measure dynamic contact angles over a range of organosilane, fluoro-alkyl, and polymeric surfaces. NG contact angles change over a wide range depending on the nature of the surface chemistry used, demonstrating major variations of the NG interfacial interactions for surfaces with different functionalities. We revisit surface tension measurements generated over eighty years ago, and include the measurement of NG surface tension as a function of temperature up to 60°C using two versions of the classical capillary rise method. *Note: Unless referenced or specified otherwise, all photos and figures are produced by the author.*

## 1.2 Nitrocellulose and its Properties

Nitrocellulose (NC) is the commercial name for the product resulting from the reaction of cellulose with nitric acid and most commonly in the presence of sulfuric acid. In fact, the name nitrocellulose is incorrect, because it implies  $\text{NO}_2$  functionality with the nitrogen attached directly to the carbon.<sup>1</sup> However, it is actually an ester containing nitrate groups with an oxygen bridge between the carbon in the polymer backbone and the nitrogen of nitrate.<sup>1, 2</sup>

NC is a natural fibrous crystalline powder. Its structural formula and SEM picture is shown in Figure 1.1. NC is derived from cellulose made up of anhydroglucose units joined by ether linkages. The average number of units in the molecule is several thousand for most native celluloses, which ranges from 500 to 2,500 for chemically purified celluloses.<sup>1</sup>



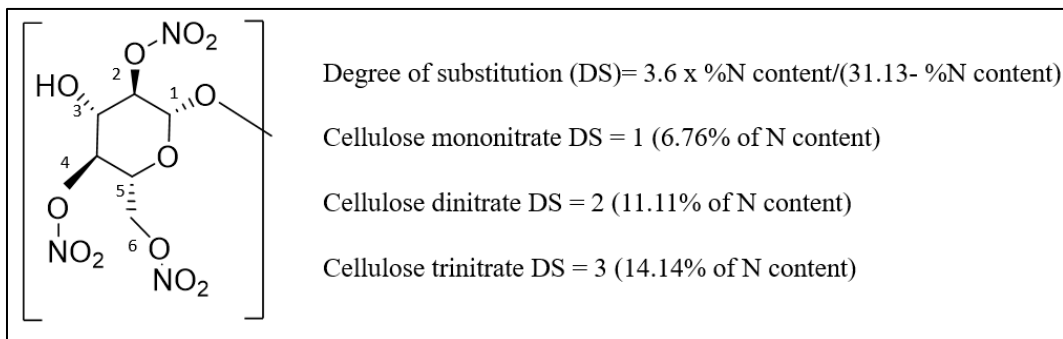
**Figure 1- 1: Nitrocellulose:** Crystalline Powder, Chemical Structure (*Chem Draw version 19.1*), and SEM Photo.

Under proper conditions, an ester is formed by reacting the cellulose with nitric acid. The esterification reaction offers the discussion of degree of substitution. In theory, it should be possible to replace the three hydroxyl groups in each anhydroglucose unit with nitrate to give cellulose trinitrate, which would result in a molecule that is 14.14% nitrogen. However,

in practice it is not possible to obtain nitrogen content higher than 13.5%. This is because the practical upper limit in substituting nitrate for hydroxyl groups is roughly 2.9 which results to a nitrogen content of 13.8%.<sup>1, 2, 3</sup> It is known that in order to provide properties that generate a stable material, NC should have an average degree of substitution<sup>4, 5</sup> between 1.8 and 2.3. On Nitrocellulose, positions C<sub>2</sub>, C<sub>3</sub>, and C<sub>6</sub> are occupied by nitro groups. However, the rate of nitration is different for each carbon because the substitution is more favorable on the C<sub>6</sub> carbon, followed by C<sub>2</sub> and C<sub>3</sub> carbons.<sup>3</sup> Figure 1.2.1 shows the chemical structure of nitrocellulose with a nitrogen content of 6.76% taking into account the carbon reactivity. The use of NC is also determined by the nitrogen content of NC. NC that has a nitrogen content lower than 12% is often used in propellant cartridge casing material, lacquers, and photographic films.<sup>2,3,4</sup> NC with a higher nitrogen content than 12%, is used in military grade propellant formulations.<sup>1,2,3</sup> The nitrogen content of nitrocellulose is important because it affects the solubility and the viscosity of nitrocellulose in organic solvents. Solubility decreases when the nitrogen content of nitrocellulose decreases.<sup>1, 2, 3</sup>

The cellulose used to react to make NC is usually made from wood pulp.<sup>6</sup> Cellulose obtained from wood pulp is separated by two methods of nitration.<sup>6,7,8</sup> The methods include sulfite and sulfate processes.<sup>6,7,8</sup> The sulfite process involves heating and boiling wood chips in a solution of calcium bisulfate at high pressure, which results in a high percentage of alpha cellulose. The sulfate process involves cooking the wood chips at high temperature and pressure in a solution of sodium hydroxide, sodium sulfide, and sodium bicarbonate. The sulfate product contains less percentage of alpha cellulose. Depending on which process is used ultimately determines the properties of the nitrocellulose to include degree of polymerization, and molecular weight.<sup>6</sup>

For the purpose of this work we demonstrated the surface functionality of NC nitrated up to 13.15%. However, in the beginning phases of this research, we studied the functionalized surface of 11.15% NC as well, which is the standard nitrogen content used in military cartridge casing increments.<sup>4</sup> Theoretically, if surface modification is possible, ~13.15% NC should result in lower lyophobicity than the ~11.00% nitrated NC. We initially used ~13.15% and ~11.00% nitrated NC to study reactions using acyl chlorides and isocyanates. However, as the research progressed we utilized a blended NC that is typically used in propellant qualified by the U.S. Army, with an average nitration of ~12.46%. The degree of substitution for this NC was ~2.4 leaving ~.6 degree of substitution for remaining hydroxyl sites to be used for surface modification.<sup>9</sup>



**Figure 1- 2: Chemical Structure of NC**  
 with nitrogen content of 6.76% and description of degree of substitution.  
*(Molecular structure produced using Chem Draw version 19.1)*

### 1.3 Nitrocellulose Double Base Propellants

Nitrocellulose (NC) based propellants are used in the initiation of ammunition systems such as rockets and projectiles. Propellants are manufactured in a variety of geometries, depending on the intended application.<sup>10</sup> Figure 1-3a-h show a variety of geometries ranging from a single grain of ball powder to multi-perforated cylinders. Figure 1-3b represents an M2 cylindrical multi-perforated propellant used for medium caliber

munitions. Figure 1-3c depicts the flake powder M9 propellant containing >20% NG, used in small caliber ammunition. In firearms, propellants fill the interior of an ammunition cartridge chamber of a gun or cannon, leading to the expulsion of a bullet or shell. Numerous additives are used in solid propellants to improve their burn rate, stability, sensitivity, and mechanical properties.<sup>10-12</sup> NC is the primary ingredient in military grade propellants, and are used in the initiation of ammunition systems such as rockets and projectiles.<sup>10</sup>

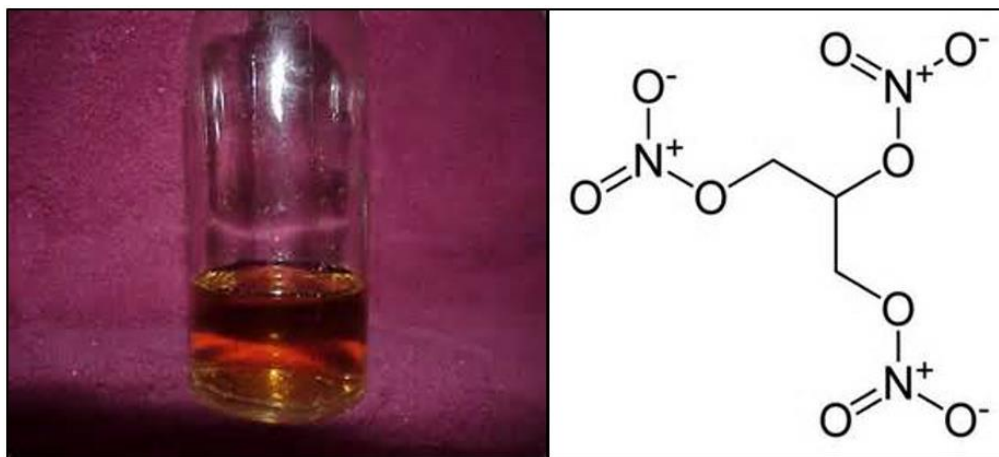
NC is also used in the manufacturing of cartridge casing increments that house the propellant within a munition system. Numerous additives are used in solid propellants to improve their burn rate, stability, sensitivity, and mechanical properties.<sup>11</sup> Energetic plasticizers are the most common additive in propellant manufacturing to increase overall energetic performance.<sup>12</sup> NG is incorporated in the propellant formulation as a powerful liquid explosive, and it also functions as a plasticizer.<sup>4,10, 11, 12</sup> Figure 1-4 Shows NG in neat form and the chemical structure of NG.



**Figure 1- 3: Propellant Types**

(a) Various geometries of solid propellant. (b) M2 cylindrical multi-perforated propellant. (c) M9 ball powder propellant. (d) Small caliber flake. (e-f) multi perforated. (g) Rosette perforated (h) single perforated.<sup>10</sup>





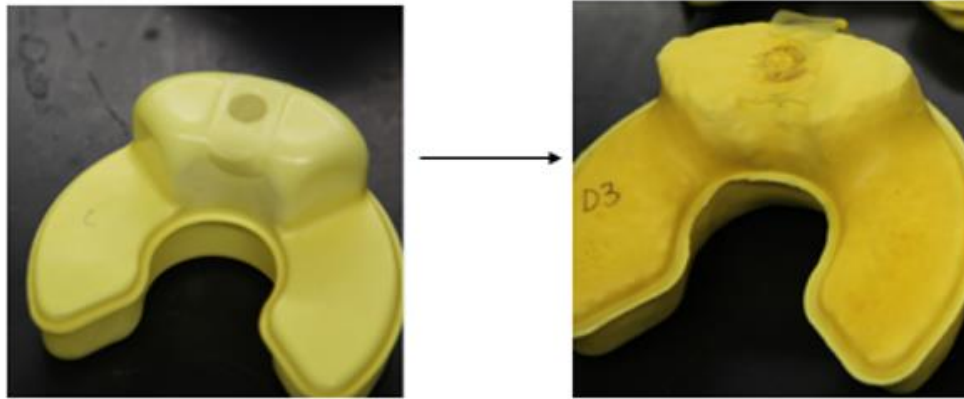
**Figure 1- 4:** Bottled nitroglycerin<sup>142</sup> and chemical structure of nitroglycerin.  
(Chem Draw version 19.1)

#### 1.4 Nitroglycerin Migration in Solid Propellant and Possible Solutions

While NG serves a significant purpose, it has the tendency to sweat throughout a propellant grain leading to performance and safety problems which have long been documented.<sup>12-14</sup> For instance, long term storage of NG based propellants have caused explosions and fires due to sweating of the energetic material through out the propellant matrix.<sup>14,15</sup> Accordingly, a need exists to prevent sweating of NG in propellant without compromising the desired energetic properties. Recently, we proposed a solution to this problem<sup>16</sup> by means of developing a “tunable” NC surface that will hopefully provide solutions pertaining to improved safety parameters, enhanced performance of NC contained products, and the potential of utilizing a surface modified NC for 3-D printable explosives.

Sweating of NG often occurs in nitrocellulose cartridge casing increments that contain ball powder propellant.<sup>14</sup> Ball powder propellant formulations comprise of 25-50% nitroglycerin by weight.<sup>4</sup> Over time, sweating of the NG from the ball powder propellant leaches into the cartridge case increments. This leaching of NG results in performance and shelf-life issues. Figure 1-5 demonstrates the effect NG has on cartridge casing increments

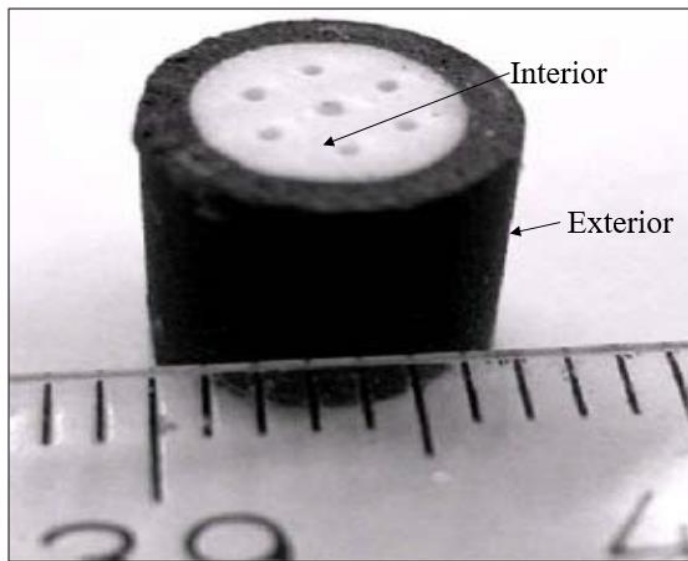
when exposed to heating at 50°C for 28 days. The sweating of NG results in a negative shape effect of the cartridge casing, including a softening of the material. A solution to this problem involves the surface chemistry of NC. Provided the correct NC surface, NG maybe contained in the interior of the cartridge casing.



**Figure 1- 5:** Nitroglycerin exposure of nitrocellulose cartridge casing at 50°C for 28 days.

#### **1.4.1 Co-extruded Propellant and the Lyophobic Barrier**

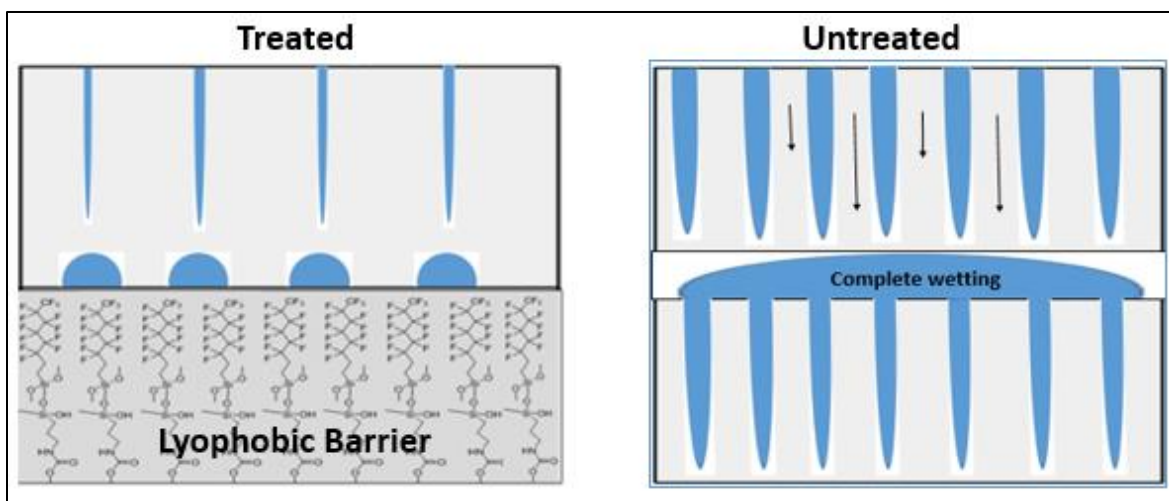
Diffusion and migration of propellant constituents can also arise with co-extruded propellants. A co-extruded propellant is a dual system with an inner and outer core having its own constituents independent of one another designed to control the propellant's burn rate. Figure 1-6 shows an example of a co-extruded propellant grain where the black colored section burns at a slower rate than the interior (white colored portion) of the grain. The inner core is known for its high energy density and burns much hotter than the outer core. The outer core may be formulated with nitrocellulose which acts to minimize the extremely hot burn of the inner core. The purpose is to have the plasticizers that burn hot contained in the inner core of the propellant, leaving the outer core as a single-based nitrocellulose. Problems arise when plasticizers such as nitroglycerin diffuse into the outer portion of the propellant grain thus, defeating the intended purpose of the co-extruded grain.



**Figure 1- 6:** Co-extruded propellant grain.<sup>141</sup>

*Zebregs, M.; van Driel. Co-extrusion of Gun Propellant. IM/EM Symposium, Tucson, AZ, May 2009*

The idea behind creating a tunable NC surface is to establish a lyophobic barrier that will allow a low surface energy interface or perhaps a surface with a slightly higher interfacial energy depending on the intended application that is to be determined. Figure 1-7 gives an example of treated NC surface versus an untreated surface. The treated surface in the diagram shows (Tridecafluoro-(1, 1, 2, 2-tetrahydrooctyltrimethoxysilane) as the functionality. The treated surface containing a lyophobic barrier would possess a low surface energy which would result in the liquid energetic plasticizer to form a contact angle on the interface of the ‘treated’ or functionalized portion of the lyophobic barrier. In comparison to the untreated interface shown on the right hand side of Figure 1.7, the liquid exposed on a higher energy surface would completely wet the surface and continue to move throughout the system. Migration of plasticizers within a propellant formulation are proposed in this work to



**Figure 1- 7:** Proposed outcome of lyophobic barrier and movement of liquid between the untreated interface.

prevent safety problems. The migration of constituents are known to be the cause of fires resulting from propellants stored for long periods of time. Propellant burn rates are compromised due to plasticizer migration. Currently, there is no true solution for plasticizer migration. Propellant coatings used in industry only remain stable in low temperature and humidity environments and will not contain the plasticizer movement once environmental factors start to fluctuate. The coatings used in industry pose compatibility issues and performance constraints on the propellant formulation. Insight on the wettability of NC may help to eliminate these problems by encapsulating/coating the propellant grains with a functionalized NC that is lyophobic, therefore containing the plasticizers within the matrix of the propellant grain. The modification of NC could replace traditional propellant coatings due to its ability to contain liquid constituents within a matrix and still maintaining the functionality of nitrocellulose without jeopardizing the performance of the propellant.

## 1.5 Nitroglycerin Wetting Properties & Surface Tension at Various Temperatures

### 1.5.1 The Young's Equation and the Contact Angle

The contact angle measurement continues to be perhaps the most useful characterization technique in the field of surface chemistry. Contact angle measurements are an important technique for probing the character of solid-liquid interfaces. 'Wetting' is the ability of a liquid to maintain contact with a solid surface.<sup>16</sup> The contact angle measures the extent to which a surface is wetted with a liquid. Wetting is uniquely valuable in characterizing surfaces to obtain high sensitivity and its application to disordered surfaces.<sup>16,17</sup>

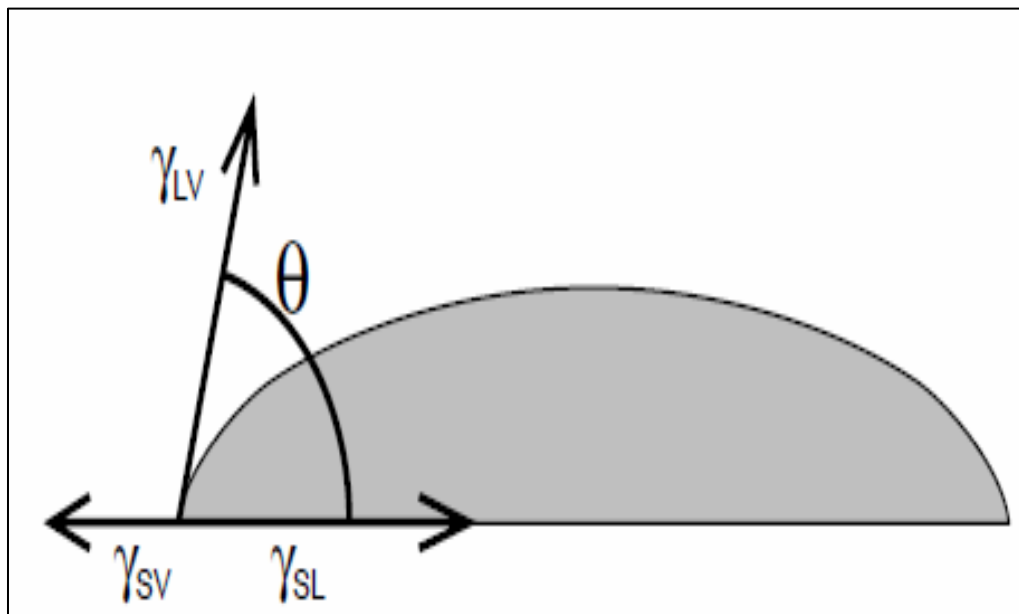
The contact angle ( $\theta$ ) is measured at a three-phase interaction between a liquid, solid, and vapor.<sup>16</sup> Young characterized this balance of the free surface energies at the liquid-vapor ( $\gamma_{LV}$ ), solid-vapor ( $\gamma_{SV}$ ), and solid-liquid ( $\gamma_{SL}$ ) Young's Equation (1-1). Figure 1-8 describes the balance of the free surface energies at the interface.<sup>16-18</sup>

$$\gamma_{LV}\cos\theta = \gamma_{SV} - \gamma_{SL} \quad \text{Eq. 1- 1}$$

The equilibrium contact angle is often stated as a balance of the work of adhesion ( $WA = \gamma_{SV} + \gamma_{LV} + \gamma_{SL}$ ) and the work of cohesion ( $WC = 2 \gamma_{LV}$ ) and is written as:

$$\cos\theta = \frac{2W_A - W_C}{W_C} \quad \text{Eq. 1- 2}$$

When  $W_A \geq W_C$ , the contact angle approaches zero, the liquid will spread over the surface resulting in complete wetting.<sup>19</sup>



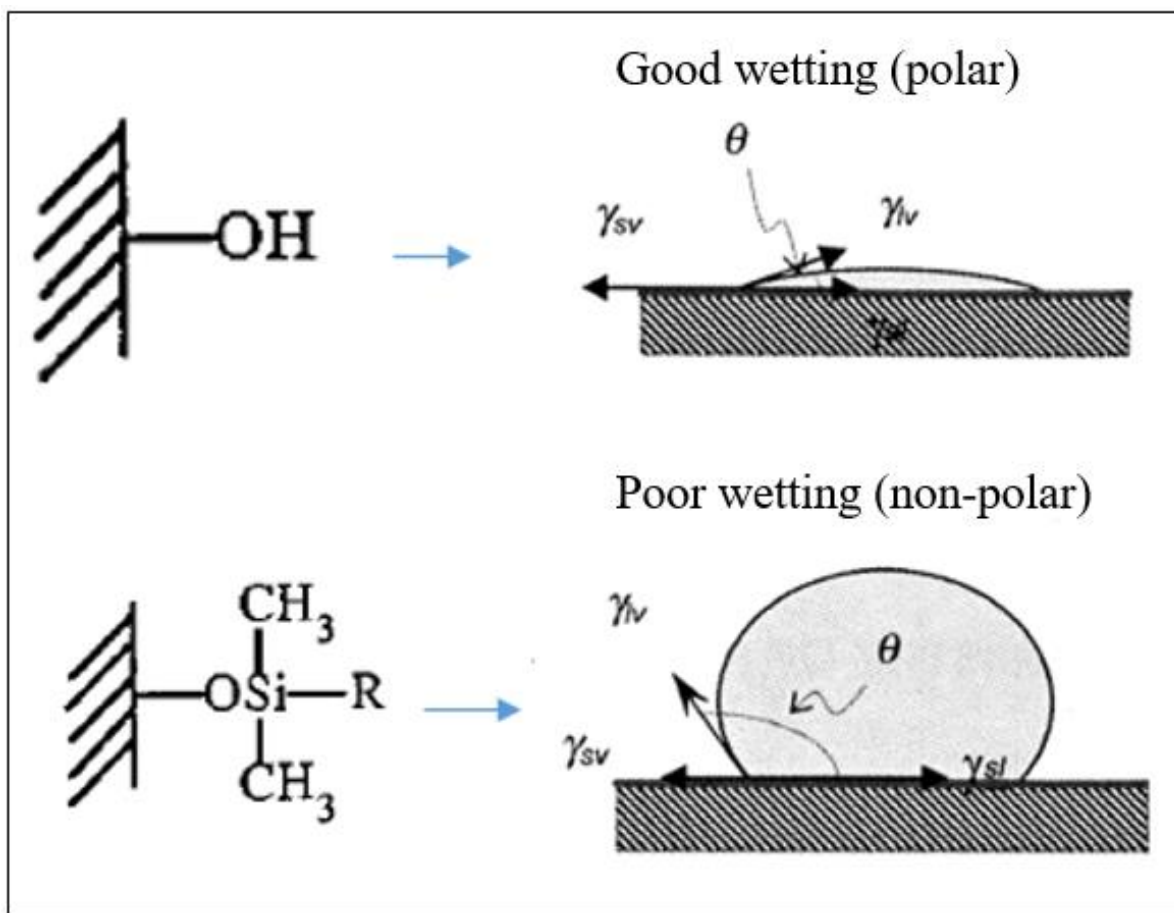
**Figure 1- 8: Young's Contact Angle.**

Three forces acting at the three phase contact line of a droplet on a solid surface where  $\theta$  is the contact angle equilibrium.<sup>16</sup>

*Image reproduced from reference 16, Permission from American Chemical Society, 2000.*

Lyophobicization of a surface will result in a decrease of surface energy and in return, decreases  $W_A$ , and therefore increasing the contact angle. The description shown in Figure 1-9 represents the attachment of organic groups to polar substrates, converting a lyophilic surface into a lyophobic surface by means of surface functionalization with siloxane compounds.<sup>19</sup> With the creation of the hydrophobic surface, when  $W_A$  is less than  $0.5 W_C$ , the contact angle will be  $> 90^\circ$ . Theoretically, when  $W_A$  approaches zero, the contact angle approaches<sup>19</sup>  $180^\circ$ . When working with a uniform surface, the intermolecular attraction across the interface is always greater than zero, in which contact angles are less than  $180^\circ$ . In practice, however, most real surfaces have some level of heterogeneity which results in

hysteresis.<sup>19, 20</sup> Hysteresis, in this case, refers to the difference between the advancing  $\theta_A$  (as wetted area increases) and receding  $\theta_R$  (as wetted area decreases) contact angles.<sup>19-21</sup>



**Figure 1- 9:** Comparison of a water contact angle on polar and non-polar surface.<sup>19</sup>  
*Image reproduced from reference 19, Permission from Taylor and Francis Publishing, 2006.*

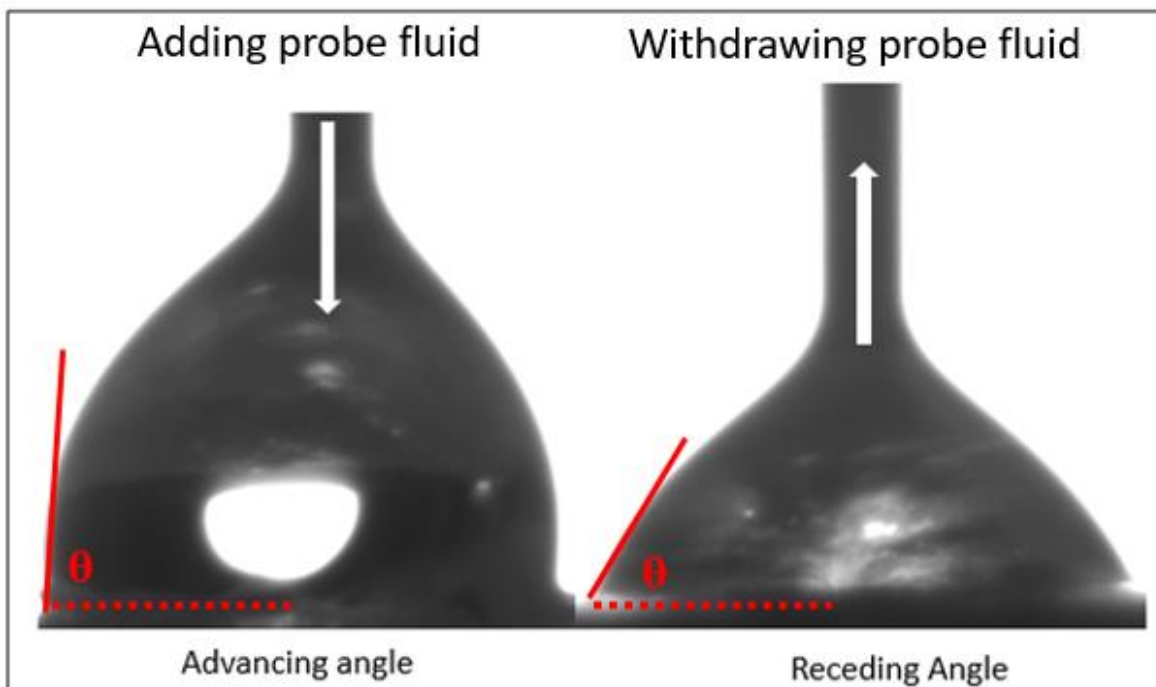
Due to this phenomenon, full characterization of the hydrophobicity of materials requires evaluation of both advancing and receding contact angles.<sup>20, 21</sup> Hysteresis demonstrates the useful sensitivity of wetting to the depth of functional groups below the organic-water interface.<sup>21</sup> The difference between the advancing and receding contact angle is far from zero for most systems.<sup>21</sup> A large value in hysteresis usually means a system is not at equilibrium.

Contact angle measurements rely heavily on comparisons of measurements in similar systems rather than on interpretation of absolute values obtained from only one system.<sup>22</sup> Thus, we use contact angles because they are convenient, very sensitive to obtain details of interfacial structure even at the angstrom scale, and because they are applicable to the characterization of solid-liquid interfaces.<sup>23</sup> These measurements at least correlate with thermodynamically significant measures of surface and interfacial free energies.<sup>24</sup> The technique used to obtain advancing and receding contact angle measurements for our studies was the use of a digital contact angle tensiometer. This instrumentation allowed real-time video analysis while advancing and thus the receding of a droplet of liquid back through the syringe needle. We were then able to measure the angles at different positions of the contact angle experiment. As an example, the action of performing the advancing and receding contact angle with NG as probe fluid on a fluoroalkyl treat NC surface.

In open literature there is very little data concerning the surface properties of nitroglycerin. During our investigations we find that the measurement of NG surface tension was first measured circa 1934.<sup>24</sup> The accurate measurement of liquid surface tension is temperature dependent and is characteristic of the liquid.<sup>25</sup> Confirmation of purity is of absolute necessity when measuring the surface tension of a liquid.<sup>25</sup> The surface tension of NG as a function of temperature, which may be of importance in several industries, is lacking entirely in literature. We performed an extensive literature search only to discover that we are unable to locate data related to the wetting properties of nitroglycerin. This is most likely due to the hazards of sensitivity and potential of explosion when isolating pure NG.<sup>4, 5, 6</sup> According to previous studies, pure nitroglycerin has a surface tension of  $\sim 50.5 \text{ (mJ/m}^2\text{)}$ <sup>25</sup> at room temperature (20°C) similar in value to methylene iodide<sup>26</sup>. Methylene iodide is a



common probe fluid used commonly by researchers such as Zisman et al.<sup>26</sup> in surface characterization. With few exceptions, NG should have similar wetting properties.



**Figure 1- 10:** Advancing and Receding ( $\theta_{Adv}/\theta_{Rec}$ ) contact angle.

The similarity in surface tensions may allow the use of methylene iodide as safe inert replacement for NG, either for surface analyses or laboratory scale propellant formulating. In this study, we utilize NG as a probe fluid on a variety of surfaces. We compare NG and methylene iodide contact angles. We measure the surface tension of NG at variable temperatures up to 60°C after which degradation and increased vapor pressure starts to have direct influence on the measurements.<sup>28</sup>

## 1.5.2 Experimental

### 1.5.2.1 General Information

Nitroglycerin (NG, 99.9%) was supplied as 5% solution in ethanol (SDM 36) by

Copperhead Chemical Company (Tamaqua, PA). Methylene iodide was purchased from Sigma Aldrich 50 mL >99% pure.

#### **1.5.2.2 Nitroglycerin Purity**

The purity of NG was determined by placing a known amount of 5% NG in ethanol on an electronic balance and monitoring the weight loss over time. Observed stabilization of the weight loss was determined to be ~50 hours. GC/MS was then performed to confirm the purity of NG monitoring the loss of ethanol and water. 2 mL of stock solution was evaporated and weight loss was monitored over two days and tested, the final residue was confirmed to contain no ethanol. The final purity of the NG was detected at 98.9 % weight NG verified by GC/MS. Surface water was contributed to the percent error. The procedure to obtain and monitor NG purity from the NG/ethanol solution is described in Appendix-B.

#### **1.5.2.3 Wetting and Contact angles**

Contact angles were measured by a Dataphysic OCA contact angle instrument using GASTIGHT #1750 Hamilton Company micro-syringe. The probe fluids used were nitroglycerin (NG) and methyl iodide. Dynamic contact angles ( $\theta_{Adv}/\theta_{Rec}$ ) were recorded while the probe fluid was added to ( $\theta_{Adv}$ ) and withdrawn ( $\theta_{Rec}$ ) from the drop, respectively. The dynamic contact angles with NG as a probe fluid were measured using a Drummond WIRETROL 5  $\mu$ L pipette to add and withdraw the probe fluid while recorded under the video capability of a Dataphysic OCA tensiometer. Due to safety concerns, we used this technique rather than using a syringe filled with NG. *Filling a syringe with a sufficient amount of NG to obtain measurements could result in initiation of NG. Great care must be taken when performing measurements with nitroglycerin.*

#### 1.5.2.4 Surface Tension of Nitroglycerin

Surface tension measurements were performed using two versions of the classic capillary rise method.<sup>29</sup> First, we used a graduated capillary (.05 cm in diameter) with a surface tension gauge developed by Surf gauge. We also used an off the shelf glass capillary .06 cm in diameter. The length of the capillary column was measured with a ruler graduated in centimeters. .5 mL NG was dispensed into a shallow Teflon dish. The Teflon dish containing the NG and the capillaries were placed in a 150 mL beaker and placed in a Thermo-Fischer conditioning chamber where the samples can maintain a constant temperature while being measured. The NG and capillary tubes were held for 2 hours at each desired temperature. While sampling, the tip of the capillary was placed on the surface of the NG while keeping the capillary vertical. The capillary was turned over and drained at the back end by placing towels until the NG fluid comes out. Each measurement was performed five times to get a consistent read value.

#### 1.6 Results and Discussion

The surface tension (mN/m) of NG at variable temperatures using two capillary diameters were obtained using equation 1-3  $g$  is the gravitational constant.  $\rho$  is the density of the liquid.  $r$  is the radius of the capillary tube and  $h$  is the capillary rise measured from the plane surface of the liquid. The contact angle of NG on a glass surface is assumed to be  $\sim 0$  ( $\cos \theta = 1$ ). The data is reported according to equation 1-4. The data is described in Table 1-1 and Figure 1-11. We see that the surface tension of NG decreases linearly as a function of temperature, confirming that it is in equilibrium with its own vapor.<sup>27</sup> In our measurements, we determined two parameters influencing the measured percent error. The first being the

measured height of the capillary and the second being the density of nitroglycerin at various temperatures. Due to the sensitivity of NG, the challenge was to obtain accurate density readings of NG at low volume for each temperature interval. We therefore utilize data found in literature<sup>29</sup> for the density values ranging from 10-25°C and extrapolate to 60°C.

$$\gamma = \frac{1}{2} \rho g r h \quad \text{Eq. 1- 3}$$

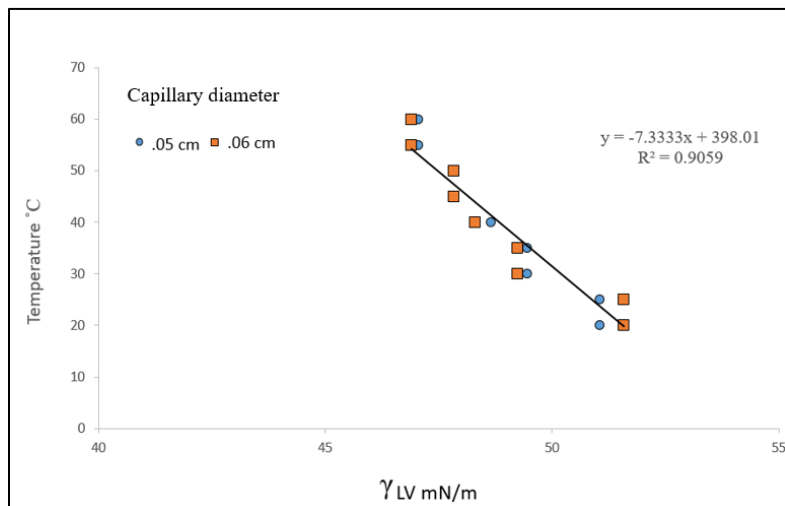
$$\gamma_{\text{NG}}(T) = \gamma_{\text{NG}}^{\circ} - \frac{d\gamma}{dT} T \quad \text{Eq. 1- 4}$$

**Table 1- 1:**  $\gamma_{\text{LV}}$  (mN/m) Measurements at Different Temperatures.

Temperature °C	Capillary diameter (cm)	
	0.05	0.06
20	51.04	51.58
25	51.04	51.58
30	49.445	49.24
35	49.445	49.24
40	48.65	48.3
45	47.85	47.83
50	47.85	47.83
55	47.05	46.89
60	47.05	46.89

To access wetting the properties of NG, surfaces were characterized by dynamic contact angles using NG as a probe fluid. Table 1-2 displays advancing and receding contact angle for NG and methylene iodide. The contact angles of NG show major changes depending on the nature of surface groups demonstrating different levels of wettability (Table 1-2). For all the surfaces studied, the contact angles of NG fell close to the contact angles of methylene iodide in accord with the surface tensions of the probe fluids (mJ/m<sup>2</sup>) at ~20°C: CH<sub>2</sub>I<sub>2</sub> (50.1), NG (50.4). Methylene iodide, in most cases, demonstrated contact angles several degrees

lower than that of NG for the same surface.



**Figure 1- 11:** Graphical representation of temperature vs. surface tension of NG using two different capillary diameters.

However, like for methylene iodide probe fluid, the highest value of NG contact angles  $95^\circ/83^\circ$  (adv/rec) was observed for PDMS/Ti PET substrate, poly(tetrafluoro ethylene) (Teflon)  $87^\circ/78^\circ$  (adv/rec), and perfluoroalkyl  $85^\circ/74^\circ$  (adv/rec) representing the low-energy surface of  $\text{CF}_2$  functionalities. Non-polar hydrophobic surfaces of poly (ethylene), phenyl, and monolayers of octadecyl silane, supported on Si wafers, projecting respectively  $\text{CH}_2$  and mixed  $\text{CH}_2\text{-CH}_3$  functionalities, were poorly wetted by NG and showed contact angles in the range  $\sim 75^\circ/65^\circ$  (adv/rec). For the dimethyldichlorosilane surface, NG contact angle hysteresis was the lowest, which agrees with data obtained using known probe fluids on polydimethylsiloxane surfaces.<sup>30</sup> For relatively polar surfaces of poly (ethylene terephthalate) and polyvinyl alcohol, as evidenced by intermediate value of water contact angles, wetting of NG improved with the advancing contact angle being  $35^\circ$  and the receding angle less than  $10^\circ$ . For the high-energy polar surface of cleaned Si-wafer, NG, demonstrated complete wetting with both advancing and receding contact angles being near zero ( $<10^\circ$ ). On all the model surfaces tested, the contact angles hysteresis of NG was  $\sim 10\text{-}15^\circ$  which was similar to

the values normally reported for methylene iodide on previously tested surfaces.<sup>25,26,27</sup>

Comparing the contact angles for NG on the model surfaces<sup>101</sup>, we concluded that NG, as a probe fluid, produced similar results as methylene iodide probe fluid.<sup>25</sup> The NG contact angles show formation of high quality lyophobic surfaces comparable with the closely-packed monolayers of organosilanes on Si wafers or homogeneous polymer films of similar chemical composition. In this work we explored the wetting of NG with different groups ranged as follows: fluoroalkyl- ( $\theta_{Adv}/\theta_{Rec}$  ~90°/~50°), alkyl- (~75°/~35°), oligo (dimethylsiloxy)- (~65°/~35°), phenyl- (~40°/~10°), demonstrating major variations in the NG interfacial interactions.

**Table 1- 2:** Dynamic Contact Angles ( $\theta_{Adv}/\theta_{Rec}$ , deg) for Nitroglycerin and Methylene Iodide on Model Surfaces, Polymer Films, and Functionalized Si Wafers.

Sample	Probe fluids	
	Nitroglycerin	Methylene iodide
Nylon silica filled	56/42	55/38
Polychloro trifluoroethylene	55/28	53/22
Polyvinyl alcohol	35/27	34/23
Polymethyl pentane	75/62	72/48
PDMS/Ti PET substrate	95/83	87/68
Cleaned Si-wafer: Si/SiO <sub>2</sub> *	<10	<10
Si/SiO <sub>2</sub> -OSi(CH <sub>3</sub> ) <sub>2</sub> C <sub>18</sub> H <sub>37</sub>	75/65	65/50
Si/SiO <sub>2</sub> C <sub>6</sub> H <sub>5</sub>	71/60	68/42
Cl <sub>2</sub> Si(CH <sub>3</sub> ) <sub>2</sub>	80/78	74/70
(CH <sub>3</sub> O) <sub>3</sub> Si(CH <sub>2</sub> ) <sub>2</sub> C <sub>6</sub> F <sub>13</sub>	85/74	84/72
Poly(tetrafluoroethylene), Teflon: -[CF <sub>2</sub> ] <sub>n</sub> -	87/78	86/78
Poly(ethylene): -[CH <sub>2</sub> ] <sub>n</sub> -	65/58	62/54
Poly(ethylene terephthalate): -[C(O)C <sub>6</sub> H <sub>4</sub> COO(CH <sub>2</sub> ) <sub>2</sub> O] <sub>n</sub> -	35/<10	30/<10

\*Si-wafers were cleaned and functionalized by organosilanes as described in ref 19.

Because of the lack of wetting data for NG in open literature, we investigated the surface properties of NG. NG demonstrates surface tension values similar to methylene iodide in which the latter may be used as a probe fluid replacement for the extremely friction and

impact sensitive properties of NG. The surface tension of NG shows ~5 percent decrease for every 10°C temperature increase up to 60°C. The information gathered from this study will hopefully serve as a reference should the need arise to evaluate surface interactions with NG. For this reason, NG contact angles were measured on a variety of well-defined surfaces of known composition including monolayers of organosilanes and fluoro-alkyls supported on Si-wafers, and smooth polymer films.

## **1.7 Conclusions**

In this chapter we discussed the properties of nitrocellulose and its uses in solid propellant formulations. We described the various geometries and uses of formulated nitrocellulose based propellants. We look at the negative impact nitroglycerin movement has on propulsion systems, demonstrating specific examples pertaining to cartridge casing increments and co-extruded propellant grains. Finally, in the experimental section, we look at the surface tension of NG at various temperatures and compare the results to methylene iodide. We utilized NG as a probe fluid for the first time, on a number of known surfaces, to gain insight on how NG may act on modified NC surfaces.

Because of the lack of wetting data for NG in open literature, we investigated the surface properties of NG. The information gathered from this study is to serve as a reference for parameters describe in the following chapters. For this reason, NG contact angles were measured on a variety of well-defined surfaces of known composition including monolayers of organosilanes and fluoro-alkyls supported on Si-wafers, and smooth polymer films. We will see in the next several chapters the importance in understanding NG as probe fluid and

its surface tensions at various temperature is essential in understanding the wetting of NC with NG.

In Chapter 2 we look at the structure of cellulose and with that, the chemistry used for optimal manipulation of hydroxyl sites. We examine the robust nature of silane chemistry and its unique application in surface modification in which literature provides several approaches used to functionalize the cellulose surface. We look at the aspects of organosilane chemistry and its application to surface modification. We discuss the role of silane and cellulose modification through previous work. In the experimental section of Chapter 2, we confirm cellulose surface functionalization in our laboratory, presenting successful reaction conditions performed in our laboratory with alpha cellulose and silyl isocyanate. Results from FTIR and contact angle measurements ( $\theta_{Adv}/\theta_{Rec}$  98/75) suggest successful surface modification. The confirmation of this reaction gave us insight into the use of methods selected to modify NC. Finally, in Chapter 2 We demonstrate surface functionalization on NC. We perform reactions using acyl chloride and isocyanate functionalities using chemistry from previous work and our preliminary experiments with cellulose.



## Chapter 2: Approaches for Nitrocellulose Functionalization

### 2.1 Introduction

Cellulose is the most abundant naturally occurring polymer used for the fabrication of numerous products.<sup>31</sup> For certain applications, including sensing, biomaterials, separation membranes, catalysts, emulsion stabilizers, coatings and polymer-based hybrid materials hydrophobic cellulose surfaces are needed which requires additional functionalization of inherently hydrophilic cellulose.<sup>32,33</sup> The common methods of covalent functionalization of cellulose includes alkylation, alkanoylation, carbamoylation and other reactions that utilize primary and secondary hydroxyl groups available on the surface of cellulose.<sup>34,35</sup> Numerous studies reported the use of silane coupling agents for functionalization of cellulose.<sup>31-35,85</sup> Silylation involves the reaction of cellulose with organosilanes of general formula  $R_nSiX_{4-n}$  ( $n=0-3$ , X- hydrolyzable group e.g. Cl, alkoxy-, acetoxy, and R - organic functionality).<sup>31-35</sup> Silanes are chemically binding to cellulose hydroxyl groups through Si-O-C linkages. When multifunctional silanes ( $n=0,1,2$ ) are used in presence of moisture, polymerization (cross-linking) of silanes occurs yielding siloxane network (Si-O-Si) which greatly improves stability of the coatings.<sup>86, 87</sup> The use of fluorinated silanes produce extremely non-polar surfaces with lyophobic (omniphobic) and superhydrophobic properties.<sup>40, 41</sup>

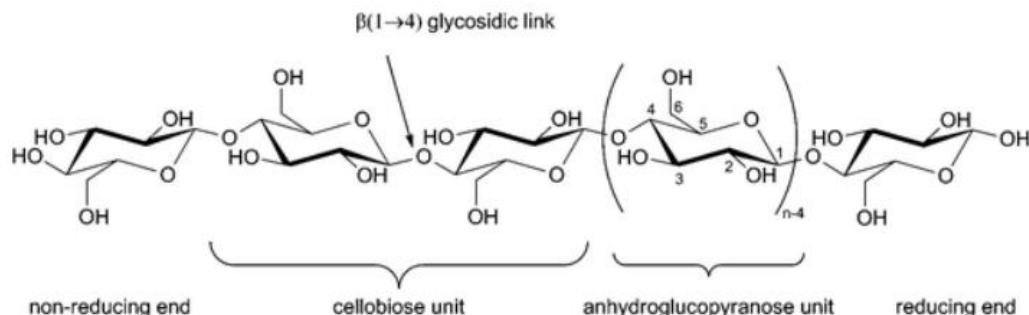
As compared to cellulose, covalent functionalization of NC is more challenging, particularly because of reduced number of hydroxyl groups available for the reaction and limited choice of the reaction conditions that have to be mild enough to preserve nitro groups. The latter is particularly important for the functionalization of highly-nitrated energetic NC materials. Nitrocellulose paper membrane is the common substrate for lateral

flow diagnostics, biosensors, and immunoassays.<sup>89</sup> A majority of the reported functionalization methods employ non-covalent modification of the NC paper through the physical adsorption of proteins or other polymers.<sup>89,90</sup> Several covalent functionalization methods utilizing substitution or elimination of nitro groups were reported.<sup>88</sup> There is virtually no open literature research pertaining to the surface chemistry and functionalization of NC with nitrogen content >12%. In this work, we describe the organosilicon chemistry approach for the covalent functionalization of NC fibrous material (~12.5%N) with the focus on preparing of NG-repellant surfaces of NC to inhibit sweating and leakage of NG in energetic materials.

## **2.2 Cellulose: Its Role in Understanding Nitrocellulose Surface Functionalization**

In order to understand the chemistry of nitrocellulose, it is important to look at the parent compound, cellulose. Clear understanding of the underlying structure of cellulose (Figure 2.1) is fundamental to understanding its surface chemistry. Cellulose is named for (1 → 4) -β-D-glucopyranan, a linear homopolysaccharide composed of β-D-anhydroglucopyranose units (also referred to as anhydroglucose and glucopyranose units but universally abbreviated as AGU) and linked by β(1 → 4) ether bonds called glycosidic links. β-D-anhydroglucopyranose is a six-membered heterocycle with an anomeric carbon (labeled C1) and usually found in the chair conformation.<sup>32</sup> Cellulose is the most abundant natural occurring source of raw materials for the fabrication of numerous products.<sup>30, 31, 32</sup> However, its liquid-proofing properties are poor. Much work has been done to improve its lyophobic properties by means of surface modification. Surface modification of cellulose and its derivatives have been well documented over recent decades.<sup>34-38</sup> The surface of cellulose contains hydroxyl (-OH)

groups available for chemical reactions. Clear understanding of the underlying structure of cellulose is fundamental to understanding its surface chemistry.



**Figure 2- 1: Cellulose Chain.**

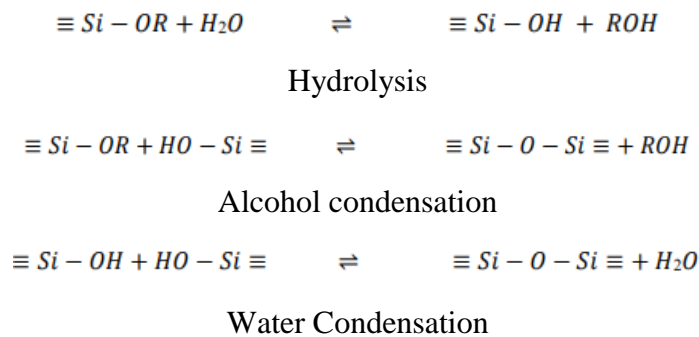
The anhydroglucose unit in the chair conformation, the glycosidic link, and both reducing and non-reducing ends of the polymer.<sup>31</sup>

*Image reproduced from reference 31, Permission from Elsevier, 2005.*

### 2.3 Silane Chemistry for Surface and Polymer Modification

The use of organosilane chemistry for tailoring surfaces and modifying polymers is a process that has been used for decades in both research and technology.<sup>39, 40, 41</sup> A variety of structures can be produced on a surface or reacted with a polymer.<sup>42, 43, 44</sup> The general formula for an organosilane is  $R_nSi X_{(4-n)}$ , showing two classes of functionality typically encountered.<sup>45, 46, 47</sup> X is a hydrolysable group which can be alkoxy, acyloxy, amine, or halogen. The reactive silanol is formed after the presence of hydrolysis which can condense with other silanol groups. The R group is nonhydrolyzable and usually provides a functionality that demonstrates characteristics of a reaction product. The final reaction product resulting from reacting an organosilane with a substrate alters the surface properties of the substrate.<sup>48, 49, 50</sup>

The use of silanes for surface chemistry applications on cellulose and its derivate can be utilized similar to steps required in the preparation of sol-gels.<sup>51, 52, 53, 54</sup> At the functional group level, three reactions to include hydrolysis, water condensation, and alcohol condensation are generally used to describe this process.<sup>51</sup> The hydrolysis reaction replaces –OR groups with –OH (hydroxyl) groups. hydrolysis occurs by the nucleophilic attack of oxygen contained in water on the silicon atom.<sup>51</sup> Alkyl oxysilanes for example, hydrolyze upon exposure to water vapor.<sup>51, 52</sup> Hydrolysis is facilitated in the presence of homogenizing agents to include alcohols, dioxane, THF, and acetone.<sup>53</sup> Condensation may occur either between two silanols or a silanol and an ethoxy group to form a siloxane group (Si-O-Si).<sup>53, 54, 58</sup> Reactions in Figure 2-2 show that polymerization to form siloxane bonds can form by either producing either an alcohol or water condensation reaction.<sup>54</sup> The most widely accepted mechanism for the condensation reaction involves the nucleophilic deprotonated silanol on a neutral silicate species as proposed by Iler<sup>54</sup> to explain condensation in aqueous silicates systems. Brinker et al. explained that silanol acidity depends on the other substituents on the Si atom.<sup>55</sup> When basic OR and OH are replaced with O-Si, the reduced electron density on Si increases the proton acidity on the remaining silanols.<sup>57</sup>



**Figure 2- 2:** Silane surface chemistry reactions.

## 2.4 Cellulose Surface Modification

For the purpose of this work, the mechanism for converting surface alcohol to ester was an obvious choice for nitrocellulose surface modification. We needed to explore reactions giving us optimal conditions, without jeopardizing nitro functional groups and allowing reaction of secondary alcohols. Literature pertaining to ester formation of cellulose provided a vast amount of information on a variety of potential reaction conditions.<sup>42-54</sup>

Reactions involving cellulose have been documented well before the 1950's. Reid and Peterson et al. gave attention to the kinetics and mechanism of cellulose esterification.<sup>11, 57, 58</sup> References confirm the primary hydroxyl groups of cellulose are intrinsically more reactive than the secondary hydroxyl groups by means of homogeneous acetylation performed in 1954 by Krassig et al. The degree of difference between them depends on reaction conditions.<sup>59</sup> In general, the primary hydroxyl is more selectively esterified in a slower reaction process.<sup>57, 58, 59</sup> Reid et al found the apparent difference in reactivity is less in suspension than in solution, perhaps because of a slow diffusion rate, rather than hydroxyl reactivity.<sup>57</sup> The workers found that relative reactivity's of aliphatic acid anhydrides toward the hydroxyl groups of cellulose vary with the reaction catalyst used.<sup>57, 58, 59</sup>

Various types of functionalities including fluoroalkyls and organosilane reagents are currently used in surface modification of cellulose.<sup>43-47</sup> For example, Perfluoroacylated derivatives of ethyl cellulose have been synthesized to improve the lyophobicity of thermoplastic and lacquer manufacturing.<sup>43, 44</sup> Improved performance of cellulose acetate membranes using silane grafting and crosslinking to enhance polymer properties for membrane based gas separations has been documented.<sup>37, 42</sup> Esters of cellulose can also be treated using acyl chlorides that react with the hydroxyl groups of cellulose. The use of

isocyanates to form a carbamate with cellulose have been used for numerous applications in paper manufacturing.<sup>59, 60, 61</sup> In the section we discuss the selection of isocyanate to react with the hydroxyl rich alpha cellulose as an experimental confirmation demonstrating the reaction feasibility by treating a hydroxyl rich surface so that we could continue with our efforts to do the same with nitrocellulose.

## **2.4.1 Experimental (Cellulose Modification)**

### **2.4.1.1 General Information**

The chemicals used in this study was provided by Sigma Aldrich Alpha cellulose (NC). di-isopropyl ethyl amine, lithium chloride, dimethylacetamide (DMAc) (>99%), 3-triethoxysilyl propyl isocyanate .

### **2.4.1.2 Cellulose Modification with 3-triethoxysilyl propyl isocyanate**

Our challenges of modifying nitrocellulose arise from the necessity to maintain nitro functional group moiety, in which the nitration of cellulose gives rise to the energetic properties of NC. We sought out reactions that are not selective to primary alcohols since it is obvious the nitration process reacts with the most sterically available hydroxyl groups on cellulose. With this in mind, it was a necessity to find conditions that would not cleave off the nitro groups or degrade the cellulose polymer chain. To verify reaction conditions which could potentially be used for NC modification, We elected to use isocyanate chemistry based on previous work.<sup>61, 62</sup> Reacting isocyanate in the presence of tin catalyst typically generates a mild exothermic reaction where low heat is generated.<sup>63, 64</sup> We reacted 3-(triethoxysilylpropyl) isocyanate with the hydroxyl rich alpha cellulose. The reaction was

performed in a Pyrex 500 mL round bottom, three prong, enclosed flask by dissolving ~1.0 gram of alpha cellulose (dried at 100°C for 1 hour) in 200mL of dimethylacetamide (DMAc) and ~1.50 grams of lithium chloride (LiCl)<sup>65</sup> in a closed vessel and stirred appropriately at 60°C until the alpha cellulose was fully dissolved. A three-fold increase of solvent amount was required for full dissolution of alpha cellulose compared to work described in literature.<sup>65</sup> Dissolution procedures concerning cellulose are often described in methods pertaining to analytical methodology, where cellulose is being dissolved at the milligram level as an analyte for size exclusion chromatography.<sup>65</sup> Excess of 3-(triethoxysilylpropyl) isocyanate was then added drop-wise. Several drops of dibutyl tin dilaurate<sup>63, 64</sup> was then added as a catalyst and stirred for 4 hours. The DMAc was then evaporated leaving behind the modified alpha cellulose. The modified alpha cellulose was then rinsed with toluene and ethanol, and placed in a 100°C vacuum oven for 1 hour. The material was then characterized using FTIR, H<sub>2</sub>O contact angle measurements, and Si elemental analysis.

#### **2.4.1.3 Results and Discussion**

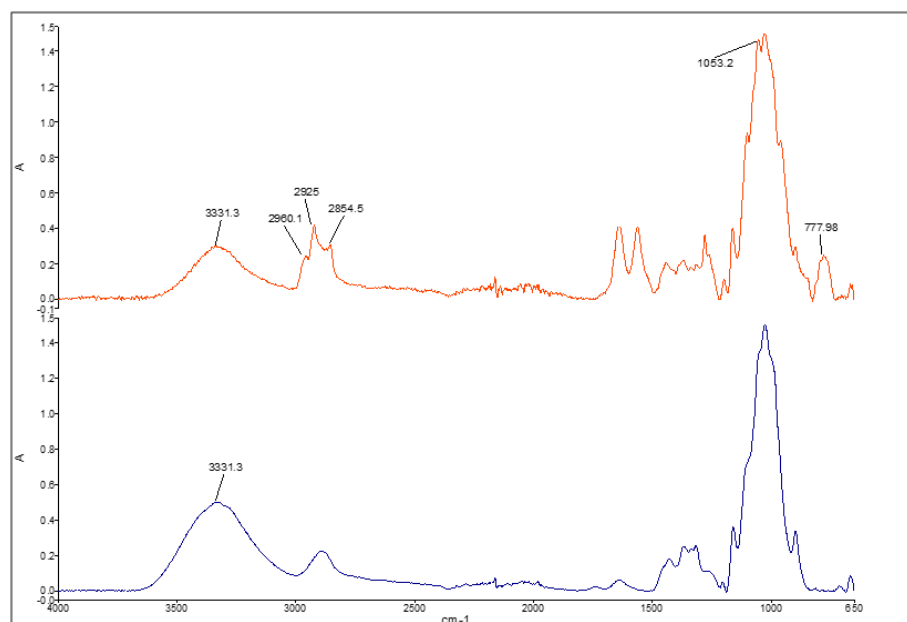
The FTIR spectrum of neat alpha cellulose versus modified alpha cellulose is shown in Figure 2-3. The band at ~2857 cm<sup>-1</sup> shows a decrease in hydroxyl functionality for the modified cellulose compared to neat cellulose, due to the uptake of hydroxyl during the esterification process of the isocyanate reaction. We speculate that without further hydrolysis there would be a decrease in surface hydroxyl functionality after reaction. In later work, we observed an increase of hydroxyl groups if promotion of hydrolysis is allowed, possibly as a result of cross-linking by the silyl propyl carbamate. The bands at ~2929 cm<sup>-1</sup> and ~2857 cm<sup>-1</sup> in the spectrum representing the modified cellulose are evident of CH<sub>3</sub> and CH<sub>2</sub> functional

groups. The band at  $\sim 1637\text{ cm}^{-1}$  and  $1562\text{ cm}^{-1}$  is distinctive of C=O stretch and NH bend from and amide band respectively.<sup>66, 67</sup> The peaks at  $\sim 1100\text{ cm}^{-1}$  and  $1055\text{ cm}^{-1}$  are distinctive of organosilane Si-O and Si-O-C stretch respectively.<sup>68</sup> More details involving FTIR data related to functionalized nitrocellulose will be described in chapter 3.

The alpha cellulose modified with silyl isocyanate and the neat alpha cellulose were subjected to H<sub>2</sub>O contact angle measurements for comparison. The cellulose materials were pressed into pellets. Neat alpha cellulose show complete wetting when H<sub>2</sub>O droplets were dispensed on the pellet surface. The modified alpha cellulose showed a  $\theta_{\text{Adv}}/\theta_{\text{Rec}}$  contact angle of 98/75 respectively. Chapter 4 will describe the wetting of functionalized NC surfaces in detail.

Finally, elemental analysis of the modified alpha cellulose show a percent silicon at  $\sim 3\%$ . This result, along with the promising results obtained from FTIR and contact angle measurements, provided evidence of chemical functionalization of a carbamate layer, and buildup of silane. These findings gave us the information we needed to proceed with the work described in the following section.





**Figure 2- 3: FTIR comparison of neat alpha cellulose**  
(bottom) and alpha cellulose reacted with 3-(triethoxypropyl isocyanate) (top).

## 2.5 Nitrocellulose Functionalization with Acyl Chloride and Isocyanate

### 2.5.1 Preconditioning of Nitrocellulose

NC was laid out on a Pyrex 125 mm watch glass surface and heated at 100°C for one hour in an a Binder explosion proof oven to eliminate excess moisture. Sample was allowed to cool in a Pyrex desiccator in the presence of a calcium sulfate desiccant. 1.5 grams of NC was weighed out in a 3 necked round bottom flask under a nitrogen purge. A stir bar and 50ml THF was added to vessel. A 100 ml condenser was fitted in the center neck while the other two necks were capped with a rubber septum to provide a moisture free environment. A thermocouple was penetrated through a septum to monitor temperature. The NC solution was allowed to stir for 48 hours at room temperature. As previously mentioned, NC must be efficiently stirred to promote optimal dissolution in THF. We have conducted experiments to

determine an optimal stir time at a fixed stir rate of 400 rpm and up to one week using a Chem Glass stir plate.

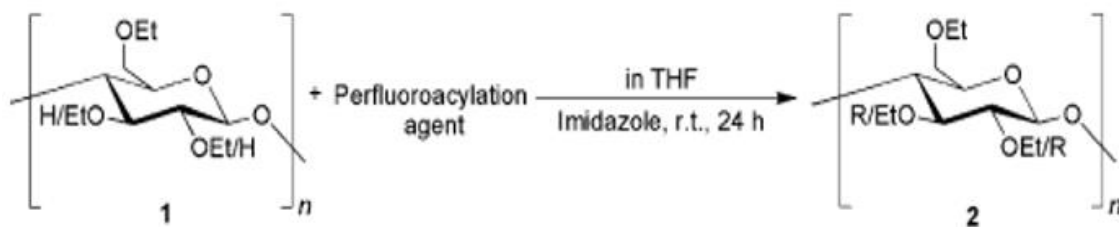
### 2.5.2 General Information

Imidazole (>99%), (acyl chlorides (>95%): pentafluorooctanoyl, nonafluorooctanoyl, pentafluorobenzoyl, 3,3,3-trifluoropropionyl), (Isocyanates: pentafluorophenyl (95%), 3-(triethoxysilylpropyl) (95%), trifluoromethylphenyl (95%), trimethylsilyl (95%)), dibutyl tin dilaurate (95%), toluene (99.8%), Tetrahydrofuran (THF) (HPLC grade, uninhibited), *n*-hexadecane (used as probe fluid) (>99%), (all from Sigma-Aldrich, St. Louis, MO). Water was purified using a Hydro company ultrapure UV pump and filters.

### 2.5.3 Nitrocellulose Surface Functionalization with Acyl Chlorides

Our literature search sent us in the direction using perfluorinated acyl chlorides to functionalize NC for the purpose of increasing the hydro/lyophobicity of NC. The use of acid chlorides appeared to be a potentially mild reaction in the presence of cellulose,<sup>42-45</sup> specifically, with the perfluoroacylation of ethyl cellulose.<sup>45</sup> The challenge with NC was the need to identify a mild base to use for the reaction. We initially chose imidazole as a base, which is described in literature<sup>43</sup> (Figure 2-4) for reacting acyl chlorides with ethyl cellulose, however, reactions resulted in noticeable degradation of nitrocellulose in the presence of imidazole. During the reaction process, the products turned a brown color indicating the NC had crashed out of the solution, possibly due to the proton on the imidazole reacting with the nitrate ester on the surface of NC. We then proceeded to use di-isopropyl ethyl amine (Hunig's base). Hunig's base is known to act as a protecting agent (Figure A-14 Appendix A). The nitrogen atom is shielded by two isopropyl groups and an ethyl group, in which only

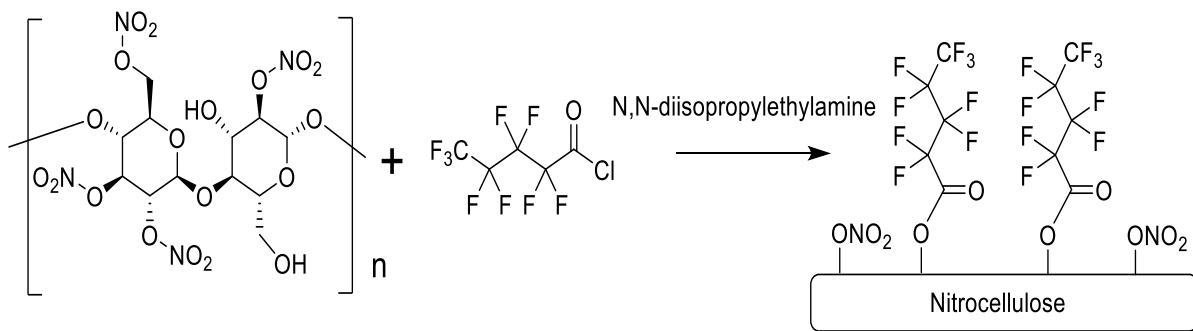
a proton is small enough to fit.<sup>71</sup> Therefore, we hoped that the Hunig's base would prove as a good candidate for the mild reaction needed to modify nitrocellulose. We used 2.0 grams of nitrocellulose (13.15% nitrated) dissolved in THF (50ml) and stirred at room temperature until fully dissolved and stirred for 48 hours, based on our previous findings pertaining to optimal stir time.



**Figure 2- 4:** Perfluoroacylation of ethyl cellulose.<sup>43</sup>

*Image reproduced from reference 43, Permission from American Chemical Society, 2006.*

The fluorinated acyl chlorides chosen for NC surface modifications include 3,3,3-trifluoropropionyl, pentadecafluorooctanoyl, pentafluorobenzoyl, and nonafluoropentanoyl acyl-chlorides. According to literature, these structures show significant increase in lyophobicity of surfaces containing hydroxyl moieties.<sup>41, 42, 43</sup> The reaction was performed for each acid chloride in the presence Hunnig's base (1ml) and stirred for 12 hours at room temperature. An example of a reaction with NC and perfluorinated acyl chloride is shown in Figure 2-5. Reactions were filtered through a 25 $\mu$ m PEP filter membrane and precipitated out with 1 liter of H<sub>2</sub>O. Samples were dried at 100°C for 1 hour.

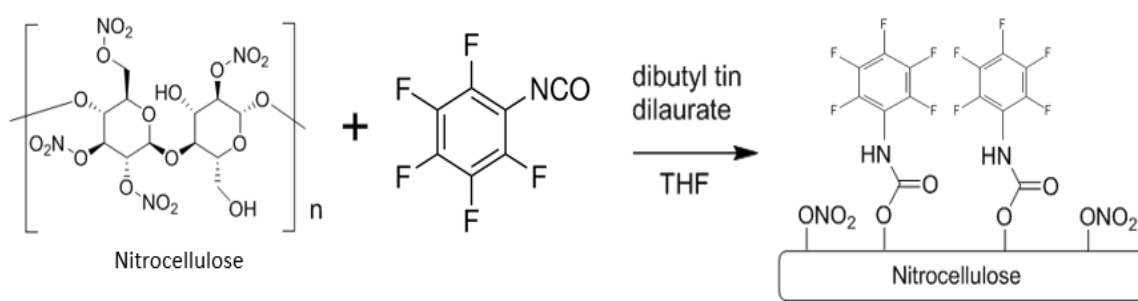


**Figure 2- 5:** Reaction of nitrocellulose with perfluorinated acyl chloride.  
(Chem Draw version 19.1)

#### 2.5.4 NC Surface Functionalization with Isocyanates

It is well known that fluorinated and silyl isocyanates can react with the hydroxyl groups of cellulose via nucleophilic substitution.<sup>44, 73, 74, 78</sup> This nucleophilic substitution forms a carbamate through the alteration of the isocyanate (NCO) group.<sup>73</sup> Procedures in which NCO reacts with the hydroxyl groups of cellulose to produce a more lyophobic/hydrophobic ester group is referenced in vast amounts of work pertaining to cellulose surface modification.<sup>72-78</sup> As described in section 2.2.1 we performed a reaction using alpha cellulose and silyl isocyanate. The successful results from the characterization of this reaction proved it to be promising for further work with NC. However, there has been no work to our knowledge on isocyanate reactions with NC. We therefore performed the surface modification of 13.14 % and 11.04 % NC with fluorinated and silyl isocyanates. The compounds used in this study included pentafluorophenyl, trifluoro-methyl-phenyl, 3-(triethoxysilyl propyl), and trimethylsilyl isocyanates. We chose dibutyl tin dilaurate (DBTDL) as reaction catalyst based on previous work reacting isocyanates.<sup>63</sup> Pentafluorophenyl and 3-(triethoxysilyl propyl) NCO were chosen as the initial reaction candidates with nitrocellulose for their availability and well-defined functionality. The reaction proceeded with 2.0 grams of NC being dissolved in 50 milliliters of tetrahydrofuran

and stirred for forty eight hours in a moisture free environment. 1mL of isocyanate was dispensed drop wise in the reaction vessel. Several drops of DBTDL was added to the reaction. Reactions were stirred for two hours at room temperature, filtered through a polypropylene filter membrane and precipitated out with 1 liter of H<sub>2</sub>O and washed with excess H<sub>2</sub>O. Samples were dried in an oven at 100°C for 1 hour. The reaction chemistry of NC and pentafluorophenyl isocyanate is depicted in Figure 2-6.



**Figure 2- 6:** Reaction of nitrocellulose with 3-(triethoxysilyl propyl) isocyanate.  
(Chem Draw version 19.1)

### 2.5.5 Discussion

Results from characterizing acyl chloride reactions in the presence of Hunnig's base show polymer chain degradation and reduction of nitro group functionality. Therefore, at this point in our work, we turned our attention to the isocyanate chemistry and what would hopefully provide a more mild reaction to successfully modify the surface of NC, without jeopardizing its chemical structure. Disregarding large contact angle hysteresis, the chemical and thermal results for isocyanate reactions looked promising. Although we hadn't totally ruled out the possibility of revisiting the use of acyl chlorides for NC modification, in order to optimize reaction conditions, we decided to search for a reaction that would give us more promising characterization results in terms of stable functionalization of NC. With further

research we demonstrated the use 3-triethoxysilylpropyl isocyanate and its potential as viable candidate for NC surface functionalization. After its initial treatment with NC, we noticed this functionality demonstrated adequate characterization results pertaining lyophobicity and stability. 3-(triethoxysilylpropyl) isocyanate presented the most promising results out of the isocyanates chosen for surface modification of nitrocellulose. What is especially interesting based on further review, previous work details the cross linking functionality of the 3-(triethoxysilylpropyl) isocyanate in the presence of hydrolysis.<sup>44,84</sup> We hoped that the crosslinking properties of 3-(triethoxysilylpropyl) isocyanate may provide an increased formation of hydroxyl groups, acting as a primer layer on the surface of NC, for further surface functionalization.

## **2.6 Surface Chemistry Approach to Control Wetting of Nitrocellulose with Nitroglycerin**

In this section we discuss several approaches of surface functionalization to reduce wettability of NC with energetic plasticizer NG. In the first approach we use two dissolution reactions in which NC is treated with either 3-(triethoxysilylpropyl) isocyanate or tetramethoxysilane (TMOS) in THF, followed by hydrolysis. The silyl isocyanate is chemically grafted to NC via propyl carbamate linkages. TMOS forms a siloxane network directly to the surface of NC. Both reactions yield silanol rich surfaces.

Next, the silanol-modified NC was reacted with various organosilanes of general formula  $\text{RSiX}_n$  ( $\text{R}$ =alkyl-, phenyl-, fluoroalkyl-; ( $\text{X}$ =Cl or  $\text{CH}_3\text{O}$ )) producing a series of lyophobic NC materials. The second approach used for modifying the surface of NC is a direct approach that introduces TMOS vapor to a flat NC pellet, forming a silanol rich surface. The silanol rich NC surface is then further exposed to dimethyldichlorosilane vapor

or monofunctional organosilane to produce the desired lyophobic NC surface. We also had the need to search for reactions that would sufficiently establish surface silanol for lyophobic reactions on a solid surface. We found that TMOS performs well in vapor phase<sup>90, 91</sup> producing surface silanol on NC (Figure 2-7). We turn to the well understood, robust Si-O-Si functionality that is highly chemically and thermally stable.<sup>19,20,21</sup> The organosilane functionality is commercially available, possessing an endless variety of R groups that provide various degrees of lyophobicity<sup>20</sup> detrimental to our work.

Nitroglycerin (NG) is incorporated in the propellant formulations as a powerful liquid explosive, and it also functions as a plasticizer.<sup>1,3,5,6</sup> Due to complete wetting, NG has the tendency to sweat throughout a propellant grain leading to performance and safety problems which have long been documented.<sup>2,3</sup> Long term storage of NG based propellants has caused explosions and fires due to sweating of the energetic material throughout the propellant matrix.<sup>5,6</sup> Accordingly, a need exists to prevent sweating and leakage of NG in propellant without compromising the desired energetic properties. Recently, we proposed a surface chemistry approach to address this problem by means of developing lyophobic NC surfaces<sup>15</sup> that inhibit sweating of NG, improve safety parameters, enhance performance of NC contained products, and show the potential of utilizing a surface modified NC for 3-D printable explosives.

### **2.6.1 Organosiloxanes $R_{4-n}SiX_n$**

Organosilanes with the general formula  $R_{4-n}SiX_n$  ( $n=1,2,3$ .) where X is a hydrolysable group ( $X=Cl, OR, NR_2, H$ ) are very powerful reagents for surface modification.<sup>19</sup> A large variety of organosilanes are commercially available, allowing an expanse of surface functionalities.<sup>72, 81</sup> The linkage of Si-O is synonymous with the word “robust”. Meaning the

linkage between the silane and the surface show good thermal and chemical stability. The fundamental properties of siloxane (Si-O-Si) backbones is high flexibility and high thermal stability.<sup>19, 20</sup> Silanes greatly expand the versatility of surface functionalization.<sup>19</sup> Here we primarily use functional groups with the formula RSiX<sub>3</sub>. The molecules deemed as ‘parent molecules’ in Appendix A depict the organosilane structures used to lyophobicize NC.

### 2.6.2 General Information

The nitrocellulose (NC) used in this study was a blended military grade cellulose 12.47%N by mass (Radford AAP, VA). Nitroglycerin (NG, 99.9%) was supplied as 5% solution in ethanol (SDM 36) by Copperhead Chemical Company (Tamaqua, PA). Tetrahydrofuran (THF) (HPLC grade, uninhibited), 3-(triethoxysilylpropyl) isocyanate (95%), dibutyl tin dilaurate (95%), toluene (99.8%), and *n*-hexadecane (>99%) were used as received (all from Sigma-Aldrich, St.Louis, MO). Tridecafluoro-1,1,2,2,-tetrahydrooctyltrimethoxysilane (95%), *n*-octadecyldimethylchlorosilane (>97%), dimethyldichlorosilane (>99%), phenyltrichlorosilane (>95%), and tetramethoxysilane (>99%) were used as received (all from Gelest, Levittown, PA). Water was purified using a Hydro company ultrapure UV pump and filters.

### 2.6.3 Experimental

#### 2.6.3.1 Reaction of Nitrocellulose with 3-(Triethoxysilylpropyl) Isocyanate and other Silanes

The preconditioned NC (1.5 g) was dissolved in 50 mL of THF and several drops (~0.5 mL) of tin dibutyldilaurate was added to the reaction vessel as catalyst.<sup>62</sup> 3-(triethoxysilylpropyl) isocyanate (1 mL) was added drop-wise and stirring at room



temperature for 4 hours was then completed. The material (silyl- propyl-modified-NC) was rinsed on a 5  $\mu$ m polypropylene filter membrane with 50 mL of THF then rinsed several times with distilled water and dried in an oven at 100°C for 1 h. ~1.5 g of silyl-propyl-modified NC was dissolved in 50 mL of THF. Next, Either tridecafluorotetrahydrooctyl trimethoxysilane, *n*-octadecyl dimethylchlorosilane, dimethyl- dichlorosilane, or phenyltrichlorosilane was added drop wise (~1 mL) and stirred overnight. The reactions were quenched by dropwise addition of water. The functionalized NC was then collected on a filter, rinsed with 50 mL of THF then rinsed several times with distilled water and dried in an oven at 100°C for 1 h.

### **2.6.3.2 Vapor Approach for Preparation of Organosilane Surfaces**

#### **2.6.3.2.1 Preparation of Tetramethoxysilane Surface**

Formed pellets (as described in the experimental section) of either neat NC or silyl isocyanate reacted NC were placed in a 25 mL enclosed Pyrex glass weigh dish with two 1mL beakers containing 1 mL each of tetramethoxysilane (TMOS) and left overnight to react. Reactions were performed at room temperature.

#### **2.6.3.2.2 Preparation of Polydimethylsiloxane Surface**

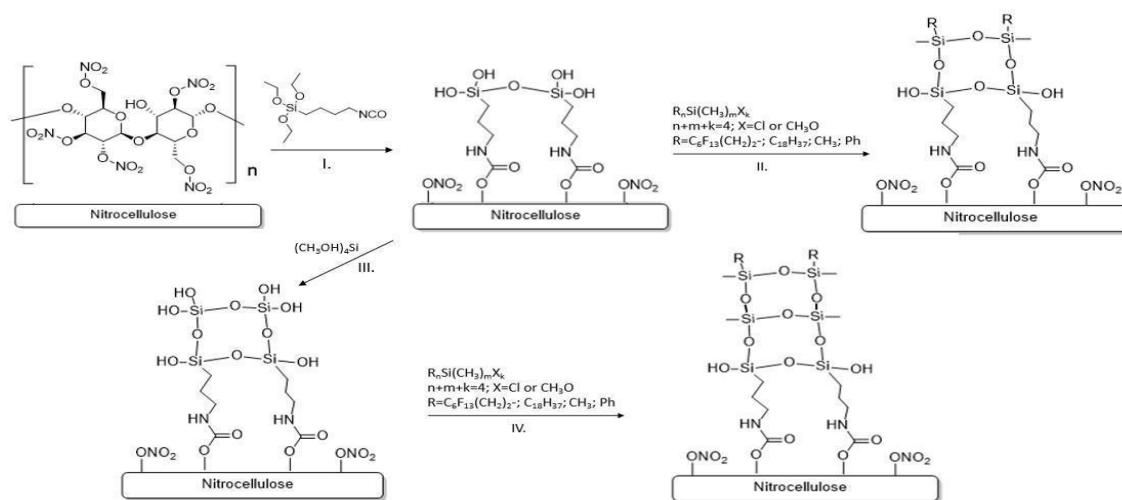
The pellets that were formed from either neat NC or reacted NC were transferred to a 25 mL enclosed Pyrex glass weigh dish containing a 1mL of dimethyldichlorosilane in a 2 mL beaker and allowed to react overnight. Reactions were performed at room temperature. The NC pellets reacted with TMOS were reacted with either 1 mL *n*-octadecyldimethylchlorosilane or fluoro-alkyl with 25 mL toluene in an enclosed rounded 50 ml glass reaction vessel. Reactions were stirred overnight at room temperature. The pellets

were removed from the toluene and placed in a vacuum oven for 1 hour at 100°C.

## 2.7 Results

In this work, we explored several synthetic pathways for surface functionalization of nitrocellulose fibers (NC). Figure 1 summarizes the structures of the reagents used and the reaction schematics. The rationale for the reactions chosen is outlined below. The NC used in this study showed 12.47% of nitrogen (by mass). Although this was considered a high degree of nitration, the number was less than the theoretical maximum of 14.14 %N (by mass) corresponding to fully nitrated cellulose. Significant portion of cellulose OH groups were not substituted with nitro groups providing centers for surface functionalization. In the preliminary research, we have tested and compared several reactions to bind to these OH groups, including the reactions of alkanoyl-, fluoroalkanoyl chlorides and alkoxy silanes. Although the use of alkanoyl- and fluoroalkanoyl chlorides was well-known for functionalization of cellulose,<sup>42-45</sup> these reactions did not fare well with NC and resulted in partial degradation of nitro groups. The direct use of alkoxysilanes, while demonstrating chemical functionalization and a buildup of siloxane surfaces, was considered compromised, primarily due to poor stability of grafted groups attached to NC via labile Si-O-C bonds (see Table 1 and more discussion below). The most effective and powerful method was proven to be the reaction of NC with triethoxysilylpropyl isocyanate. The use of this reagent was reported previously for functionalization of cellulose,<sup>44</sup> but, to the best of our knowledge, it has not been reported for the reactions with NC. Triethoxysilylpropyl isocyanate was a bifunctional reagent: the isocyanate groups were able to bind to the OH groups of NC via carbamate linkage, while triethoxysilyl moieties (in presence of moisture) were able to

hydrolyze, each producing three silanol groups that were attached to the NC backbone via propyl linker (Figure 1, reaction I). Triethoxysilyl isocyanate acted as a “priming reagent” introducing reactive silanols bonded to the NC through the set of robust covalent bonds. The silanol-modified NC could be further functionalized using known methods of silane coupling chemistry to tailor its surface properties. The silane coupling involves formation of strong Si-O-Si linkages and results in chemically and thermally stable coatings.<sup>91, 92</sup> The organosilanes having a virtually endless variety of functional groups are commercially available.<sup>71</sup> This provides powerful method to decorate the NC with desired functionalities to control its surface energy and surface properties including wetting, adsorption, and adhesion. Since the main goal of this particular work was producing non-polar low-energy NC surfaces, we focused on the functionalization of the NC with alkyl-, fluoroalkyl-, dimethylsiloxy-, and phenyl-groups generating a range of lyophobic non-polar NC materials (Figure 1, reaction II). The reaction of silanol-modified NC with tetramethoxysilane produced cross-linked silanol- siloxane network chemically attached to the NC (Figure 3-1, reaction III). This NC with silica-like surface can also be further modified using the methods of CAMs or SAMs chemistry developed for the functionalization of silicas.<sup>93, 94</sup> In this work, this approach was used to prepare NC with thicker coatings with higher surface coverage of organosilicon groups (Figure 3-1, reaction IV).



**Figure 2- 7:** Reaction Schematic for the covalent functionalization of nitrocellulose with organosilanes.

(Chem Draw version 19.1)

## 2.8 Discussion

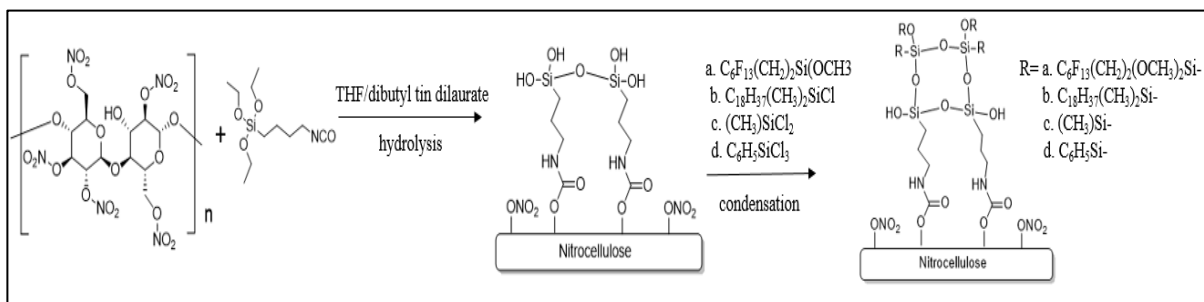
In the previous section, Figure 2-7 describes a condensed version of our reaction schemes. A further detailed discussion of the chemistry and break down of reaction schemes is warranted. Our approaches for surface modification of NC result in several avenues to obtain lyophobic surfaces. In Figure 2-8 we show the reaction in which NC is dissolved in THF and treated with 3-(triethoxysilylpropyl) isocyanate in the presence of catalyst. The silyl isocyanate is chemically grafted to NC via propyl carbamate linkages. After hydrolysis the silanol-modified NC is reacted with various organosilanes of general formula  $RSiX_n$  ( $R$ =alkyl-, phenyl-, fluoroalkyl-; ( $X=Cl$  or  $CH_3O$ )) producing a series of lyophobic NC materials. This reaction demonstrated the bi-functionality of the 3-(triethoxysilylpropyl) isocyanate. In Figure 2-9, we render the fibrous NC powder possessing the propyl carbamate termination. The solid surface is then exposed to TMOS vapor, allowing further treatment of multiple pathways to produce various surfaces with general formula  $RSiX_n$  ( $R$ =alkyl-,

phenyl-, fluoroalkyl-; (X=Cl or CH<sub>3</sub>O)). In Figure 2-10 we demonstrate a subsequent reaction for the direct functionalization of NC. First, a dissolution method that reacts NC with TMOS in THF is followed by hydrolysis. The next reaction in Figure 2-10 demonstrates a TMOS vapor method that forms a thick primer layer directly to NC. The NC reacted with TMOS is used as a powder or pellet to be used as a reaction substrate. TMOS, in both cases, forms a siloxane network directly to the surface of solid NC. Both reactions yield silanol rich surfaces. The silanol rich NC surface is then further exposed to dimethyldichlorosilane vapor or monofunctional organosilane to produce the desired lyophobic NC surface.

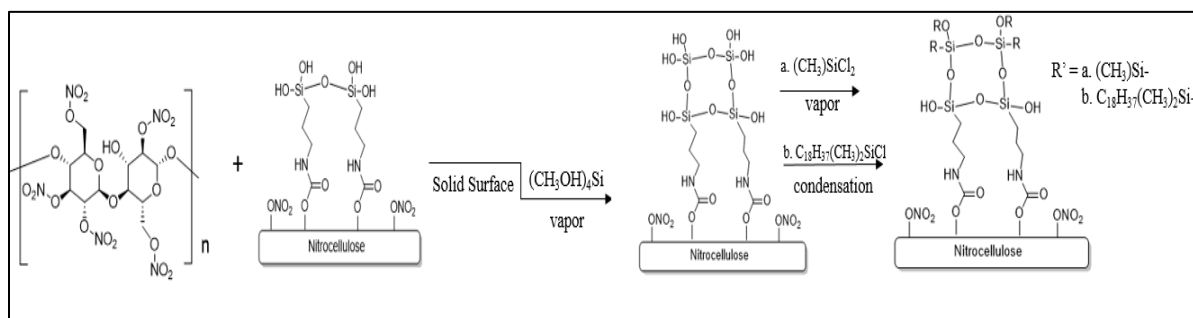
The treatment of a surface with 3-(triethoxysilylpropyl) isocyanate and tetramethoxysilane are known to have crosslinking properties that can provide more hydroxyl groups for further surface modification.<sup>60, 61, 91</sup> The effectiveness of 3-(triethoxysilylpropyl) and TMOS provide an increase of hydroxyl sites via siloxane crosslinking. We applied the term “primer layer” to illustrate the utility of the 3-(triethoxysilylpropyl) propyl carbamate on NC. We initially utilized these functionalities as dissolution phase reactions but we also needed to develop reactions that would sufficiently establish surface silanol for lyophobic reactions on the solid surface. We found that TMOS and PDMS performed well in vapor phase<sup>72, 86</sup> producing surface silanol and polysiloxane respectfully on NC.

## 2.9 Conclusion

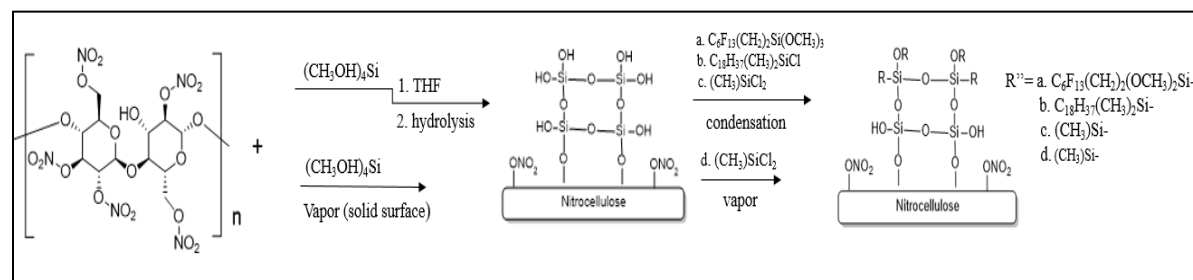
In this chapter we demonstrated surface functionalization on NC, derived from techniques used in cellulose modification. This reaction demonstrated that our selected reaction conditions were successful in the presence of optimal hydroxyl sites. We explored NC surface modification by means of hydroxyl group esterification first by using



**Figure 2- 8: Synthesis of 3-(triethoxysilylpropyl) Carbamate Linkage on Nitrocellulose**  
and hydrolysis of R=fluoroalkyltrimethoxysilane, nalkyldimethylchlorosilane,  
dimethyldichlorosilane, or phenyltrichlorosilane.  
*Chem Draw version 19.1*



**Figure 2- 9: Reaction of TMOS Vapor on Nitrocellulose**  
with the carbamate linkage generating additional surface silanol for the addition of  
R=dimethyldichlorosilane. *Chem Draw version 19.1*



**Figure 2- 10: Synthesis of Surface Silanol on Nitrocellulose**  
using TMOS and hydrolysis of R=fluoroalkyltrimethoxysilane, alkyldimethylchlorosilane,  
dimethyldichlorosilane and reaction of tetramethoxysilane vapor on NC generating additional  
surface silanol for the addition of R= dimethyldichlorosilane and alkyldimethylchlorosilane.  
*Chem Draw version 19.1*

perfluorinated acyl chlorides. However, the use of acyl chlorides and the accompanied reaction conditions, at this time, did not fare well for NC modification, due to the observed degradation of nitro functional groups during the reaction. Although it may be beneficial to return to the utilization of acyl chlorides for NC modification, this work thus lead us to investigate the use of isocyanates. We Demonstrated in this chapter this is where we discovered the effectiveness of the 3-(triethoxysilylpropyl) functionality, which we demonstrated could provide an increase of hydroxyl sites via siloxane crosslinking of 3-(triethoxysilylpropyl) to form the propyl carbamate primer layer.

We described the covalent surface functionalization of nitrocellulose (NC) focusing on the preparation of the NC materials with “tunable” surface properties, specifically with controlled wetting with energetic plasticizer nitroglycerin (NG). We found that even highly nitrated NC (12.47%N) contained sufficient amount of free hydroxyl groups that could be effectively modified leading to various functionalized NC derivatives. The most effective method involved the activation of NC by the reaction with bifunctional reagent 3(triethoxysilylpropyl) isocyanate. In Chapter 3, we discuss how FTIR and chemical analysis, demonstrates the isocyanate groups bound to the OH groups of NC via carbamate linkage, while triethoxysilyl moieties (after hydrolysis) produced cross-linked siloxane-silanol surfaces, in a similar fashion reported for conventional cellulose substrates.<sup>59, 60</sup> The silanol-grafted NC was subsequently reacted with various organosilanes of general formula  $R_3SiX$ ,  $R_2SiX_2$ , and  $RSiX_3$  ( $R$ =alkyl-, phenyl-, fluoroalkyl-;  $X$ =Cl) and  $Si(CH_3O)_4$  producing a series of surface-functionalized NC materials without degradation of its nitro groups. Also in Chapter 3, based on results from SEM and DSC, there was no significant change neither in fiber morphology nor in thermal decomposition profiles of the modified NCs as compared to

bare NC suggesting that the bulk properties of NC were not affected and that the reactions largely involved surface functionalities.



## **Chapter 3: Characterization of Nitrocellulose Reactions**

### **3.1 Abstract**

In Chapter 2 we demonstrated multiple chemical functionalization approaches aimed at the preparation of interfaces on NC to control wetting and to inhibit leaking of NG. In Chapter 3, we discuss chemical characterization approaches to confirm successful chemical reactions with NC and organosilanes. Percent atomic analyses show presence of elemental fluorine and silicon on chemically modified fibers and confirms the presence nitro groups as a comparison for post reacted NC to bare NC. Gel permeation chromatography was used to confirm nitrocellulose dissolution and polymer chain degradation of nitrocellulose. FTIR results show evidence of carbonyl functionality and silanol/siloxane build up on the functionalized NC surfaces. Differential Scanning Calorimetry (DSC) compares onset and decomposition temperature of bare and treated NC. Scanning electron microscopy (SEM) demonstrates the fibrous surface morphology of NC. X-ray photo electron spectroscopy (XPS) results demonstrate uniformed thickness of perfluoro alkyl and polydimethylsiloxane (PDMS) in which completely attenuates nitrogen on the NC and silyl propyl carbamate functionalized surfaces. Detection of carbonyl carbon at 289 eV confirms the presence of carbamate on the surface of NC reacted with of 3-(triethoxysilylpropyl) isocyanate. Deconvoluted C 1s spectra resulted in peaks at 291 and 293 eV representing presence of CF<sub>2</sub> and CF<sub>3</sub> on the surface of fluor-alkyl treated NC.

### **3.2 Introduction**

In this Chapter we utilized a variety of methods to characterize the surface functionalization of military grade nitrocellulose (NC). Here, we report a rigorous set of

characterization parameters to confirm surface modification and thermal stability. DSC analysis is used to evaluate the onset and peak decomposition temperatures of treat NC surfaces compared to bare NC. Elemental analysis was used to indicate the attachment of silyl propyl groups to NC and provide evidence of silanol/siloxane build up. Percent nitrogen analysis was used to monitor the thermal stability of conditioned modified NC in the presence of surface NG. FTIR was used to monitor reaction conditions, providing spectra in accordance with functional group formation. SEM was used to observe changes in fiber morphology of bare and treated NC.

Contact angle measurements of H<sub>2</sub>O on the surface of treated surfaces

In this chapter, we report the atomic percentage and binding energies of the treated NC surfaces determined by X-ray photo electron spectroscopy (XPS). As a surface-sensitive technique, the XPS presented information about the composition and the chemical state of the elements in the top 3-10 nm layer of the material.<sup>125, 126</sup> XPS utilizes a monoenergetic beam of soft X-rays to measure binding energies of electrons ejected by the ionizations of atoms on a solid surface of Angstrom level depth depending on the element. Here, we report a rigorous set of characterization parameters to confirm surface modification.

### **3.2.1 General Information**

The number and weight average molecular weights ( $M_n$  and  $M_w$  respectively) were determined by Gel Permeation Chromatography (GPC) at 30°C with a Viscotek TDA model 300 Triple Decker array, GPC MAX VE 2001 solvent/samples module, calibrated with PolyCal UCS-PS polystyrene standards. Column used was a linear 300 x 7.8 mm 10  $\mu$ m Phenomenex Phenogel. Onset and decomposition temperatures were recorded using

differential scanning calorimetry (DSC) Perkin Elmer DSC4000 at a rate of 5°/minute up to 400°C under nitrogen flow at 40ml/min. DSC samples were prepared in Perkin Elmer aluminum DSC pans. Scanning electron microscopy images were generated using a JOEL 5600 SEM. NC fibers (bare and modified) were sputter coated using a Denton Vacuum II sputter coater with a gold/palladium coating as to reduce charging in the SEM. Elemental analysis of C,H,N was determined by a Perkin Elmer Model 2400 CHN analyzer under a helium carrier gas at an operating temperature of 950°C. A Cahn electro balance was used to weigh samples into tin sample capsules which were 6 x 4 mm in size. Calibration standard used was a 141d acetanilide standard. Elemental fluorine was determined by a fluorine ion specific electrode, F-ISE, Orion. Elemental analysis for Si was determined by using inductively coupled plasma optical emission spectroscopy (ICP-OES).

The X-ray photoelectron spectra were recorded at the Surface Analysis Laboratory, Polymer Science and Engineering Department, University of Massachusetts-Amherst (courtesy of Director J. Hirsh and Prof. T.J. McCarthy) with a Physical Electronics Quantum 2000, Scanning ESCA Microprobe using Al monochromatic X-Rays. Spectra were obtained at 45° take off angle with the spot size ~200  $\mu m$ . The spectra were analyzed using the MultiPak software.<sup>124</sup> Unless specified otherwise, spectra were collected in duplicates and the results on the reported atomic compositions were average of two runs.

### **3.3 Gel Permeation Characterization (GPC) of Nitrocellulose**

In this section, we discuss using a size exclusion (GPC) method to monitor the stability of the NC polymer chain before and after exposure to reaction conditions. We discuss NC surface modification by hydroxyl group esterification using perfluorinated acyl

chlorides and isocyanates.<sup>42,43,44</sup> Procedures obtained from the literature described successful surface functionalization of ethyl cellulose.<sup>43</sup>

Gel permeation chromatography (GPC) is a size exclusion technique used to study the molar mass distribution (Mw), and the number-average molar mass distribution (Mn) of NC. Historically, it has been the standard method for estimating the molecular weight and polydispersity of nitrocellulose samples. However, there are issues using this method related to a standard method of calibration of the GPC equilibrium curve and adequate detector selection.<sup>9</sup> Narrow molecular weight range of polystyrene standards are used to calibrate the elution volume of the GPC instrument. The separation is based on hydrodynamic volume and not molecular weight. A problem arises because a molecule of nitrocellulose that has the same elution volume as a molecule of polystyrene may have a different molecular weight.<sup>9, 69, 70</sup> Therefore, proper correction must be used or an error in absolute molecular weight measurement occurs.<sup>9, 69, 70</sup> We found with the instrumentation used for our studies, the most common problem was solvation of NC by tetrahydrofuran (THF). Previous experiments suggests that NC contains a high stiffness structure.<sup>9</sup> The stiffness of the NC polymer causes observed changes in Mw values with dissolution time of nitrocellulose in THF. Previous work explains that it can take up to seven days for an NC solution in THF to obtain stable molecular weight results. NC with higher percent nitrogen content needs less time to achieve complete dissolution.<sup>9, 70</sup> With this in mind monitored the dissolution time of NC in THF in order to help us capture a consistent molecular weight distribution so we would have a tool to compare molecular weight distributions of bare NC with treated NC.

In the early stages of our work, we found it necessary to optimize size exclusion (GPC) methods to characterize our work, as molecular weight of NC relates to providing a

sufficient method to confirm polymer chain stability. We needed to be able to identify a baseline molecular weight distribution for our lots of bare NC. Establishing a reproducible Mn & Mw was essential so we could compare molecular weight changes with functionalized NC. We hoped that GPC could provide reproducible data points that relate to NC polymer chain stability. Our initial experiments were performed to identify the solubility of NC in tetrahydrofuran (THF). THF is known to be a suitable solvent for NC dissolution.<sup>9</sup> We performed experiments with GPC to identify the optimal stir times in THF for NC used in this study. Stir times ranged from 8 hours to 1 week. GPC data showed a stabilized molecular weight distribution of 13.15% nitrated NC at 48 hours of stirring (Table 3-1). We observed after 48 hours the Mn and Mw would fluctuate between ~72-79 kDa and ~862-892 kDa respectively. Each stir time value is based on an average of ten runs. As will be seen in the following sections, the values for reactions that result in polymer chain degradation are quite evident, and are backed up by complementary methodology that indicate instability.

**Table 3- 1:** Molecular Weight Distribution (in thousands) for Timed Stirring of Nitrocellulose in THF.

Stir time	M <sub>n</sub> (kDa)	M <sub>w</sub> (kDa)
8 hours	53	470
24 hours	56	592
36 hours	67	692
48 hours	79	880
3 days	78	862
4 days	76	881
5 days	72	892
6 days	79	878
1 week	77	879

### 3.4 Characterization of Acyl Chlorides and Isocyanate Modified NC

GPC analysis was performed to determine NC polymer chain stability after reaction condition exposure. Bare and reacted NC were compared for changes in molecular weight

distribution. Results in Table 3-2 shows an increase in Mn for pentadecafluorooctanoyl and pentafluorobenzoyl acyl chlorides and a decrease in Mn for nonafluoropentanoyl and 3,3,3-trifluoropropionyl acyl chlorides compared to bare nitrocellulose. Mw decreases for all selected acyl chloride reactions with NC compared to bare nitrocellulose. The low Mw results compared to bare NC is most likely a result of potential degradation of the larger polymer chain during the reaction. GPC analyses was also performed on NC treated with NCO. Mw and Mn for NC treated with pentafluorophenyl and 3-triethoxysilyl propyl NCO was compared to bare NC. Results in Table 3-2 shows an increase in both the number average molecular weight Mn and the weight average molecular weight Mw for both the surface modified 13.15 % and 11.04% NC. The increase of molecular weight distribution for the isocyanate treated NC suggest a presence of surface functionalization, and maintained stability of the polymer chain.

**Table 3- 2:** Gel Permeation Chromatography (GPC)

Data for Bare and Treated Nitrocellulose (in thousands).

GCP samples	Mn (kDa)	Mw (kDa)
<b>Perfluorinated acyl Chlorides</b>		
pentadecafluorooctanoyl	92	396
nonafluoropentanoyl	29	176
pentafluorobenzoyl	76	340
3,3,3-trifluoropropionyl	48	372
<b>Isocyanates</b>		
11.04% NC Pentafluorophenyl	76	995
13.15% NC Pentafluorophenyl	92	980
11.04 % 3-triethoxysilyl propyl	94	916
13.15 % 3-triethoxysilyl propyl	96	979
<b>Bare NC reference 13.15/11.06%</b>	<b>64/58</b>	<b>586/502</b>

To determine if nitro groups remained intact during the reaction and if fluorine was present, the treated NC was analyzed to obtain percent elemental analysis for nitrogen and

fluorine. Results in Table 3-3 show percent nitrogen decreased for the listed acyl chloride modified NC reactions. The decrease in percent nitrogen provided conformation of polymer chain instability, in line with the data obtained from the GPC results, suggesting degradation due to reaction conditions. Pentadecafluorooctanoyl, nonafluoropentanoyl, and pentafluorobenzoyl acyl chloride modified NC show a degree of fluorination, whereas 3, 3, 3-trifluoropropionyl acyl chloride modified NC was absent of fluorine.

Fluorine was present (~4 % and ~3 %) for 11.04% and 13.15% pentafluorophenyl isocyanate functionalized NC respectively. The slightly higher amount of fluorine for the 11.04% nitrated cellulose may suggest increased availability of hydroxyl groups. Elemental Si analysis for 3-triethoxysilyl propyl isocyanate functionalized NC resulted in 1.22% for the reaction with 11.04% NC and 0.43% for the 13.15% NC reaction, indicating again that the 11.04% NC may have more reaction sites due to the higher percentage of Si.

**Table 3- 3:** Elemental Analysis Data for Nitrocellulose Functionalized with Acylchlorides and Isocyanates.

Sample	Elemental analysis	Elemental analysis	Elemental analysis
<b>NC/fluorinated acyl chlorides</b>	~ % Fluorine	% Nitrogen	% Silicon
13.15% 3,3,3 Trifluoropropionyl	0	9.69	Not applicable
13.15 % Pentadecafluorooctanoyl	3	10.98	Not applicable
13.15% Pentafluorobenzoyl	2	7.79	Not applicable
13.15% Nonafluoropentanoyl	2	12.13	Not applicable
<b>NC/pentafluorophenyl NCO</b>			
11.04 % Pentafluorophenyl NCO	4	11.56	Not applicable
13.15 % Pentafluorophenyl NCO	3	12.25	Not applicable
11.04 % 3-triethoxysilyl propyl NCO	Not applicable	12.51	1.22
13.15 % 3-triethoxysilyl propyl NCO	Not applicable	12.58	0.43-0.82
Neat NC 13.15%	Not applicable	12.47	Not applicable

\*From triple repeat analysis, the standard errors were estimated to be <0.15% for C,H,N,Si and <0.5% for F.

Differential Scanning Calorimetry (DSC) was used to compare peak decomposition temperatures of the fluorinated acyl chloride modified NC with baseline NC. Nitrocellulose is known to have peak temperature at ~200°C when analyzed on DSC instrumentation at 5°C per minute.<sup>83</sup> Table 3-4 shows that 3, 3, 3-trifluoropropionyl modified NC decomposition temperature is over a 20°C decrease in temperature than that of bare NC again suggesting instability caused by reaction conditions. The decomposition temperatures of the remaining perfluoroacyl chloride functionalized NC are consistent with bare NC. The peak height and therefore enthalpy, however, decrease for all of the acyl chloride treated NC. DSC thermal scans located in Appendix B show reduction in decomposition peak heights for 3,3,3,-trifluoropentanoyl and nonafluoropentanoyl acyl chloride modified NC compared to the distinct peak decomposition of bare NC. The peak height/enthalpy and decomposition temperature of pentafluorophenyl and 3-triethoxysilyl propyl NCO isocyanate modified NC are consistent with bare NC at 5°/minute.

**Table 3- 4:** DSC Decomposition Temperatures for Nitrocellulose Reacted with Acylchlorides and Isocyanates.

<b>DSC samples</b>	<b>Decomposition temperature °C</b>
<b>NC/fluorinated acyl chlorides</b>	
3,3,3 Trifluoropropionyl	168.01
Pentadecafluorooctanoyl	195.58
Pentafluorobenzoyl	194.73
Nonafluoropentanoyl	200.48
<b>NC/pentafluorophenyl NCO</b>	
11.04 % Pentafluorophenyl NCO	206.35
13.15 % Pentafluorophenyl NCO	207.29
11.04 % 3-triethoxysilyl propyl NCO	198.56
13.15 % 3-triethoxysilyl propyl NCO	198.52
<b>Bare NC 13.15%</b>	<b>201.66</b>

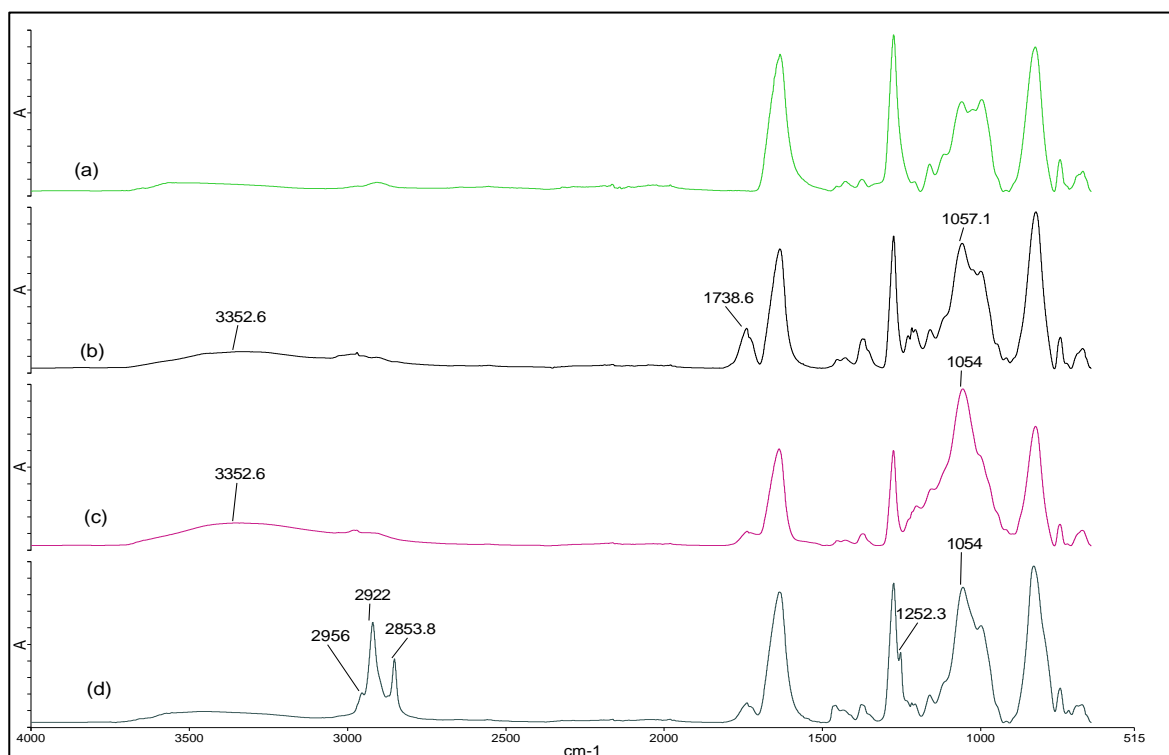


### 3.5 Characterizing the Reaction of Nitrocellulose Isocyanate and Organosilanes

Analysis by FTIR was performed using a Perkin Elmer Spectrum 100 spectrometer. FTIR samples were prepared by weighing out 1 milligram of NC materials to 200 milligrams of potassium bromide to form pellets or by using solid state ATR. FTIR samples were pressed using a Perkin Elmer 13mm IR die under a Carver Laboratory Press at 8 metric tons pressure and held for 1 minute to ensure adequate pellet formation.

The progress of the reactions was monitored by FTIR. Figures 3-1 presents an overlay of representative FTIR spectra illustrating changes in the absorption bands for a sequential functionalization of NC with organosilanes. Spectra of neat NC (Figure 3-1a) showed three strong bands at  $\sim 1665\text{ cm}^{-1}$ ,  $\sim 1275\text{ cm}^{-1}$ , and  $\sim 826\text{ cm}^{-1}$ , which represented O-NO<sub>2</sub> asymmetric, symmetric stretching, and N-O stretching respectively.<sup>65-68</sup> These bands were also present in all the spectra of modified NC, indicating the preservation of nitro-groups of NC in the reactions. Figure 3-1b shows the spectra of NC that reacted with triethoxysilylpropyl isocyanate. It showed a new band at  $\sim 1738\text{ cm}^{-1}$ , which was attributed to carbonyl stretching, supporting the formation of carbamate species due to reaction between isocyanate and hydroxyl groups of NC. The broad band centered  $\sim 3350\text{ cm}^{-1}$  was attributed to hydrogen-bonded silanol groups<sup>66-68</sup> obtained after hydrolysis of triethoxysilane moieties. Certain portion of these silanols condensed yielding siloxanes as evidenced by the increased band at  $\sim 1057\text{ cm}^{-1}$  (Si-O stretching).<sup>79</sup> The reaction of this sample with tetramethoxysilane (in presence of water to promote hydrolysis and condensation) demonstrated growth of bands at  $3350\text{ cm}^{-1}$  (O-H) and  $\sim 1054\text{ cm}^{-1}$  (Si-O) evidencing a buildup of the silanol-siloxane network grafted to NC (Figures 3-1c & 3-2). This silanol-grafted NC could be further

functionalized with organosilanes. As an example, Figure 3-1d demonstrates the spectra of the silanol-grafted NC that was subsequently reacted with *n*-octadecyldimethylchlorosilane. The decrease of the band at  $\sim 3350\text{ cm}^{-1}$  was attributed to the consumption of silanols due to their coupling with chlorosilanes. The new bands at  $\sim 2922$ ,  $\sim 2853\text{ cm}^{-1}$  and  $\sim 1252\text{ cm}^{-1}$  attributed to  $\text{CH}_2$  and  $\text{Si-CH}_3$  stretching respectively,<sup>67</sup> representing attachment of octadecyldimethylsilyl groups to the NC.

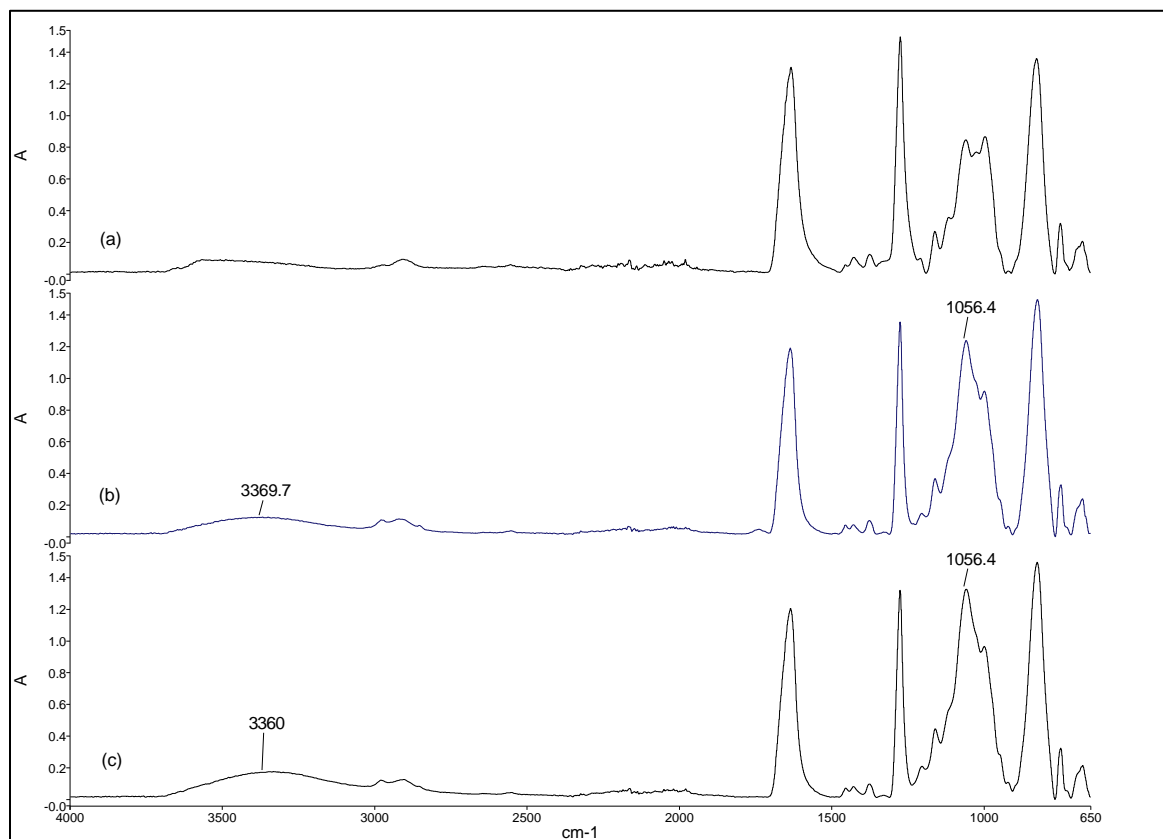


**Figure 3- 1: FTIR spectra**

(a) nitrocellulose, (b) NC reacted with silyl isocyanate, (c) nitrocellulose reacted with silyl isocyanate and exposed to TMOS vapor. (d) nitrocellulose + silyl isocyanate + TMOS reacted with *n*-octadecyldimethylchlorosilane.

Chemical analysis data supported the findings from FTIR and provided quantitative information about the extent of substitution in the cellulose chain (Table 3-5). Bare NC showed 12.47% N, from which the degree of nitration<sup>9</sup> was determined to be 2.4. Thus, on

average 2.4 out of 3 hydroxyl groups per cellulose repeat unit were substituted with nitro groups and 0.6 hydroxyls (~20%) remained free.



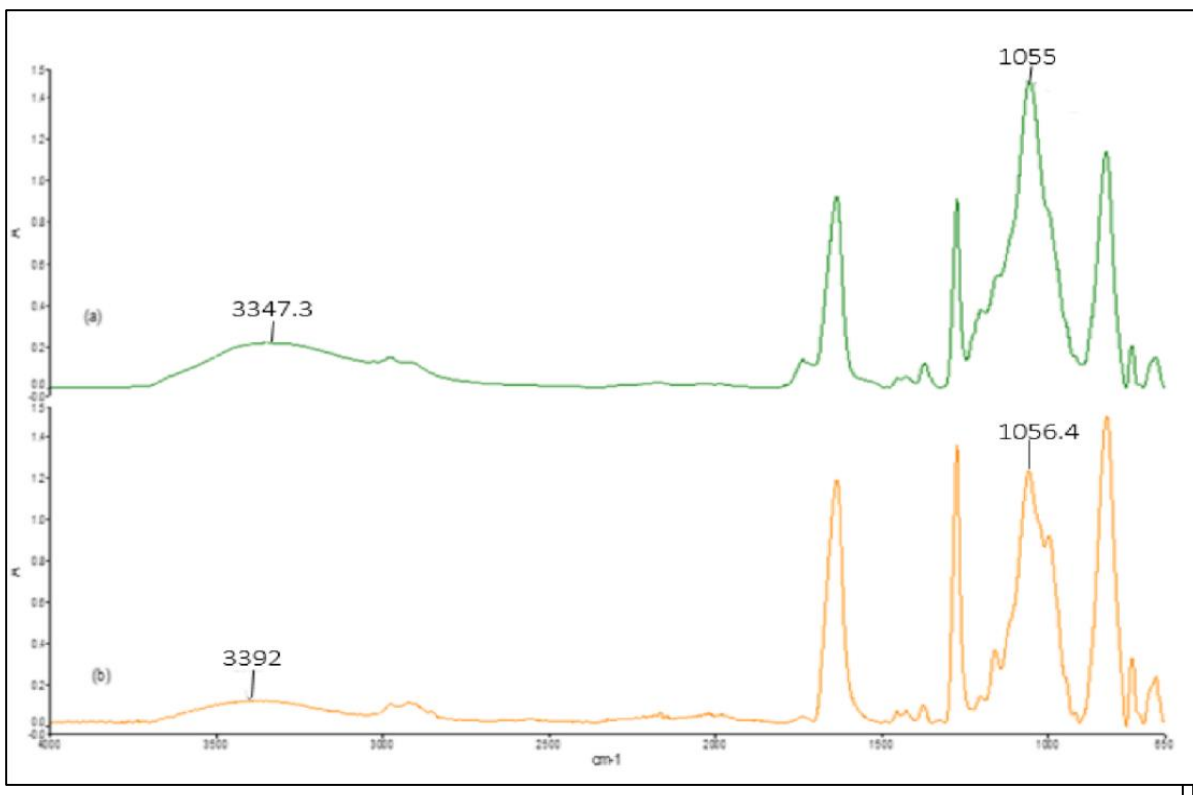
**Figure 3- 2: FTIR spectra**

(a) Nitrocellulose (b) Nitrocellulose reacted with tetramethoxysilane in THF, and (c) Nitrocellulose reacted with tetramethoxysilane vapor.

The chemical formula of this compound was  $[C_6H_7O_2(OH)_{0.6}(ONO_2)_{2.4}]_n$ . For the NC reacted with triethoxysilylpropyl isocyanate, the presence of 0.82% Si along with small increase in % C as compared to bare NC indicated attachment of trisilanol propyl groups to NC. From the silicon content in this compound, we estimated that ~one out of six OH groups of NC reacted with triethoxysilylpropyl isocyanate. Assuming uniform distribution, this corresponded to ~one trisilanol-propyl group per 10 repeat units of NC. The reactions of this silanol-modified

NC with mono-, di-, tri and tetra-functional organosilanes showed further increase in %Si and %F (when present) indicating attachment of organosilane groups to the NC. This was illustrated by the reactions of n-octadecyldimethyl chlorosilane, dimethyldichloro silane, 1,1,2,2-tetrahydro- perfluorooctyl trimethoxysilane, phenyl trichlorosilane, and tetramethoxy silane (Table 3-5, lines 3- 8). The reaction with tetramethoxy silane produced samples with significant Si content (>10%) indicating a build-up of silica-like surfaces grafted to NC. High Si content was also observed for the reaction with dimethyl dichlorosilane in presence of moisture, the conditions known to facilitate polycondensation and formation of poly(dimethylsiloxanes) grafted to the hydroxyl surfaces.<sup>94, 95</sup> Table 3-5 also includes the data for the direct reaction of TMOS with NC (two bottom lines). The presence of 0.48% of Si suggested the attachment of TMOS directly to OH groups of NC. Although these samples could be further functionalized with organosilanes in a similar way to the reactions of silyl-propyl NC (Table 3-5) this approach was fundamentally inferior to the one involving triethoxysilylpropyl isocyanate. In the direct reaction of alkoxysilanes with cellulose, the organic groups were attached to NC via Si-O-C linkages that are prone to hydrolysis. So these coatings were inherently unstable upon exposure to moisture. Also, we noted that the amount of silanes grafted in the direct reaction with NC was greatly reduced as compared to the reactions using triethoxysilylpropyl isocyanate. This was evidenced by lower Si content (Table 3-5) and by weaker silanol band  $\sim 3350\text{ cm}^{-1}$  (H-bonded OH stretching) in the FTIR spectra Demonstrated in Figures 3-2 and 3-3. This emphasized the key role of the initial activation reaction of NC with triethoxysilylpropyl isocyanate. The latter bonded to NC through the set of robust chemical bonds yielding silanol-rich surface thereby providing basis for the subsequent functionalization of NC with various organosilanes. Crude kinetics of the

water vapor adsorption was performed at room temperature and 100% RH for bare and modified NC materials.



**Figure 3- 3: FTIR spectra**

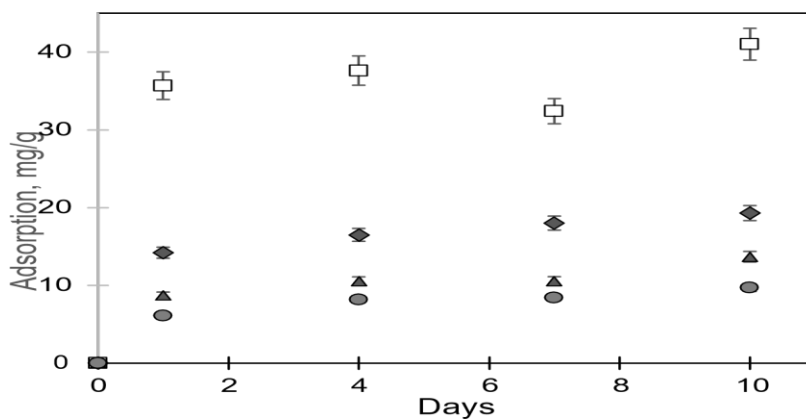
(a) silyl-propyl nitrocellulose reacted with tetramethoxysilane and (b) bare nitrocellulose reacted with tetramethoxysilane.

The moisture adsorption experiments provided further insight in the surface properties of the modified NC materials. The rate of adsorption (Figure 3-4) was also lower than for bare NC: for hydrophobized NCs, only ~60-70% from the maximum was adsorbed within the first 24 h and the adsorption kept growing even after seven days of contact. In terms of the maximal amount of water adsorbed after 10 days of contact, the NC materials ranged as follows: bare NC >> poly(dimethylsiloxane)-NC > fluoroalkyl-NC  $\geq$  alkyl-NC. More detailed studies of adsorption is explained in Chapter 5.

**Table 3- 5:** Chemical Analysis Data for Bare and Treated Nitrocellulose.

Sample	% C	% H	% N	% F	% Si
Bare NC	25.19	2.54	12.47	<0.5	<0.1
NC + (C <sub>2</sub> H <sub>5</sub> O) <sub>3</sub> Si(CH <sub>2</sub> ) <sub>3</sub> NCO	32.21	3.02	12.58	-	0.82
NC + (C <sub>2</sub> H <sub>5</sub> O) <sub>3</sub> Si(CH <sub>2</sub> ) <sub>3</sub> NCO + (CH <sub>3</sub> O) <sub>3</sub> Si(CH <sub>2</sub> ) <sub>2</sub> C <sub>6</sub> F <sub>13</sub>	25.87	2.16	12.70	26.2	1.15
NC + (C <sub>2</sub> H <sub>5</sub> O) <sub>3</sub> Si(CH <sub>2</sub> ) <sub>3</sub> NCO + Cl <sub>3</sub> SiC <sub>6</sub> H <sub>5</sub>	31.17	2.42	12.57	-	1.90
NC + (C <sub>2</sub> H <sub>5</sub> O) <sub>3</sub> Si(CH <sub>2</sub> ) <sub>3</sub> NCO + ClSi(CH <sub>3</sub> ) <sub>2</sub> C <sub>18</sub> H <sub>37</sub>	36.90	5.07	12.63	-	3.05
NC + (C <sub>2</sub> H <sub>5</sub> O) <sub>3</sub> Si(CH <sub>2</sub> ) <sub>3</sub> NCO + Cl <sub>2</sub> Si(CH <sub>3</sub> ) <sub>2</sub>	27.35	4.30	12.18	-	9.88
NC + (C <sub>2</sub> H <sub>5</sub> O) <sub>3</sub> Si(CH <sub>2</sub> ) <sub>3</sub> NCO + (CH <sub>3</sub> O) <sub>4</sub> Si	31.35	4.20	12.32	-	10.30
NC + (C <sub>2</sub> H <sub>5</sub> O) <sub>3</sub> Si(CH <sub>2</sub> ) <sub>3</sub> NCO + (CH <sub>3</sub> O) <sub>4</sub> Si + ClSi(CH <sub>3</sub> ) <sub>2</sub> C <sub>18</sub> H <sub>37</sub>	33.62	4.82	12.52	-	10.70
NC + (CH <sub>3</sub> O) <sub>4</sub> Si	32.73	3.04	12.42	-	0.48
NC + (CH <sub>3</sub> O) <sub>4</sub> Si + (CH <sub>3</sub> O) <sub>3</sub> Si(CH <sub>2</sub> ) <sub>2</sub> C <sub>6</sub> F <sub>13</sub>	38.92	4.26	12.5	10.3	0.68

\*From triple repeat analysis, the standard errors were estimated to be <0.15% for C,H,N,Si and <0.5% for F.

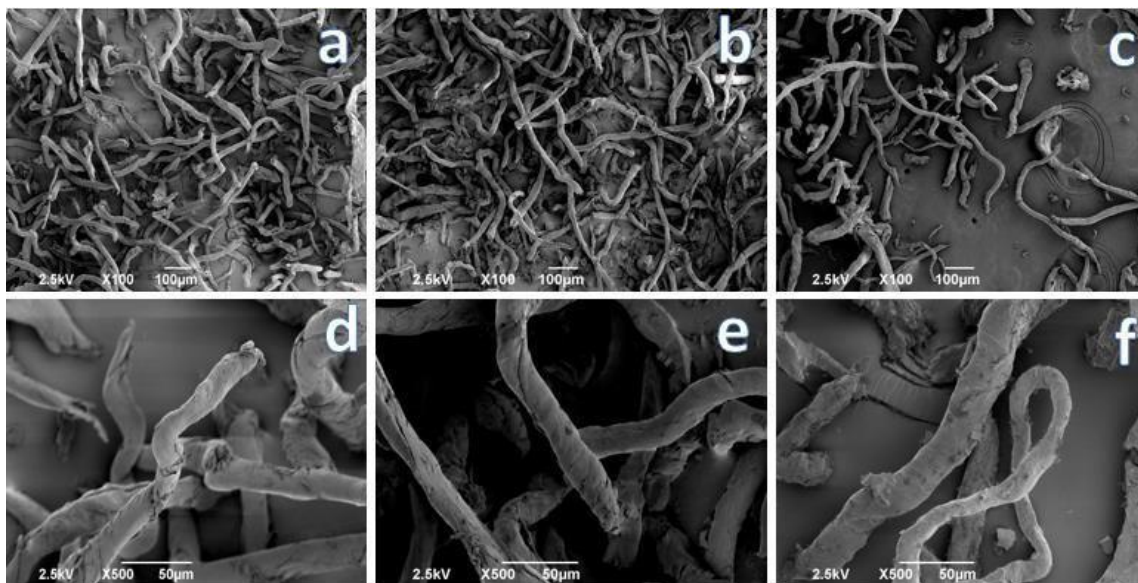
**Figure 3- 4:** Kinetics of water adsorption (RH 100%, 298K) on NC powder:

(□) bare NC, (▲) C<sub>6</sub>F<sub>13</sub>-NC, (●) C<sub>18</sub>H<sub>37</sub>-NC, (◆) -[(CH<sub>3</sub>)<sub>2</sub>SiO]<sub>n</sub>-NC.

When error bar is nonvisible, standard error is less than the symbol size.

### 3.6 SEM and DSC of Functionalized Nitrocellulose.

The possible effects of surface functionalization on the bulk properties of NC were evaluated by scanning electron microscopy (SEM) and differential scanning calorimetry (DSC). Morphologies of bare and modified NC were observed by SEM. Representative SEM images of bare NC and NC treated with organosilanes at magnitudes of 100X and 500X are compared in Figure 3-5. SEM image of bare NC showed twisted individual fibers of ~10-30  $\mu\text{m}$  wide with somewhat rough surfaces. SEMs of treated NC showed somewhat increased surface roughness notable at a magnification of 500X (Figure 3-5f), which was attributed to the deposition of organosilicon coatings. Overall, the images of bare and treated NC showed similar fibrous structure and porosity.

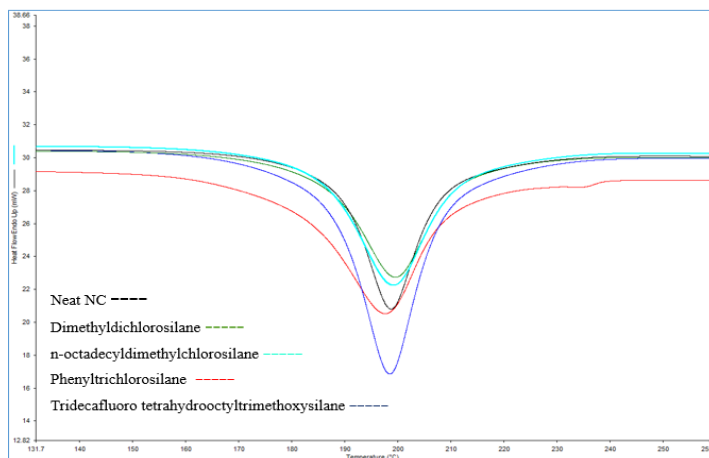


**Figure: 3-5: Representative SEM images of NC materials.**

(a) and (d) bare NC, (b) and (e) NC reacted with tetramethoxysilane, (c) and (f) NC reacted with tetramethoxysilane followed by the reaction with octadecyldimethyl chlorosilane.

Magnification: 100X (Top row) and 500X (Bottom row).

DSC was used to evaluate the effect of chemical functionalization on the thermal decomposition and thermal stability of the NC materials. The onset and peak temperatures for bare and silane modified NCs were compared to confirm the equivalence of their energetic properties. Representative DSC curves of bare and modified NCs are shown in Figure 3-6. Table 3-6 gives a comparison of their decomposition temperatures. For both bare and modified NC the DSC graphs showed a broad exothermic peak attributed to deflagration of the materials. The onset and the peak temperatures of bare NC were  $187.3\pm0.5$  and  $198.5\pm0.5^\circ\text{C}$  respectively, which was in close agreement with the data reported previously.<sup>83</sup> For the modified NCs, the onset and the peak temperatures showed only minor variation with the type of the silane and for all the samples studied averaged at  $186.8\pm1.5$  and  $198.3\pm1.0^\circ\text{C}$  respectively which was essentially indistinguishable from bare NC. To conclude this section, the morphology and the DSC peaks and temperatures of the modified NC were very close to those of the bare NC demonstrating that the reactions with silanes did not affect the bulk properties of the material



**Figure 3-6:** DSC thermograms of unmodified and modified nitrocellulose decomposition.

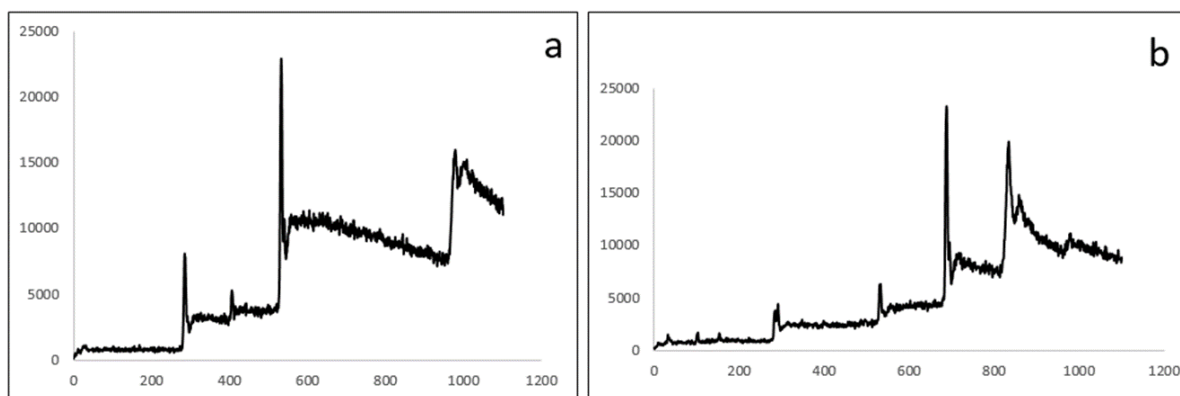


**Table 3- 6:** Onset and Peak Decomposition Temperatures of Bare and Modified Nitrocellulose.

Sample	Onset, °C	Peak, °C
Bare NC	187.3	198.5
NC + (C <sub>2</sub> H <sub>5</sub> O) <sub>3</sub> Si(CH <sub>2</sub> ) <sub>3</sub> NCO	185.3	197.5
NC + (C <sub>2</sub> H <sub>5</sub> O) <sub>3</sub> Si(CH <sub>2</sub> ) <sub>3</sub> NCO + (CH <sub>3</sub> O) <sub>3</sub> Si(CH <sub>2</sub> ) <sub>2</sub> C <sub>6</sub> F <sub>13</sub>	185.8	199.5
NC + (C <sub>2</sub> H <sub>5</sub> O) <sub>3</sub> Si(CH <sub>2</sub> ) <sub>3</sub> NCO + ClSi(CH <sub>3</sub> ) <sub>2</sub> C <sub>18</sub> H <sub>37</sub>	185.1	199.2
NC + (C <sub>2</sub> H <sub>5</sub> O) <sub>3</sub> Si(CH <sub>2</sub> ) <sub>3</sub> NCO + Cl <sub>2</sub> Si(CH <sub>3</sub> ) <sub>2</sub>	188.3	198.8
NC + (C <sub>2</sub> H <sub>5</sub> O) <sub>3</sub> Si(CH <sub>2</sub> ) <sub>3</sub> NCO + Cl <sub>3</sub> SiC <sub>6</sub> H <sub>5</sub>	187.4	195.9
NC + (C <sub>2</sub> H <sub>5</sub> O) <sub>3</sub> Si(CH <sub>2</sub> ) <sub>3</sub> NCO + (CH <sub>3</sub> O) <sub>4</sub> Si	185.6	199.0
NC + (C <sub>2</sub> H <sub>5</sub> O) <sub>3</sub> Si(CH <sub>2</sub> ) <sub>3</sub> NCO + (CH <sub>3</sub> O) <sub>4</sub> Si + ClSi(CH <sub>3</sub> ) <sub>2</sub> C <sub>18</sub> H <sub>37</sub>	188.3	198.2
NC + (CH <sub>3</sub> O) <sub>4</sub> Si	187.5	198.3
NC + (CH <sub>3</sub> O) <sub>4</sub> Si + (CH <sub>3</sub> O) <sub>3</sub> Si(CH <sub>2</sub> ) <sub>2</sub> C <sub>6</sub> F <sub>13</sub>	185.7	198.0
NC + (CH <sub>3</sub> O) <sub>4</sub> Si + Cl <sub>2</sub> Si(CH <sub>3</sub> ) <sub>2</sub>	189.3	198.2
NC + (CH <sub>3</sub> O) <sub>4</sub> Si + ClSi(CH <sub>3</sub> ) <sub>2</sub> C <sub>18</sub> H <sub>37</sub>	188.2	199.0

### 3.7 X-Ray Photoelectron Spectroscopy (XPS)

Chemical composition of the NC materials were analyzed by XPS. As a surface-sensitive technique, the XPS presented information about the composition and the chemical state of the elements in the top 3-10 nm layer of the material.<sup>122, 123</sup> The survey spectra (Figure 3-7) were used to identify the main elements present on the surfaces, while high-resolution spectra of bare NC is shown in Figure 3-9. The spectrum revealed the main peaks that were identified as C1s (290 eV), N1S (~400 eV), and O1s (~530 eV) and KLL Auger group (~1000 eV) respectively.<sup>122-125</sup> The multiplex scans for the elements are shown in Figure 3-9. For C1s, three components were identified from the deconvolution that were labeled C<sub>1</sub>, C<sub>2</sub>, C<sub>3</sub> As shown in Figure 3-8.

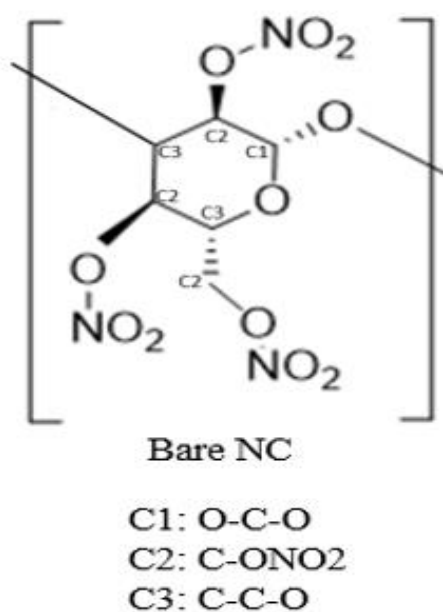


**Figure 3- 7: XPS Survey Spectra**

(a) Bare nitrocellulose and (b) Bare nitrocellulose treated with  $C_6F_{13}$ .

These peaks were attributed to different chemical states of the carbon atoms in nitrocellulose. The main component  $C_2$  (~58% from the peak area) at 286.4 eV was attributed to carbon atoms bound to nitrate groups.  $C_3$  (28%) at 284.2 eV and  $C_1$  (14%) at 287.9 eV were attributed to C-C and C-O respectively. The ratio of peak areas  $C_2$ :  $C_3$ :  $C_1$  observed was in reasonable agreement with the ratio 3:2:1 predicted from the structure of the repeat unit. The  $N1s$  and  $O1s$  spectra (Figure 3-7) showed single main features at 407.2 eV attributed to nitrogen in nitro-groups<sup>124</sup> and at 532.8 eV for oxygen, which was consistent with oxygen in organic compounds and nitrates.<sup>123-125</sup>

The average atomic composition of bare NC surfaces was obtained from the multiplex spectra as an average of three measurements of different NC samples. The result was  $47.2 \pm 0.7$  (C),  $45.8 \pm 0.7$  (O), and  $6.8 \pm 0.5$  atomic % (N) respectfully. From the chemical analysis data reported in our previous work<sup>102</sup>, the bulk composition of the NC was determined as follows:  $33.0 \pm 0.15$  (C),  $54.2 \pm 0.15$  (O), and  $13.3 \pm 0.15$  atomic % (N). The bulk composition was notably different from the surface composition by XPS.



**Figure 3- 8:** Chemical states of carbon atoms in nitrocellulose determined by XPS.  
(Chem Draw version 19.1)

As compared to the bulk, the surface of NC was enriched with carbon and depleted with oxygen and nitrogen. Here we offer two possible explanations for the difference observed between bulk and surface composition. First, this could be due to the physisorbed adventitious carbon contaminants that attenuated peaks from other elements. Also, it was conceivable that the surface was depleted in nitrogen compared to the bulk due to more facile degradation of the exposed nitrate groups.

Bulk chemical analysis of bare NC showed 12.47% N, from which the degree of nitration<sup>4,9</sup> was determined to be 2.4. Thus, on average 2.4 out of 3 hydroxyl groups per cellulose repeat unit were substituted with nitrates while 0.6 hydroxyls (~20%) remained free. In the previous work<sup>101</sup>, we described the use triethoxysilylpropyl isocyanate to bind to these OH groups via carbamate linkage. The triethoxysilyl moieties (after hydrolysis and

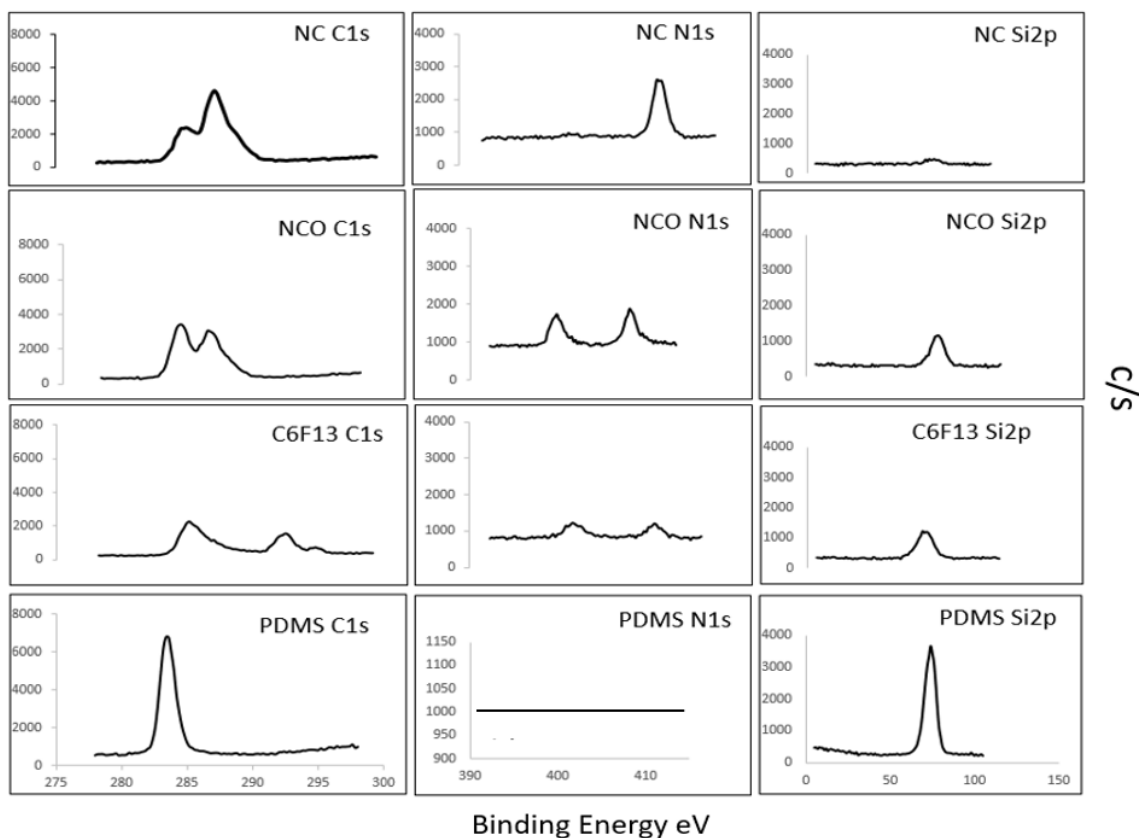
cross-linking) produced the NC supported silanol-rich surface that could be further functionalized using the silane coupling chemistry.<sup>101</sup> In this work, we used XPS to investigate these reactions and to characterize the surface grafted layers of organosilanes supported on the NC.

XPS survey spectra for bare NC and NC reacted with organosilanes is presented in Figure 3-9. The attachment of silanes to NC was evident by the appearance of two new peaks ~100 and ~150 eV for Si2p and Si2s and (when F was present in organosilane) by a strong peak ~680 eV for F1s accompanied with F KLL Auger peaks ~830-860 eV. The atomic compositions of the silane treated NCs are shown in Table 3-7. Besides the changes in the atomic surface composition, chemical binding of organosilanes to NC was evident from the changes of the chemical states of carbon and nitrogen that were observed in the multiplex spectra of these elements.

As a representative example, Figure 3-9 shows an evolution of the C1s spectra for NC treated with 3-(triethoxysilylpropyl)isocyanate and then subsequently reacted with either dimethyl-dichlorosilane, or tridecafluoro-1,1,2,2,-tetrahydrooctyl-trimethoxysilane. As compared to bare NC, the C1s spectra of NC reacted with 3-(triethoxysilylpropyl)isocyanate presented notable increase of the component at 284.2 eV (aliphatic carbon) and the appearance of the split peak at 287.9 eV which was attributed to carbon in carbonyl. Even more prominent changes were observed in the N1s spectra, which revealed two components with intensity ratio ~1:1 at 407.2 eV (nitrate) and a new peak at 399.6 eV (organic amide). Together with ~10-folds increase of Si vs bare NC (Table 3-7), these changes supported the covalent attachment of trisiloxy-propyl groups via amide bond to the free OH groups of NC.

**Table 3- 7:** XPS Atomic Compositions for Nitrocellulose Reacted with Organosilanes (atomic %).

Sample label	Silane reagent(s)	C	O	N	Si	F
Bare NC	None	47.2±0.7	45.8±0.7	6.8±0.5	0.5±0.2	<0.1
NC-(CH <sub>2</sub> ) <sub>3</sub> Si(OH) <sub>3</sub>	(C <sub>2</sub> H <sub>5</sub> O) <sub>3</sub> Si(CH <sub>2</sub> ) <sub>3</sub> NCO	50.6±0.5	38.6±0.8	5.5±0.5	5.5±0.7	<0.1
NC-(SiO <sub>2</sub> ) <sub>x</sub>	(C <sub>2</sub> H <sub>5</sub> O) <sub>3</sub> Si(CH <sub>2</sub> ) <sub>3</sub> NCO + (CH <sub>3</sub> O) <sub>4</sub> Si	24.3±0.4	55.1±1.0	2.0±0.5	18.0±0.6	<0.1
NC-PDMS	(C <sub>2</sub> H <sub>5</sub> O) <sub>3</sub> Si(CH <sub>2</sub> ) <sub>3</sub> NCO + (CH <sub>3</sub> ) <sub>2</sub> SiCl <sub>2</sub>	48.5±0.5	26.1±0.7	0.5±0.3	21.2±0.6	<0.1
NC-C <sub>6</sub> F <sub>13</sub>	(C <sub>2</sub> H <sub>5</sub> O) <sub>3</sub> Si(CH <sub>2</sub> ) <sub>3</sub> NCO + (CH <sub>3</sub> O) <sub>3</sub> Si(CH <sub>2</sub> ) <sub>3</sub> C <sub>6</sub> F <sub>13</sub>	34.9±0.8	12.0±1.0	2.2±0.5	4.0±0.3	46.7±0.7



**Figure 3- 9:** Results of deconvolution of XPS high resolution spectra.

The subsequent reaction of this tri-siloxy-propyl-NC with dimethyldichlorosilane produced PDMS-like surfaces. The C1s spectra of these samples resolved into two unequal components: ~90% at 284.2 eV (methyl from PDMS) and ~10% at 287.9 eV (carbonyl and ether from NC). The Si concentration showed further increase to ~21%, while nitrogen signal was reduced almost to the noise level indicating formation of relatively thick and uniform PDMS coating that attenuated the signal from the underlying NC. The C:Si:O concentrations ratio for these samples was 2.3:1:1.2, which was close to the 2:1:1 ratio for pure PDMS. The reaction of the tri-siloxy-propyl-NC with tridecafluoro-1,1,2,2,-tetrahydrooctyl-trimethoxysilane produced fluoroalkyl-like surfaces. Deconvolution of the C1s spectra of these samples revealed five components with the binding energies attributed to CF<sub>3</sub> at 293.8 eV (~8% from the total signal), CF<sub>2</sub> at 291.4 eV (~34%), C=O 287.8 eV (~9%), C-O at 286.3 eV (~25%), and C-H at 284.6 eV (~24%), respectively. The CF<sub>3</sub>:CF<sub>2</sub> intensity ratio was 1:4.25, close to 1:5 ratio for C<sub>6</sub>F<sub>13</sub> group in the silane reagent. As compared to tri-siloxy-propyl-NC, N1s signal in fluoroalkyl-treated NC was also significantly reduced (Table 3-8) indicating formation of densely-packed coatings of perfluoroalkyl-groups. Attenuation of the N1s signal (407.2 eV) from the nitrate groups of the NC due to surface reactions with organosilanes was used to determine thicknesses of grafted layers using the equation<sup>125</sup>:

$$\text{Thickness} = \ln(N_0/N) \lambda \sin 45^\circ \quad \text{Eq. 3- 1}$$

where  $N_0$  and  $N$  were the intensity of the 407.2 eV peak for bare and functionalized NC, respectively.  $45^\circ$  was the XPS take-off angle and  $\lambda$  - the N1s photoelectron mean free path  $\lambda = 2.5$  nm was assumed.<sup>123,124</sup> The results summarized in Table 3-8 demonstrate that the

thickness of the organosilanes layers were in the range of monolayers or, in case of easily polymerizable tetramethoxysilane and dimethyldichlorosilane – thin oligomeric layers.

**Table 3- 8:** Thickness of Organosilanes Layers Grafted to Nitrocellulose.

Sample label	Silane reagent(s)	N1s (407.2 eV), at. %	Thickness, nm
Bare NC	None	6.8±0.5	-
NC-(CH <sub>2</sub> ) <sub>3</sub> Si(OH) <sub>3</sub>	(C <sub>2</sub> H <sub>5</sub> O) <sub>3</sub> Si(CH <sub>2</sub> ) <sub>3</sub> NCO	5.5±0.5	0.4±0.2
NC-(SiO <sub>2</sub> ) <sub>x</sub>	(C <sub>2</sub> H <sub>5</sub> O) <sub>3</sub> Si(CH <sub>2</sub> ) <sub>3</sub> NCO + (CH <sub>3</sub> O) <sub>4</sub> Si	2.0±0.5	2.2±0.5
NC-PDMS	(C <sub>2</sub> H <sub>5</sub> O) <sub>3</sub> Si(CH <sub>2</sub> ) <sub>3</sub> NCO + (CH <sub>3</sub> ) <sub>2</sub> SiCl <sub>2</sub>	0.5±0.3	5.0 ±1.1
NC-C <sub>6</sub> F <sub>13</sub>	(C <sub>2</sub> H <sub>5</sub> O) <sub>3</sub> Si(CH <sub>2</sub> ) <sub>3</sub> NCO + (CH <sub>3</sub> O) <sub>3</sub> Si(CH <sub>2</sub> ) <sub>3</sub> C <sub>6</sub> F <sub>13</sub>	2.2±0.5	1.9±0.5

### 3.8 Conclusion

According to FTIR and chemical analysis, the isocyanate groups bound to the OH groups of NC via carbamate linkage, while triethoxysilyl moieties (after hydrolysis) produced cross-linked siloxane-silanol surfaces, in a similar fashion reported for conventional cellulose substrates.<sup>18</sup> The silanol-grafted NC was subsequently reacted with various organosilanes of general formula R<sub>3</sub>SiX, R<sub>2</sub>SiX<sub>2</sub>, and RSiX<sub>3</sub> (R=alkyl-, phenyl-, fluoroalkyl-; X=Cl) and Si(CH<sub>3</sub>O)<sub>4</sub> producing a series of surface-functionalized NC materials without degradation of its nitro groups. According to SEM and DSC, there was no significant change neither in fiber morphology nor in thermal decomposition profiles of the modified NCs as compared to bare NC suggesting that the bulk properties of NC were not affected and that the reactions largely involved surface functionalities. XPS was performed

on bare and NC treated with perfluoro-alkyl, thick polydimethylsilane and TMOS surfaces. Survey scans of bare NC revealed the presence of C, N, O. Survey spectra after the surface functionalization of silyl and fluoro-alkyl species clearly show the change in composition on the surface of treated NC. The significant presence of atomic percent silicon and fluorine was evident on treated NC surfaces. As shown in Figure 3-6, bare NC demonstrated relatively fast initial adsorption, where ~90% from the maximum was adsorbed within the first 24 h. This initial growth was followed by the saturation plateau corresponding to the maximal adsorption of water at ~40 mg/g. For the NC modified with fluoroalkyl-, alkyl-, and poly(dimethylsiloxane) groups, the maximal adsorption of water was significantly reduced (~3-5 fold) as compared to bare NC.



## Chapter 4: Macroscopic and Microscopic Wetting

### 4.1 Abstract

Macroscopic contact angles demonstrated Trifluoro-methyl-phenyl and tri-methyl-silyl functionalized NC resulted in low advancing and receding contact angles for H<sub>2</sub>O and hexadecane as probe fluids. and the best quality surfaces were produced using the vapor phase reactions of organosilanes. The wettability of the bulk treated NC surfaces were characterized by dynamic contact angles using water, hexadecane, and NG as probe fluids. The NG contact angles of the modified NC pellets ranged as follows: fluoroalkyl-NC ( $\theta_{Adv}/\theta_{Rec} \sim 90^\circ/\sim 50^\circ$ ), alkyl-NC ( $\sim 75^\circ/\sim 35^\circ$ ), oligo(dimethylsiloxy)-NC ( $\sim 65^\circ/\sim 35^\circ$ ), phenyl-NC ( $\sim 40^\circ/\sim 10^\circ$ ), untreated NC ( $<10^\circ$ ). NG contact angles of the treated fibers ranged as follows: fluoroalkyl-NC ( $\theta_{clam}/\theta_{barrel-shape} \sim 90^\circ/\sim 50^\circ$ ), alkyl-NC ( $\sim 75^\circ/\sim 35^\circ$ ), oligo(dimethylsiloxy)-NC ( $\sim 65^\circ/\sim 35^\circ$ ), phenyl-NC ( $\sim 40^\circ/\sim 10^\circ$ ), untreated NC ( $<10^\circ$ ), demonstrating major variations in surface energy in accordance with the nature of surface functionalities.

### 4.2 Introduction

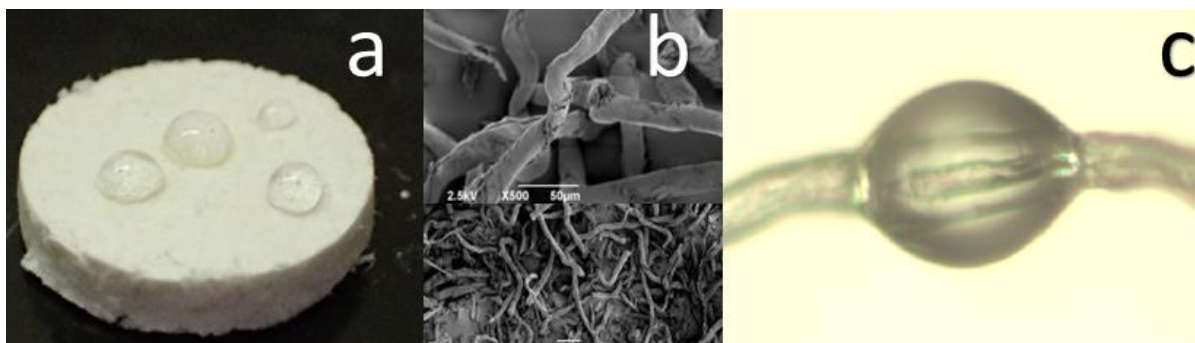
The terms ‘lyophilic’ and ‘lyophobic,’ derived from the Greek words to describe a love (philos) or fear (phobos) of dissolving or mixing with (Lyo), as well as ‘hydrophobic’ and hydrophilic’ (also Greek for “water fearing” and “water loving”, respectively) are terms that help to qualitatively describe the energy and intensity of interactions at the interface between a solid and liquid. Strong interactions with a lyophilic/hydrophilic material describe a polar surface. Weak interactions with a lyophobic/hydrophobic material describe non-polar surfaces. Hydrophobic surfaces are often prepared by modifying the surfaces with

hydrocarbons (alkanes), fluorinated alkanes, and methylsiloxanes. As described in several sections in this document, the surface of cellulose expose high energy hydroxyl groups (OH). The OH group allows for hydro/lyophobicization of the cellulose surface. There exists a number of functional groups that can be used to construct low energy surfaces.<sup>19-24</sup> The lowest surface energies are observed for the surfaces composed of perfluorinated alkyls (CF<sub>3</sub>), along with following functional groups displaying an increase in hydro/lyophobicity and an increase in surface energy respectively: fluoromethylene (CF<sub>2</sub>), methyl (CH<sub>3</sub>), and dimethylsiloxane [OSi(CH<sub>3</sub>)<sub>2</sub>].<sup>19</sup> According to Fadeev, the presence of virtually any other functionality at the surface will increase the surface energy of the solid.<sup>19</sup> In this study we found that the long chain fluoro-alkane allowed the greatest surface phobicity. Siloxane on the other hand, proved to be the most versatile and robust in terms of a surface that allows different degrees of phobicity.

Nitrocellulose is made up of natural fibers that vary in shape, dimensions, and physical properties. The inhomogeneous nature of natural fibers that make up the bulk material, promote a rough surface.<sup>102</sup>

In this chapter we discuss the fundamental wetting properties of the interface of treated NC. We utilized two levels of wettability. The first being the macroscopic wetting in which demonstrates wetting parameters taken from the bulk surface in which the intrinsic or apparent contact angle is estimated using goniometry in which the drop profile is measured from a droplet on a plane. The measurement of a contact angle on treated NC is taken from a pressed pellets. Our research also pointed us into the direction of developing methodology to study drop morphology using contact angles of NG and other probe fluids on treated NC fibers, Figure 4-1 depicts examples of nitroglycerin on treated surfaces and NC fiber

morphology. Figure 4-1a shows NG droplets for contact angle measurements on a bulk surface. Figure 4-1b shows SEM pictures demonstrating fiber morphology. Figure 4-1c shows a NG droplet in equilibrium on a treated perfluoroalkyl NC fiber.



**Figure 4- 1:Treated Nitrocellulose**

(a) Nitroglycerin droplets on  $C_6F_{13}$  treated Nitrocellulose pellet. (b) SEM of treated Nitrocellulose fiber (c) Nitroglycerin droplet on  $C_6F_{13}$  treated fiber.

While the contact angle measurements on the bulk surface are important for our research, the measurement on a bulk surface provides the apparent contact angle in which surface roughness and capillary effect of bulk material results in the instability of liquid to reach equilibrium. In contrast, the droplet on a fiber is known to represent the true, intrinsic contact angle. Therefore, a more reliable determination of the lyophobicity on a single fiber is warranted.<sup>103</sup> Contact angle measurements on bulk material can be hindered by capillary effect, which most often may not represent the true phobicity of a fibrous material.<sup>104</sup> According to Carrol et al, the accurate measurement of a contact angle on a fiber assume a cylindrical solid taking on a liquid. The droplet on a fiber can exist as an axisymmetrical barrel shape or nonaxisymmetrical clam shape conformation.<sup>99</sup>

Several methods for determining contact angles of liquid droplets on cylinder surfaces are currently used as standard practice.<sup>105-108</sup> In this chapter, we utilize methodology

based on geometry provided by Carrol et al. and several other researchers who have optimized models designed to increase the accuracy of fiber droplet measurements.<sup>105-108</sup>

This methodology employs a dimensionless description of the liquid drop profile to measure fiber contact angles with a barrel shape. A direct measurement of the contact angle can also be employed in fiber studies using microscopy software.<sup>99, 108</sup> For our work we also utilize similar direct measurement techniques that are available using a Zeiss microscope software package.

In this chapter, we discuss how contact angle measurements on the surface of natural fibers allow insight of a surface with increased curvature and reduced capillary effect giving the intrinsic contact angle, whereas the bulk surface gives an apparent contact angle.

The wettability of modified NC fibers was characterized using optical microscopy observing droplets of water, NG, hexadecane, dodecane, undecane, decane, and nonane. Contact angles of fibers were measured using methods based on geometry originally developed by Carroll et al.<sup>99</sup> Surface energy and critical surface tension was measured based on the estimated contact angles.

### **4.3 Macroscopic Contact Angles**

#### **4.3.1 General Information**

The surfaces for contact angle measurements were obtained by pressing ~0.2 grams of NC (neat or functionalized) using a Perkin Elmer 13mm IR die under a Carver Laboratory Press at 4 metric tons of pressure for 1 min. We found that pressurization at 4 metric tons for 1 min were sufficient to produce pellets with reproducible contact angles. Further increase of pressure or time had no effect on the wettability of the pellets. Contact angles were measured by a Dataphysic OCA contact angle instrument using GASTIGHT #1750

Hamilton Company micro-syringe. The probe fluids used were water, *n*-hexadecane, and nitroglycerin (NG). NG was rendered from ethanol evaporation from a 5% NG/ethanol solution. Dynamic contact angles ( $\theta_{Adv}/\theta_{Rec}$ ) were recorded while the probe fluid was added to ( $\theta_{Adv}$ ) and withdrawn ( $\theta_{Rec}$ ) from the drop, respectively. The dynamic contact angles with NG as a probe fluid were measured using a Drummond WIRETROL 5  $\mu$ L pipette to add and withdraw the probe fluid while recorded under the video capability of a Dataphysic OCA tensiometer. A tilting stage fabricated by Dataphysic OCA was used with the instrumentation to obtain contact angle hysteresis for NG droplets. Due to safety concerns, we used this technique rather than using a syringe filled with NG. *Filling a syringe with a sufficient amount of NG to obtain measurements could result in initiation of NG. Great care must be taken when performing measurements with nitroglycerin.* Three-four measurements of advancing and receding angles were taken for each sample and the average result was reported. The standard error of the contact angles for NC surfaces was estimated  $\sim 2^\circ$ .

#### **4.3.2 Contact Angles on Nitrocellulose treated with Acyl Chlorides and Isocyanates**

Contact angle measurements using water and hexadecane as probe fluids were measured using a surface tensiometer (Table 4-1). Each contact angle result is an average of 10 measurements. Samples were pressed into .2 grams pellets using a 12 millimeter die and compression press. Pentafluorobenzoyl and nonafluoropentanoyl acyl chloride functionalized NC demonstrated advancing contact angle measurements with H<sub>2</sub>O at values between 85-90° indicating a degree of surface phobicity. The receding contact angles show low measurements after the probe fluid has already been in contact with the surface. Over all, the surfaces of the prepared pellets of the acyl chlorides treated NC resulted in large contact

angle hysteresis possibly due to surface roughness and inhomogeneity.

Pentafluorophenyl functionalized NC demonstrated adequate hydrophobicity with an advancing contact angle of  $\sim 90^\circ$ . The contact angles of hexadecane provided low advancing and receding angles of  $35/15^\circ$ . Trifluoro-methyl-phenyl and tri-methyl-silyl functionalized NC resulted in low advancing and receding contact angles for  $H_2O$  and hexadecane as probe fluids. 3-triethoxysilylpropyl isocyanate on the surface of NC gave an initial theta of  $75/45^\circ$ . In general, the isocyanate reactions NC demonstrated large contact angle hysteresis, possibly due to surface roughness and inhomogeneity.

**Table 4- 1:** Advancing/Receding Contact Angle Measurements of Perfluoro Acyl Chloride and Isocyanate Modified NC ( $^\circ$ ).

\*For NC-supported surfaces the standard error for contact angles was  $\sim 2^\circ$ .

	$H_2O$ $\theta_{Adv}/\theta_{Rec}$	$C_{16}H_{34}$ $\theta_{Adv}/\theta_{Rec}$
Unmodified (neat) NC	<10	<10
<b>Acyl chlorides</b>		
3,3,3-trifluoropropionyl + NC	72/24	26/<10
Pentadecafluorooctonyl + NC	68/35	48/10
Pentafluorobenzoyl + NC	86/35	28/<10
Nonafluoro pentanoyl + NC	84/37	35/<10
<b>Isocyanates</b>		
Pentafluorophenyl + NC	90/15	35/15
Trifluoromethylphenyl + NC	57/<10	<10
3-(triethoxy)silyl propyl + NC	75/45	25/10
Trimethylsilyl + NC	55/0	35/<10

#### 4.3.3 Wetting Properties of Functionalized Nitrocellulose

For the contact angles on model surfaces (that included Si-supported monolayers of octadecyldimethylchlorosilane<sup>33</sup> and smooth polymer films of poly (tetrafluoroethylene), poly (ethylene), and poly (ethelene terephthalate)) the standard error was  $1^\circ$  or better.

To access wetting properties, pressed pellets of the NC materials were characterized by dynamic contact angles using water, hexadecane, and NG as probe fluids. Table 4-2 displays advancing and receding contact angle for bare NC and for NC reacted with organosilanes. Bare NC showed low contact angles ( $<10^\circ$ ) demonstrating complete wetting by water, hexadecane, and NG. The reaction of triethoxysilylpropyl isocyanate produced moderately hydrophobic surfaces with the advancing contact angle by water at  $75^\circ$ .

Functionalized NCs and on selected surfaces of known composition.\*

**Table 4- 2:** Dynamic Contact Angles ( $\theta_{Adv}/\theta_{Rec}$ , deg) of Water Hexadecane, and Nitroglycerine on Pellets of Functionalized NC and Selected Surfaces of Known Composition.\*

Sample	Probe fluids		
	Water	Hexadecane	Nitroglycerin
Unmodified (neat) NC	$<10$	$<10$	$<10$
NC + $(C_2H_5O)_3Si(CH_2)_3NCO$	75/45	25/10	35/10
NC + $(C_2H_5O)_3Si(CH_2)_3NCO$ + $(CH_3O)_3Si(CH_2)_2C_6F_{13}$	115/85	80/55	90/50
NC + $(C_2H_5O)_3Si(CH_2)_3NCO$ + $Cl_2Si(CH_3)_2$	112/90	60/30	65/35
NC + $(C_2H_5O)_3Si(CH_2)_3NCO$ + $ClSi(CH_3)_2C_{18}H_{37}$	102/68	$<10$	75/35
NC + $(C_2H_5O)_3Si(CH_2)_3NCO$ + $Cl_3SiC_6H_5$	85/60	$<10$	40/10
NC + $(C_2H_5O)_3Si(CH_2)_3NCO$ + $(CH_3O)_4Si$	$<10$	$<10$	$<10$
NC + $(C_2H_5O)_3Si(CH_2)_3NCO$ + $(CH_3O)_4Si$ + $ClSi(CH_3)_2C_{18}H_{37}$	90/75	$<10$	80/50
Cleaned Si-wafer: Si/SiO <sub>2</sub>	$<10$	$<10$	$<10$
Si/SiO <sub>2</sub> -OSi(CH <sub>3</sub> ) <sub>2</sub> C <sub>18</sub> H <sub>37</sub>	101/91	25/15	75/66
Poly(tetrafluoroethylene), Teflon: $-[CF_2]_n-$	110/98	25/10	87/77
Poly(ethylene): $-[CH_2]_n-$	86/78	$<10$	74/60
Poly(ethylene terephthalate): $-[C(O)C_6H_4COO(CH_2)_2O]_n-$	78/68	$<10$	35/ $<10$

\*For NC-supported surfaces the standard error for contact angles was  $\sim 2^\circ$ . For Si wafers and polymer films, the standard error was  $1^\circ$  or better.

This value of water contact angle was attributed to mixed surface containing polar and non-polar functionalities. To evaluate the contribution of different surface functionalities to wettability, we used the Israelachvili-Gee equation <sup>96</sup>

$$(1 + \cos\theta)^2 = f_1(1 + \cos\theta_1)^2 + f_2(1 + \cos\theta_2)^2$$

**Eq. 4- 1**

$$f_1 + f_2 = 1$$

We treated the surface of silyl-propyl-NC as a mixture of silanol and methylene groups. Using the water contact angle 0° for a silanol surface ( $\theta_1$ ) and 100° for a methylene surface ( $\theta_2$ ),<sup>26</sup> we found that the observed water contact angle of 75° corresponded to a mixture of ~30% silanols and ~70% methylene groups. Considering that triethoxysilylpropyl group after hydrolysis has 1:1 silanol-to-methylene ratio, we concluded that on the surface some silanols were likely cross-linked forming non-polar siloxanes. The contact angle data was consistent with the surface composed of silanol and propyl groups. Recalling that from the bulk chemical analysis only 10% of cellulose repeat units reacted with triethoxysilylpropyl isocyanate, we concluded that silane largely concentrated on the surface. The reaction of silyl-propyl-NC with tetramethoxy-silane produced surfaces that were completely wettable by all probe fluids which was in agreement with formation of silica-like polar surface rich in silanol groups. The reactions of silyl-propyl-NC with perfluoroalkyl, alkyl, and phenyl silanes produced lyophobic surfaces with water and hexadecane advancing contact angles that were on par with those reported for the closely-packed monolayers of CF<sub>3</sub>, CH<sub>3</sub>, and Phenyl-functionalities supported on Si wafers.<sup>19</sup> The receding angles, however, were lower than the reference values reported for SAMs and CAMs on Si wafers<sup>19</sup> demonstrating



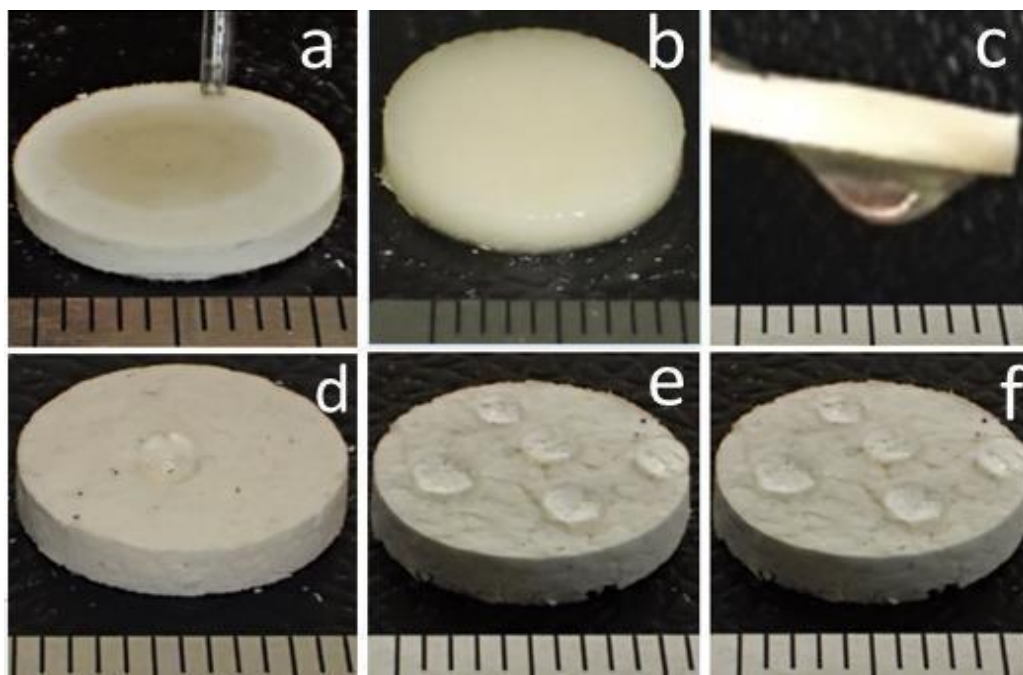
significant wetting hysteresis, which was attributed to greater surface heterogeneity and roughness of pressed pellets as compared to smooth surfaces of Si wafers. For silyl-propyl-NC reacted with long-chain alkyl (n-C<sub>18</sub>H<sub>37</sub>) and phenyl- silanes, the water contact angles were high in the range of 85-100° while the hexadecane contact angles were low (<10°) providing examples of hydrophobic yet oleophilic surfaces. The contact angles of NG also showed major changes depending on the nature of surface groups demonstrating different levels of wettability and the potential of “tuning” the strength of the NG-NC interactions by chemical functionalization. For all the surfaces studied, the contact angles of NG fell in between the contact angles of water and hexadecane in accord with the surface tensions of the probe fluids (20° C, in mJ/m<sup>2</sup>): water (72.8) <sup>97</sup>, NG (50.4) <sup>24</sup>, hexadecane (27.7) <sup>97</sup>. Due to the near absence of wetting data for NG in open literature, we had no reference values to evaluate contributions of different surface functionalities to the NG contact angles. For that purpose, the NG contact angles were measured for several well-defined surfaces of known composition including monolayers of organosilanes supported on Si-wafers and smooth polymer films. The results are shown in the bottom section of Table 4-2. Like for water and hexadecane probe fluids, the highest value of NG contact angles 87°/78° (adv/rec) was observed for poly(tetrafluoro ethylene) (Teflon) representing the low-energy surface of CF<sub>2</sub> functionalities. Non-polar hydrophobic surfaces of poly(ethylene) and monolayers of octadecyl silane supported on Si wafers, projecting respectively CH<sub>2</sub> and mixed CH<sub>2</sub>-CH<sub>3</sub> functionalities, were also poorly wetted by NG and showed contact angles in the range ~75°/60° (adv/rec). For relatively polar surface of poly(ethylene terephthalate), as evidenced by intermediate value of water contact angles, wetting of NG improved with the advancing contact angle being 35° and the receding angle less than 10°. For the high-energy polar

surface of cleaned Si-wafer, water, NG, and hexadecane demonstrated complete wetting with both advancing and receding contact angles being near zero ( $<10^\circ$ ). On all the model surfaces tested, the contact angles hysteresis of NG was  $\sim 10$ - $15^\circ$  which was similar to the values normally reported for water and hexadecane on this type of surfaces.<sup>19, 97</sup> Comparing the contact angles for NG on the model surfaces with the contact angles of NG on the modified NC surfaces, we concluded that NG, as a probe fluid, produced similar results as water and hexadecane probe fluids. Namely, for the NC modified with perfluoroalkyl, alkyl, poly(dimethylsiloxyl), and phenyl silanes, the NG advancing contact angles showed formation of high quality lyophobic surfaces comparable with the closely-packed monolayers of organosilanes on Si wafers or homogeneous polymer films of similar chemical composition.

As a demonstration of the effect of surface functionalization on the NG-NC interfacial interaction and as an illustration supporting the first portion of the title of this chapter, Figure 4-2 compares the time behavior of the NG droplets placed on two different NC pellets: (a) bare NC and (b) NC modified with  $C_6F_{13}$  groups (respectively, top and bottom rows, Figure 4-2). On bare NC, the first drop of NG ( $\sim 5 \mu\text{L}$ ) was instantly wicked by the porous surface due to capillary forces (Figure 3-5a). Further addition of liquid (total volume  $\sim 75 \mu\text{L}$ ) produced an NC pellet that was completely saturated with NG (Figure 4-2b). Over time, the excess of NG driven by gravity started to leak (“sweat out”) from the pellet. After 5 h, the growing drop of NG was clearly visible on the bottom side of the pellet (Figure 4-2c). In contrast to that, the drops of NG did not spread and beaded up on the surface of  $C_6F_{13}$ -treated NC (Figure 4-2d-e). The NG-repellant properties of the treated NC maintained over time, as the size and shape of the drops did not change after period of 12 h, Figure 4-2f. As

shown in Table 4-2, initial contact angle measurements demonstrate the high surface energy of unmodified military grade NC. NC used in this study completely wets ( $<10^\circ$ ) with probe fluids  $\text{H}_2\text{O}$ ,  $\text{C}_{16}\text{H}_{34}$ , and NG. Previous reports show a degree of hydrophobicity on the surface of highly nitrated cellulose thin films.<sup>99</sup>

The 3-(triethoxy) silyl propyl carbamate linkage shows an adequate phobicity to  $\text{H}_2\text{O}$ . We expected the hydrophobicity of this linkage on NC to be lower, based on the increase in silanol functionality shown by FTIR results described in Chapter 3.



**Figure 4- 2: Time Behavior of the NG Droplets**

(a) Droplet ( $\sim 5 \mu\text{L}$ ) of nitroglycerin on a pellet of neat NC; (b) NC pellet saturated with nitroglycerin (total volume added  $\sim 75 \mu\text{L}$ ); (c) Side view of sample (b) after 5 h. (d) Droplet ( $\sim 5 \mu\text{L}$ ) of nitroglycerin on  $\text{C}_6\text{F}_{13}\text{-NC}$ ; (e); Multiple droplets of nitroglycerin on  $\text{C}_6\text{F}_{13}\text{-NC}$ ; (f) sample (e) after 12 hours. Scale bar: one unit is 1 mm.

The higher than expected  $\text{H}_2\text{O}$  contact angles on silyl isocyanate NC pellets may be due to the high polarity of water and its hydrogen bonding.  $\text{H}_2\text{O}$  as a probe fluid often offers limited

conclusive results in terms of the true nature of a surface.<sup>19</sup> *n*-Hexadecane on the surface of the NC functionalized with the propyl carbamate linkage displays  $\theta_{Adv}/\theta_{Rec}$  of 25/10° respectively. The true dispersive properties of a long chain hydrocarbon used as a probe fluid more times than not offers more insight into the true physical properties of a surface.<sup>19</sup> In the case of the propyl carbamate linkage on NC, we see a low contact angle with *n*-hexadecane. NG used as a probe fluid also shows a relatively low contact angle on the surface of the NC functionalized with the propyl carbamate linkage. We can speculate that the low contact angle measurements on the surface of NC functionalized with the propyl carbamate linkage is due to the increase in surface silanol and the hydroxyl availability, which is a direct result from the crosslinking of the 3-(triethoxysilylpropyl) isocyanate.

The reaction of TMOS with NC in vapor phase and solvent dissolution reactions demonstrate complete wetting by the probe fluids. This suggests an increase in surface silanol for further reaction with lyophobic organosilanes and is confirmed by spectra presented in the previous chapter.

Contact angle results for reactions promoting a lyophobic surface on NC show that the silyl isocyanate and tetramethoxysilane reacted NC when modified with tridecafluoro 1,1,2,2-tetrahydrooctyltrimethoxysilane, show the highest degree of lyophobicity to NG, water, and hexadecane compared to the other organosilanes used in this work. For fluorinated alkyl monolayers, contact angles of polar and non-polar probe fluids repeatedly increase with the number of perfluorinated carbons and level off at typically 4-6 fluorinated carbons. The surface energies of fluoro alkyl monolayers decrease as the number of perfluorinated carbons increase.<sup>19</sup> The octadecyl silane functionality was chosen primarily based on its use in a variety of different applications based on its adequate surface lyophobicity.<sup>34, 93</sup> For our

work, H<sub>2</sub>O and NG probe fluids present sufficient non-wetting on the surface of *n*-octadecyldimethylchlorosilane modified NC, while complete spreading/wetting was observed with *n*-hexadecane as a probe fluid. The noticeable wettability of the dispersive liquid on *n*-octadecyldimethylchlorosilane may be a lack of surface packing density.<sup>33</sup> The imposition of steric hindrance by the presence of the two methyl groups attached to the silica atom is known to prevent close packing at the head groups and polymethylene chains.<sup>33</sup>

Dimethyldichlorosilane functionalized NC has a reasonable degree of lyophobicity to H<sub>2</sub>O, hexadecane, and NG. Dimethyldichlorosilane reacts with the NC propyl carbamate linkage, tetramethoxysilane reacted NC surface, and to some degree, directly to the NC surface via vaporization to form an oligomeric dimethyl siloxane surface. Surfaces that are generated using dimethyldichlorosilane are known to be very homogeneous and show low adsorption energy (CH<sub>3</sub> termini).<sup>33, 95</sup> Typically, no accessible silano groups can be detected on these types of surfaces, which proves the ability of short poly (dimethyl siloxane) chains to shield the silica substrate.<sup>95</sup> The adequate non-wetting of hexadecane on the NC dimethyl siloxane surface suggests the structural performance of dimethyldichlorosilane. H<sub>2</sub>O contact angle results for phenyl trichlorosilane functionalized NC indicate a sufficient degree of hydrophobicity.

According to previous work, aromatic moieties are forced to assume an orientation perpendicular to the surface.<sup>19,33</sup> However, contact angles of a non-polar probe fluid such as hexadecane display complete wetting on the phenyltrichlorosilane NC surface. Previous work suggests that the addition of compounds containing phenyl rings increase the surface energy in comparison to CF<sub>2</sub>, CF<sub>3</sub>, CH<sub>3</sub> functionalities.<sup>19,32</sup>

For the purpose of this work we utilized phenyl trichlorosilane to demonstrate the

capability of our “tunable” surface in providing different levels of NG wettability, in which the phenyltrichlorosilane functionality demonstrates the lowest NG contact angle measurements in comparison to the other parent compounds used for this work. One final observation must be noted concerning contact angle hysteresis. The difference in ( $\theta_{Adv}/\theta_{Rec}$ ) can to an extent, be attributed to the rough surface and inhomogeneity of the pellet samples prepared for contact angle measurements. From an application standpoint, the lyophobicity of the NC modified surfaces have increased substantially in comparison to the complete wetting of probe fluids ( $H_2O$ ,  $C_{16}H_{34}$ , and NG) on unmodified military grade NC.

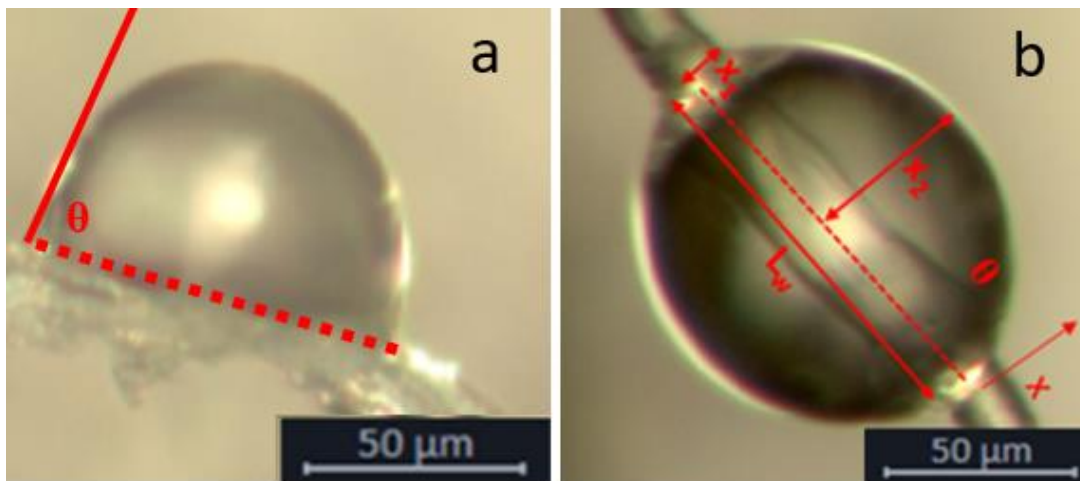
#### 4.4 Discussion

As assessed by the contact angles of water, hexadecane, and NG probe fluids, wettability of the functionalized NC changed over a wide range in accordance with the nature of surface functionalities. The least wettable surfaces were obtained for NC grafted with tridecafluorooctyl- (the NG contact angles  $\theta_{Adv}/\theta_{Rec}$   $90^\circ/50^\circ$ ), octadecyl- ( $\sim 75^\circ/\sim 35^\circ$ ) and dimethylsiloxo-groups ( $\sim 65^\circ/\sim 35^\circ$ ), which was in general agreement with the range of lyophobicity reported for well-defined surfaces composed of the corresponding functionalities.<sup>28,35</sup> While a pellet of bare NC readily wicked drops of NG, for NC grafted with fluoroalkyl- and alkyl-groups, the penetration of liquid NG inside the pellet was inhibited. The moisture adsorption in the hydrophobized NC was also greatly reduced ( $\sim 3$ -5 folds) as compared to bare NC thus improving longevity and performance of the modified NC materials. To the best of our knowledge, this was the first demonstration of covalent surface functionalization to control surface properties of nitrocellulose.

## 4.5 Contact Angle on Fibers

A microscopic approach was used to obtain micrographs of probe fluid droplets on the surface of modified NC fibers ranging from  $\sim 10\text{-}30\text{ }\mu\text{m}$  with rough surfaces. The reactions of silyl-propyl-NC with perfluoroalkyl, alkyl, and phenyl silanes produced lyophobic surfaces with NG, water, hexadecane, dodecane, undecane, decane, and nonane. Droplets on fibers resulted in both barrel and clam shell shapes in which the first possesses axial symmetry and the latter, symmetry only about a plane containing the fiber axis and drop apex.<sup>111</sup> Figure 4-3a shows a micrograph of clam shell shape NG droplet on silyl propyl perfluoroalkyl functionalized NC. Contact angles of clam shell and barrel shape droplets were measured directly using Zeiss Axioplan 2 Imaging software in interactive measure mode. The barrel shape droplets were also measured by a second method using a method based on geometry originally developed by Carroll,<sup>99</sup> in which an analytical expression was derived relating to length, surface area, volume, and Laplace pressure of a liquid drop adhering to a fiber, assuming a cylinder shape. Figure 4-3b describes the measurements used to estimate the contact angle on a droplet assuming a barrel shape, where  $x_1$  is the fiber radius,  $x_2$  is the maximum radius of the drop in a plane normal to the filament axis,  $L_w$  is the drop length along the fiber, and  $\theta$  is the contact angle. Tables of dimensionless forms are used to estimate contact angles from barrel shape droplet. An example can be found in Appendix B. Carroll was the first to develop this method using parameters based on geometry. Carroll's method has since been optimized by several researchers allowing increased accuracy of contact angle measurements on natural fibers, although ample percent error poses a problem in the methodology.<sup>102, 103-108</sup> When changing the material geometry from a flat surface to a fiber, a smaller contact angle is often observed.<sup>112</sup> This is in part due to capillary effect of the bulk

material and the inability of the liquid to form a continuous film around fibers in a bulk system.<sup>113</sup> The cylindrical shape of the functionalized NC fiber allows curvature to take place with the NG droplet.<sup>114, 115</sup>



**Figure 4- 3: Droplet Measurement**

(a) Direct measurement parameters on a clam-shell shape droplet and (b) Measurements of a barrel shape droplet.<sup>99</sup>

The treated fibers demonstrate an elongated flat, irregular curved cylinder shape comparable to bare NC, allowing probe fluid droplets to either rest in nonaxisymmetrical or take on a classical axisymmetrical shape on the low energy fiber surfaces.<sup>115</sup> Previous work involving the development of phase diagrams of droplet volume against contact angle have been reported.<sup>112,116</sup> Experiments from this work show barrel and clam shape conformations can co-exist for the same droplet volumes and thus indicates the existence of multiple stable states. In our work we frequently observed both types of conformations. Probe fluids were sufficiently dispensed on the surface of the fibers by use of aerosol.

As a demonstration of the effect of surface functionalization on NC fibers in the presence NG interfacial interaction, Fig. 4-4a shows complete soaking of NG throughout,

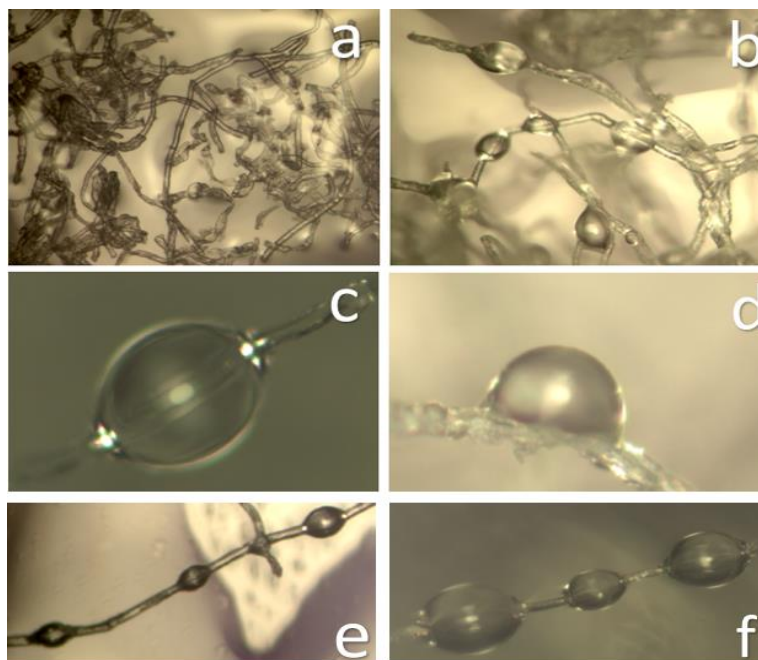


demonstrating high surface energy of individual nitrated fibers. It was not possible to observe liquid droplets on bare NC fibers. Table 4-3 gives contact angle values  $<10^\circ$  on bare NC with probe fluids, showing the wicking effects of bare NC. Barrel contact angles were measured using the two methods described above using the geometry of a cylinder shape and a direct measurement using Zeiss Axioplan 2 Imaging software. A comparison of the two methods used in this study estimating barrel shaped contact angles presented a range of percent errors depending on the surface and probe fluid. The largest differences in barrel contact angles between methods were observed on the NC + NCO +  $C_6F_{13}$  surface in which there was  $\sim 18^\circ$  difference in the NG and nonane  $\theta$ , and  $\sim 11^\circ$  for  $H_2O$   $\theta$ . The difference in  $H_2O$  and NG  $\theta$  for the PDMS surface was  $\sim 9^\circ$  and  $5^\circ$  respectfully. The largest  $\theta$  differences observed on the octadecyl surface were for probe fluids  $H_2O$  ( $9^\circ$ ) NG ( $11^\circ$ ). The NC + NCO + phenyl surface demonstrated a difference of  $\sim 11^\circ$  for undecane. The TMOS +  $C_6F_{13}$  surface resulted in a  $\sim 18^\circ$  difference for NG and a  $\sim 11^\circ$  difference for  $H_2O$ . The difference in  $\theta$  for the selected methods for barrel shape droplet estimation can be attributed to several factors. The difficulty of selecting locations on the droplet and fiber using the direct software method results in errors caused by manual interpretation. The same can be said in respect to the Carrol method. The diagrams used in geometry methods were developed for estimating low contact angles ( $<60^\circ$ ). This presents an increased source of error in estimation when the barrel droplet contact angle approaches or exceeds  $60^\circ$ . Despite the apparent percent error, the two methods used to estimate  $\theta$  on barrel shaped droplets were acceptable to use for our work. Researchers in the area of fiber analysis have accepted these methods as part of their routine characterization process.<sup>99, 103-112</sup> Finally, our results show that the trend of the barrel shaped contact angles were consistent with the properties of our probe fluids based on the contact

angle measurements estimated from our clam shell and bulk surface measurements .

The imaging software was also used to estimate the contact angles measured from clam shell droplets shown in Table 4-3. The NC fibers treated with triethoxysilylpropyl isocyanate demonstrate a degree of phobicity confirming from our previous work with the formation of cross-linked non-polar silanes.<sup>61</sup> Fig 4-4b illustrates a micrograph at 10X (low resolution) providing observation of multiple droplet formation of NG on silyl propyl perfluoralkyl modified NC fibers. The visualization of multiple droplets on the low energy surface demonstrates effectiveness of surface treatment in controlling NG wetting. Contact angles measured from barrel-shaped droplets of NG on individual fibers treated with perfluoralkyl demonstrated an average contact angle of  $\sim 59^\circ$ . The average of ten barrel-shaped droplets was determined by estimating left and right contact angles on the top and bottom portions of the barrel shaped droplets surrounding the fiber. A comparison of contact angle measurements between multiple barrel shaped droplets of NG on the same perfluoralkyl treated NC fiber was estimated in the same manner. The average NG contact angles of multiple barrel shaped droplets on perfluoroalkyl treated NC surface was  $\sim 55^\circ$ , in line with the average NG contact angle measurements on individual fibers. Estimates were based on ten separate treated fibers and selecting two droplets from each fiber for consistency, averaging a total of twenty droplets. Figures 4.4e-f depict multiple barrel-shaped droplets of NG on the same fiber. Figure 4-4e shows three droplets on the same fiber with the appearance of similar volumes of NG in equilibrium forming the barrel shape conformation. Figure 4.4f depicts three droplets with different volumes maintaining  $\sim 50^\circ$  contact angles, demonstrating homogeneity of a single fiber of perfluoro-alkyl treated NC. Table 4-3 gives the estimated contact angles on individual treated fibers with common probe fluids. The least

wetted fibers were observed on the silyl propyl perfluoralkyl surface representing low-energy surface of  $\text{CF}_2$  functionalities. Fig. 4-4c and 4-4d depict barrel ( $\sim \theta 59^\circ$ ) and clam shape NG droplets ( $\sim \theta 81^\circ$ ) in equilibrium with perfluoralkyl treated NC fibers.



**Figure 4- 4: Droplets on NC fibers**

(a) Bare NC fiber soaked with NG: (b) Multiple NG droplets on  $\text{C}_6\text{F}_{13}$ -NC fibers: (c) NG Barrel shape droplet formation on  $\text{C}_6\text{F}_{13}$ -NC fibers: (d) Clam-shape droplet on  $\text{C}_6\text{F}_{13}$ -NC fibers. (e-f) Multiple NG barrel-shape droplets on  $\text{C}_6\text{F}_{13}$ -NC fibers.

The perfluoralkyl treated fibers show moderately high contact angles of water, NG, and hexadecane with an approximate even distribution of clam and barrel shape droplets observed under the microscope. The NC fibers treated with alkyl and phenyl silanes produced lyophobic surfaces with water, NG, hexadecane, dodecane, undecane, decane, and nonane. *N*-alkane demonstrated lower contact angles on fiber surfaces forming exclusive barrel-shape equilibrium for the exception of silyl-propyl-flouroalkyl treated fibers. PDMS treated fibers retained clam shape droplets of water ( $\sim \theta 85^\circ$ ) and barrel shape ( $\sim \theta 70^\circ$ ) showing adequate hydrophobicity.

**Table 4-3:** Estimated average contact angles ( $\theta_{\text{clam shape/barrel shape}}$ ) and surface tension values of water, nitroglycerin, hexadecane, dodecane, undecane, decane, and nonane on treated NC fibers.

x = droplet shape not detected on a surface with probe fluid.

Standard %error +/-5

Functionalized NC Fiber	$\gamma_{LV}$ mJ/m <sup>2</sup>	H <sub>2</sub> O (72.8)	NG (50.4)	C <sub>16</sub> H <sub>34</sub> (27.7)	C <sub>12</sub> H <sub>26</sub> (25.4)	C <sub>11</sub> H <sub>24</sub> (24.7)	C <sub>10</sub> H <sub>22</sub> (23.8)	C <sub>9</sub> H <sub>20</sub> (22.9)
(C <sub>2</sub> H <sub>5</sub> O) <sub>3</sub> Si(CH <sub>2</sub> ) <sub>3</sub> NCO	Clam shape	63	37	47	x	x	x	x
	Barrel shape method 1	46	33	36	28	27	26	23
	Barrel shape method 2	49	36	41	35	31	26	24
(C <sub>2</sub> H <sub>5</sub> O) <sub>3</sub> Si(CH <sub>2</sub> ) <sub>3</sub> NCO + (CH <sub>3</sub> O) <sub>3</sub> Si(CH <sub>2</sub> ) <sub>2</sub> C <sub>6</sub> F <sub>13</sub>	Clam shape	93	81	64	58	47	43	x
	Barrel shape method 1	60	50	48	53	43	40	24
	Barrel shape method 2	71	68	55	48	45	41	37
(C <sub>2</sub> H <sub>5</sub> O) <sub>3</sub> Si(CH <sub>2</sub> ) <sub>3</sub> NCO + Cl <sub>2</sub> Si(CH <sub>3</sub> ) <sub>2</sub>	Clam shape	85	70	59	x	x	x	x
	Barrel shape method 1	57	50	47	42	34	33	24
	Barrel shape method 2	66	55	50	44	37	34	27
(C <sub>2</sub> H <sub>5</sub> O) <sub>3</sub> Si(CH <sub>2</sub> ) <sub>3</sub> NCO + ClSi(CH <sub>3</sub> ) <sub>2</sub> C <sub>18</sub> H <sub>37</sub>	Clam shape Direct method	89	66	x	x	x	<10	<10
	Barrel shape method 1	53	49	43	34	26	<10	<10
	Barrel shape method 2	62	58	45	39	33	<10	<10
(C <sub>2</sub> H <sub>5</sub> O) <sub>3</sub> Si(CH <sub>2</sub> ) <sub>3</sub> NCO + Cl <sub>3</sub> SiC <sub>6</sub> H <sub>5</sub>	Clam shape	61	x	x	x	x	<10	<10
	Barrel shape method 1	52	29	31	26	16	<10	<10
	Barrel shape method 2	56	37	35	28	25	<10	<10
(CH <sub>3</sub> O) <sub>4</sub> Si + (CH <sub>3</sub> O) <sub>3</sub> Si(CH <sub>2</sub> ) <sub>2</sub> C <sub>6</sub> F <sub>13</sub>	Clam shape	67	65	56	45	x	x	x
	Barrel shape method 1	56	54	52	43	38	32	25
	Barrel shape method 2	58	53	54	43	41	36	31

Barrel shape method 1 = Contact angle estimate base on geometry method.  
Barrel shape method 2= Contact angle measurement based on direct software measurement.

Clam shape droplets of NG on the dimethyl siloxy surface demonstrating contact angles of NG ( $\sim 70^\circ$ ) were observed. Fibers treated with TMOS further modified with perfluoroalkyl demonstrated a sufficient degree of lyophobicity but slightly increased in wetting compared to NC fibers treated with silyl propyl perfluoroalkyl.

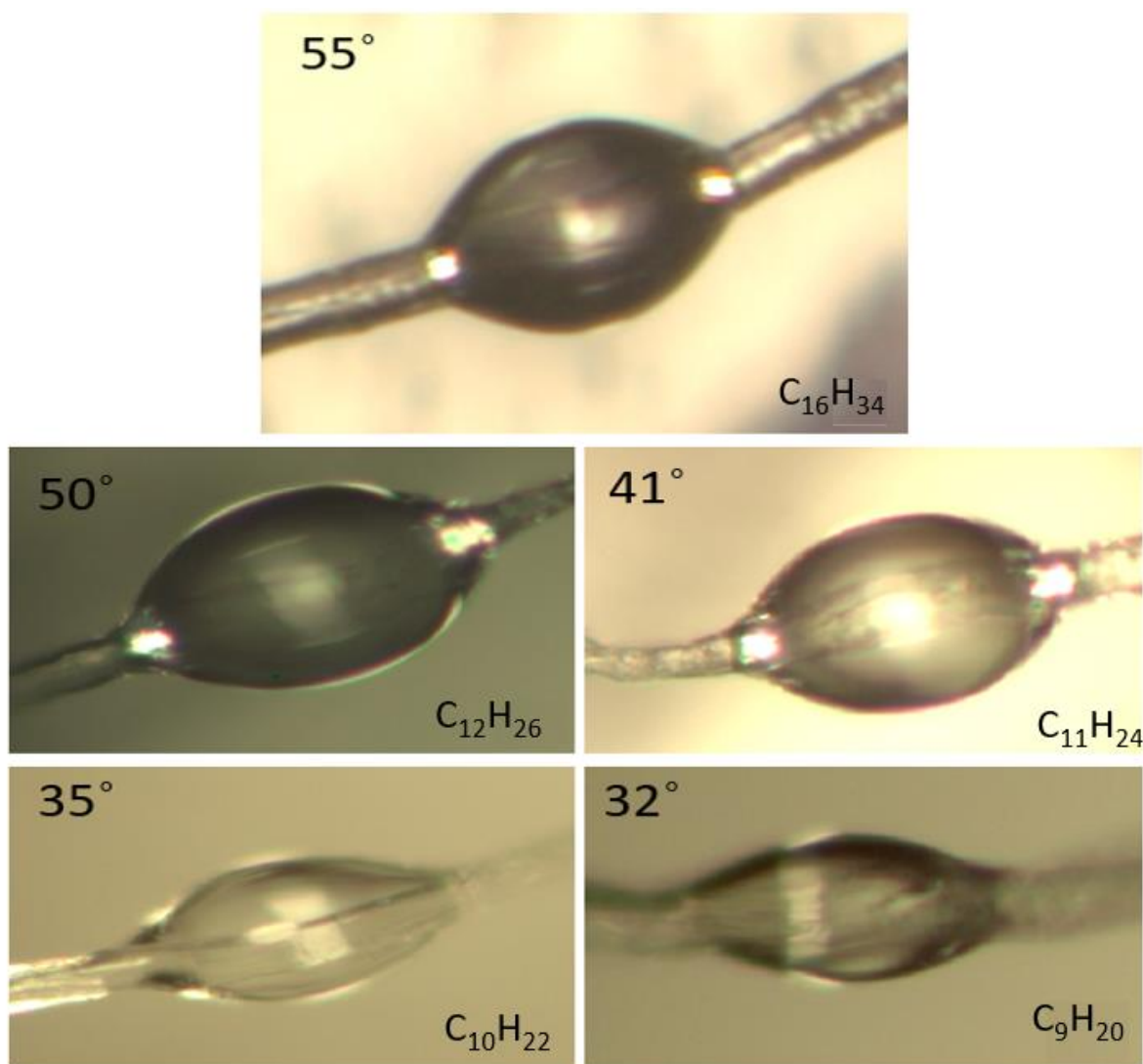
Previous work states that cylindrical fibers can cause the drop to take on a different shape when compared to probe fluids placed on a flat surface.<sup>116</sup> It has been determined that even a contact angle of  $0^\circ$  measured on a bulk surface may result in droplet formation on cylindrical fibers.<sup>108</sup> This is evident for alkane hydrocarbon droplets in equilibrium with NC fibers treated with octadecylsilane. Wetting with dispersive alkane liquids, i.e. (hexadecane ( $C_{16}$ ), dodecane ( $C_{12}$ ), undecane ( $C_{11}$ ), decane ( $C_{10}$ ), nonane ( $C_9$ )), on surfaces treated with octadecylsilane have been previously reported.<sup>33, 101</sup> In our work we observed the presence of  $C_{16}$ ,  $C_{12}$ , and  $C_{11}$  droplets on octadecyl silane reacted on silyl-propyl treated NC fibers, demonstrating the exclusive formation of barrel shape droplets. Hexadecane shows an average estimated contact angle of  $\sim 43^\circ$  for both top and bottom barrel shape droplets. Droplets of dodecane were also prevalent on octadecylsilane treated NC with decreasing contact angle measurements ranging  $\sim 30$ - $35^\circ$ . Undecane droplets were observed less frequently with contact angles estimated  $\sim 25$ - $27^\circ$ . Silyl-propyl treated fibers demonstrate a degree of lyophobicity with *n*-alkane (*n*-hexadecane) liquid comparable to its bulk form observed from results recorded from our previous work.<sup>101</sup>

The decrease in contact angle is typical of the barrel shape formation and is due to increased droplet volume, resulting in lower contact angle values compared to clam shape droplets.<sup>104-106</sup> Typically, smaller volume droplets produce clam shaped droplets with higher contact angles, resulting in a non-axial symmetric mode on the fiber surface. However,

previous work has shown that equivalent volume droplets of barrel and clam-shaped conformations can co-exist on the same fiber.<sup>104-105</sup> Our treated NC fibers collected an observed distribution of barrel and clam shape NG droplets, resulting in two droplet formations co-existing in equilibrium. This observation was for water, hexadecane, and NG as probe fluids. The *n*-alkanes (C<sub>9</sub>-C<sub>12</sub>) presented predominantly barrel-shaped conformations on the treated fibers because of the purely dispersive properties of alkane liquids allowing the axisymmetric barrel morphology to engulf the fiber.

#### 4.5.1 Critical Surface Tension

Zisman demonstrated that contact angles ( $\theta$ ) decrease linearly with surface tension of probe fluids (Equation 4-2).<sup>26</sup> This pattern related to contact angles of different liquids on a low energy surface was first studied by Zisman et al. The workers measured contact angles for a series of probe fluids on a polytetrafluorethylene (PTFE) surface.<sup>26</sup> Zisman et al. discovered that there as a linear dependence of cosine theta with surface tension (Table 4-6). For this study, a series of dispersive hydrocarbon based probe fluids were used: octane, nonane, decane, undecane, dodecane, and hexadecane. The direct measurement of droplets of these probe fluids on NC fibers treated with C<sub>6</sub>F<sub>13</sub> are pictured in Figure 4-6. The surface tension of these liquids are plotted against the cosine value of the corresponding contact angle. Surface tension values of the probe fluids used for this work can be found in literature.<sup>23,25</sup> Critical surface tension results on NC treated fiber surfaces are shown in Table 4-4. Perfluoroalkyl NC show  $\gamma_c = 19.86 \text{ mJ/m}^2$  similar to Teflon.<sup>19</sup> Bulk surface of dimethyldichlorosilane treated nitrocellulose show a comparable critical surface tension to literature values  $\sim \gamma_c = 22.5 \text{ mJ/m}^2$ .



**Figure 4- 5:** Contact angles of n-alkanes on  $C_6F_{13}$  treated nitrocellulose fibers.

An attempt was made to incorporate nitroglycerin and water as part of the Zisman plot, but this addition resulted in lack of linearity. Therefore, it is our assumption that nitroglycerin tends to behave more like a polar solvent such as water on the surface of our functionalized NC surfaces rather than the non-polar dispersive nature of long chain hydrocarbons. With contact angle measurements from dispersive liquids we were able to construct Zisman plots to calculate critical surface tension ( $\gamma_c$ ) of treated fibers (Table 4-6).

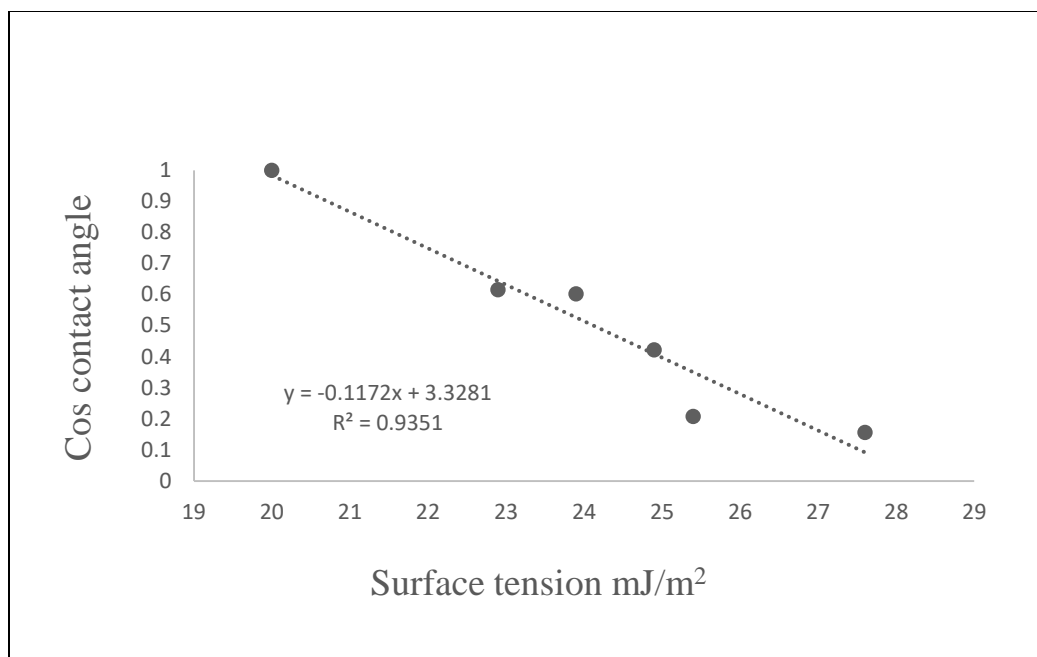
$$\cos \theta = 1 - \beta(\gamma_{LV} - \gamma_C) \quad \text{Eq. 4- 2}$$

**Table 4- 3:** Critical Surface Tension of Treated Nitrocellulose Fibers and Well Defined Solid surfaces of Different Composition.

	$\gamma_C$ mJ/m <sup>2</sup>
NC + (C <sub>2</sub> H <sub>5</sub> O) <sub>3</sub> Si(CH <sub>2</sub> ) <sub>3</sub> NCO	22
NC + (C <sub>2</sub> H <sub>5</sub> O) <sub>3</sub> Si(CH <sub>2</sub> ) <sub>3</sub> NCO + (CH <sub>3</sub> O) <sub>3</sub> Si(CH <sub>2</sub> ) <sub>2</sub> C <sub>6</sub> F <sub>13</sub>	18
NC + (C <sub>2</sub> H <sub>5</sub> O) <sub>3</sub> Si(CH <sub>2</sub> ) <sub>3</sub> NCO + ClSi(CH <sub>3</sub> ) <sub>2</sub> C <sub>18</sub> H <sub>37</sub>	19
NC + (C <sub>2</sub> H <sub>5</sub> O) <sub>3</sub> Si(CH <sub>2</sub> ) <sub>3</sub> NCO + Cl <sub>2</sub> Si(CH <sub>3</sub> ) <sub>2</sub>	22
NC + (CH <sub>3</sub> O) <sub>4</sub> Si + (CH <sub>3</sub> O) <sub>3</sub> Si(CH <sub>2</sub> ) <sub>2</sub> C <sub>6</sub> F <sub>13</sub>	21
Perfluoroeicosan: -[CF <sub>3</sub> ] <sub>n</sub> -	10.6
Poly(tetrafluoroethylene), Teflon: -[CF <sub>2</sub> ] <sub>n</sub> -	18.5
OSi(CH <sub>3</sub> ) <sub>2</sub> poly(dimethylsiloxane)	22

Unlike bulk surfaces with the same functionality,  $\gamma_C$  values from *n*-alkanes were possible on octadecyl silane (13.96 mJ/m<sup>2</sup>) and silyl-propyl (21.35 mJ/m<sup>2</sup>) treated fibers. NC fibers, because of a rigid cylindrical shape allows a capillary effect. This provides a degree of lyophobicity on the surface of the treated fiber. NC fibers treated with silyl- propyl with further addition of perfluoroalkyl generate a  $\gamma_C$  value of ~18.5 mJ/m<sup>2</sup> with contact angle measurements taken from barrel-shaped droplets and a  $\gamma_C$  of ~21.1 mJ/m<sup>2</sup> when using contact angle measurements from clam-shaped droplets. The  $\gamma_C$  of the bulk surface was measured at ~19.86 mJ/m<sup>2</sup>. NC fibers treated with TMOS with the addition of perfluoroalkyl, generate  $\gamma_C$  results of ~21.1 mJ/m<sup>2</sup> for both barrel and clam-shaped droplets.





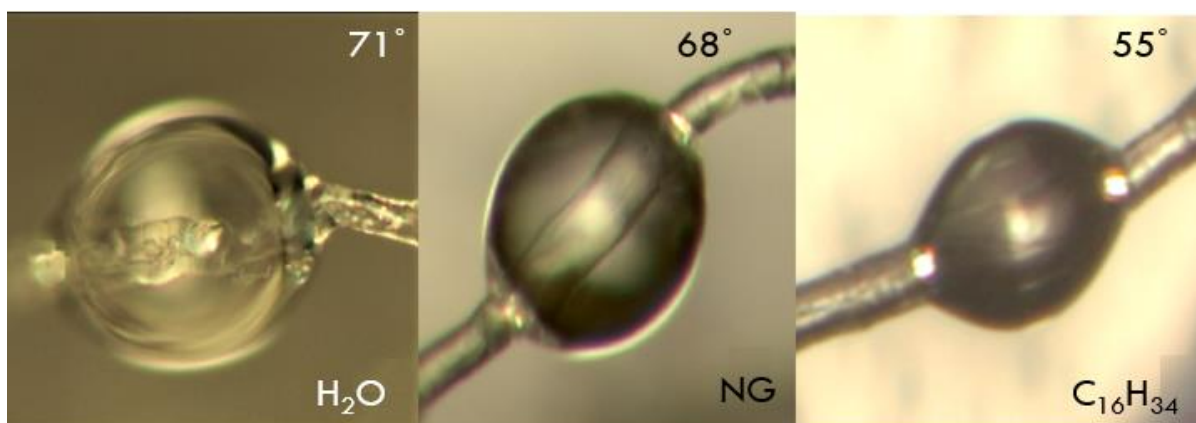
**Figure 4- 6:** Zisman plot from nitrocellulose fibers treated with perfluoroalkyl silane.

NC fibers treated with polydimethylsilane (PDMS) demonstrated exclusive barrel shaped droplets with the *n*-alkane probe fluids giving a  $\gamma_C$  value of  $\sim 21.61 \text{ mJ/m}^2$  compared to the bulk surface measured at  $\sim 22.57 \text{ mJ/m}^2$ .

#### 4.5.2 Surface Energy on Treated Fibers

When discussing the measureable parameters pertaining to the Young's equation, only  $\gamma^{LV}$  can be readily measured.<sup>118</sup> The Young equation can however, provide the difference between the solid-vapor surface tension  $\gamma^{SV}$  and the solid-liquid interfacial tension  $\gamma^{SL}$ . Extensive research providing a list of methods of solid surface tension has determined that  $\gamma^{SV}$  can be determined when  $\gamma^{LV}$  and the contact angle are known.<sup>19, 118-122</sup> In this work, we utilize two methods of calculating  $\gamma^{SV}$ .<sup>118-122</sup> We utilized our intrinsic contact angle ( $\theta_{Adv}$ ) measurements using the probe fluids *n*-hexadecane and H<sub>2</sub>O to gain insight on the surface

energies of the droplets on NC fibers. The liquid surface tension  $\gamma^{LV}$  of these two probe fluids have been confirmed in literature.<sup>25,26,27</sup> *n*-Hexadecane is known to have a liquid surface tension of ( $\gamma^{LV} = 27.6 \text{ mJ/m}^2$ ).  $\text{H}_2\text{O}$  possesses a dispersive value ( $\gamma^{LV \text{ dispersive}} = 21.8 \text{ mJ/m}^2$ ) and an acid/base component ( $\gamma^{LV \text{ A/B}} = 51 \text{ mJ/m}^2$ ).<sup>27</sup> We also use the surface tension and  $\theta_{\text{Adv}}$  of nitroglycerin ( $\sim 50 \text{ mJ/m}^2$ )<sup>25</sup> to calculate solid surface energies  $\gamma^{\text{SV}}$  of the NC functionalized surfaces using the Li-Neumann method. Figure 4-7 illustrates barrel shaped droplets of water, hexadecane, and nitroglycerin on fibers of NC treated with  $\text{C}_6\text{F}_{13}$ .



**Figure 4- 7:** Barrel droplets on NC treated with  $\text{C}_6\text{F}_{13}$  used for measuring surface energies.

The van Oss-Good-Chaudhury (OCG) theory for solid surface energy is for parameters in which the direct measurement cannot be performed. This theory estimates the acid and base components are attained by solving model equations derived from Young's equation. It takes into account the experimental values of the liquid surface tension and the appropriate contact angle for a liquid-solid pair.<sup>118-122</sup> According to the Young's equation, there is a relationship between the contact angle and the surface tension of the liquid, the interfacial transfer between the solid and liquid, and the surface energy of the solid.<sup>18</sup> This approach operates under the assumptions that only dispersive interactions are present at the interface and the

Young's equation is reduced to equation 4-3.<sup>119-121</sup>

$$\gamma_{SV} = \frac{\gamma_{LV}}{4}(1 + \cos \theta)^2 \quad \text{Eq. 4- 3}$$

The OCG method involves the surface tension of at least two liquids. In doing so, the solid surface energy is divided into a dispersive part, a Lewis acid part, and a Lewis base part.<sup>119-</sup>

<sup>121</sup> The base component describes a surface's tendency to have interactions with a second surface that has the ability to act basic by donating an electron. The acid component has opposite tendencies, and acts as an acid by accepting electrons. This method assumes free surface energies of the solid and a liquid can be presented as added properties of the dispersive and acid base components<sup>121</sup>, so Young's equation is written as described in 4-3.

$$\gamma_{LV}(1 + \cos \theta) = 2 \left( \sqrt{\gamma_{SV}^d \cdot \gamma_{LV}^d} + \sqrt{\gamma_{SV}^{AB} \cdot \gamma_{LV}^{AB}} \right) \quad \text{Eq. 4- 4}$$

For this work we utilized water and *n*-hexadecane as probe fluids to obtain contact angles on our surfaces. Since *n*-hexadecane as well as other saturated hydrocarbons are purely dispersive liquids,  $\gamma_{SV}^{AB}=0$ ,  $\gamma_{SV}^d$  can be derived from equation 4-2. The acid-base component can then be determined by using equation 4-3 using the contact angle of water.

The Li-Neumann equation of state method for solid surface tension of solids is derived from a thermodynamic point of view.<sup>118</sup> The existence of an equation of state implies that the equilibrium contact angle is a unique function of only free surface energies of solid

and liquid (equation 4-4).<sup>118</sup> This method does not take into account molecular origins of surface tension and suffers limitations because the theory only takes one liquid into account, so the choice of liquid probe fluid for contact angle measurement profoundly effects the resulting surface energy.<sup>118</sup> However, the Li-Neumann's method gives good results on low energy surfaces.<sup>19, 100</sup>

$$\cos \theta = -1 + 2\sqrt{\frac{\gamma_{SV}}{\gamma_{LV}}} \times \exp\left[-0.0001247(\gamma_{LV} - \gamma_{SV})^2\right] \quad \text{Eq. 4- 5}$$

The lowest surface energies of bulk surfaces are observed with the NC surface modified with C<sub>6</sub>F<sub>13</sub>. These surface energies are consistent with results observed in literature with the average documented results being ~12mJ/m<sup>2</sup>. The results for silane functionalized surfaces, such as dimethyl siloxane are also consistent with literature values ranging ~20-30 mJ/m<sup>2</sup>.

Surface energies ( $\gamma_{sv}$ ) were calculated using contact angle measurements estimated from and fiber contact angles using software application for contact angle estimations described above. Table 4-5 gives surface energy values fiber surfaces utilizing OCG (dispersive and acid base approach) and Li-Neumann approaches.

Surface energy measurements for NG on the silyl propyl fiber surfaces were ~42 mJ/m<sup>2</sup> for barrel droplet shapes using the Li-Newmann method, demonstrating a slightly higher surface energy consistent with mixed surface containing polar and non-polar functionalities. For silyl propyl NC surfaces, averaging the surface energies generated from H<sub>2</sub>O and hexadecane probe fluids using the Li-Newmann and the total of acid/base values using OCG methods show averaged barrel shaped droplets (HD & H<sub>2</sub>O) resulted in values of

39.4 mJ/m<sup>2</sup> (Li-Newmann) and 51.8 mJ/m<sup>2</sup> (OCG). The increase of surface energy on silyl propyl NC fibers is due to a high contribution of polar (H<sub>2</sub>O) interactions ( $\gamma_{sv}^{AB}$  29.0 and 20.25 mJ/m<sup>2</sup>) for barrel shaped droplets, because of the increased wetting by water.

The lowest surface energies were observed on silyl propyl perfluoroalkyl treated NC fibers. Average surface energies generated from H<sub>2</sub>O and hexadecane probe fluids using the Li-Newmann and OCG methods show barrel shaped droplets with values of ~31.5 mJ/m<sup>2</sup> (Li-Newmann) and ~37.4 mJ/m<sup>2</sup> (OCG). Polar contributions were estimated at  $\gamma_{sv}^{AB}$  22.44 for barrel droplets. The surface energies calculated using the Li-Newmann method for silyl-propyl-fluoro-alkyl surface using NG as a probe fluid resulted in 31.3 mJ/m<sup>2</sup> for barrel-shape droplets. The octadecyl silyl treated NC fibers gave ~34 and 28 mJ/m<sup>2</sup> for barrel shape droplets using the Li-Newmann method to estimate surface energy. The OCG surface energy values for barrel shape droplets (H<sub>2</sub>O/hexadecane) on octadecyl silane fiber surfaces was calculated at ~44 mJ/m<sup>2</sup>. NC fibers treated with PDMS show ~34.8 (Li-Newmann) and 41.74 mJ/m<sup>2</sup> (OCG) for barrel-shaped droplets on fiber surfaces. The polar contribution was estimated at more than half ( $\gamma_{sv}^{AB}$  ~21.6 mJ/m<sup>2</sup>) of the total surface energy estimated by the OCG method for the barrel-shape conformation, indicating significant increase in surface energy compared to literature values, resulting from increased wetting with water. Literature values for surface energy estimated from contact angles obtained from the PDMS surfaces are a beneficial parameter, since it has been determined that hysteresis is negligible (2-3°), suggesting a well ordered surface.<sup>93</sup> The negligible hysteresis infers a more reliable advancing contact angle for deriving surface energy.

We estimated the free surface energy (Li-Newmann method) of NC phenyl-silane surface using NG as a probe fluid. The surface energy for barrel-shaped droplets on phenyl-

silyl NC treated fibers obtained from water and hexadecane (Li-Newmman method) probe fluids was estimated at ( $\gamma_{SV}$  35.15 mJ/m<sup>2</sup>) for barrel droplets respectively). OCG surface energy estimations for barrel droplets on pheny silyl treated fibers were estimated ~49.1 and 42.09 mJ/m<sup>2</sup>, with the polar contributions  $\gamma_{SV}^{AB}$  ~24.0 and 21.24 mJ/m<sup>2</sup> respectively.

**Table 4- 4:** Surface Energy Values of Treated Surfaces.

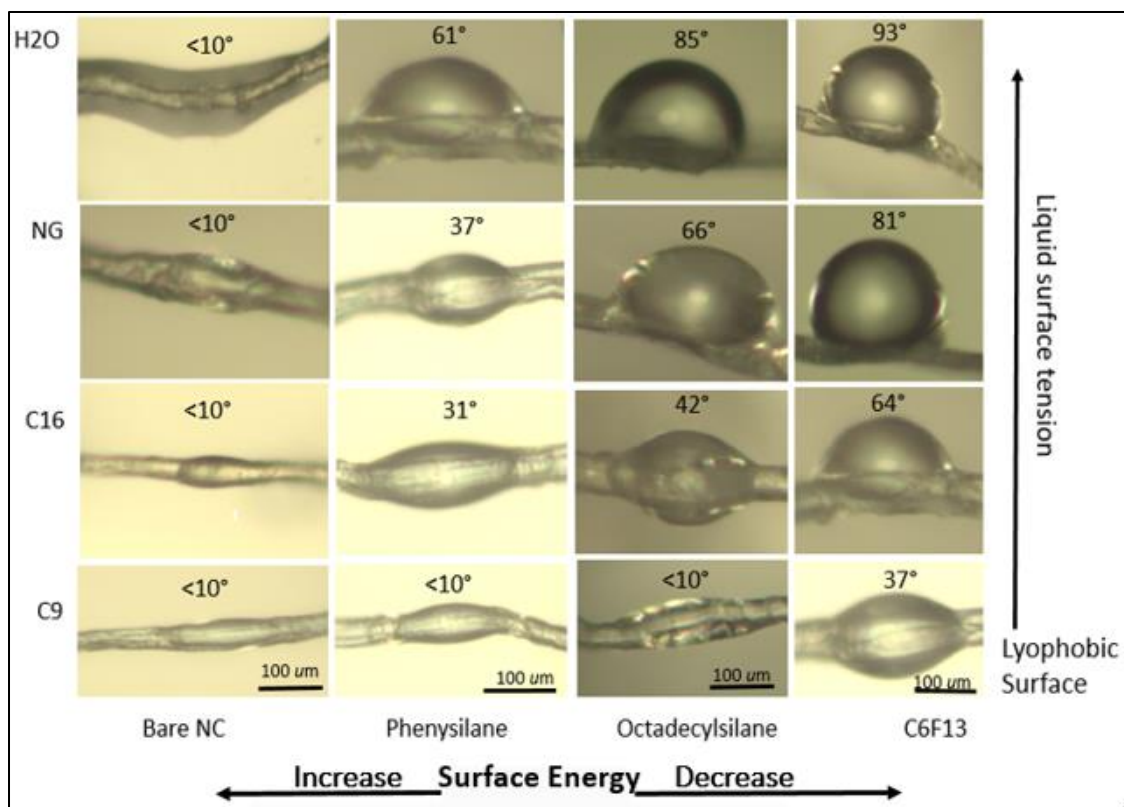
	Eq. 4-4 H <sub>2</sub> O Probe fluid	Eq. 4-4 HD probe fluid	Eq. 4-3 NG probe fluid	Eq. 4-3 Acid/ Base HD	Eq. 4-3 Acid/ Base H <sub>2</sub> O	Eq. 4-3 H <sub>2</sub> O + HD
Functionalized NC surface	$\gamma_{SV}$ (mJ/m <sup>2</sup> )	$\gamma_{SV}$ (mJ/m <sup>2</sup> )	$\gamma_{SV}$ (mJ/m <sup>2</sup> )	$\gamma_{SV}$ (mJ/m <sup>2</sup> )	$\gamma_{SV}$ (mJ/m <sup>2</sup> )	$\gamma_{SV}^{ab}$ (mJ/m <sup>2</sup> )
NC + (C <sub>2</sub> H <sub>5</sub> O) <sub>3</sub> Si(CH <sub>2</sub> ) <sub>3</sub> NCO	54.3	21.5	41.7	21.3	29.4	50.7
NC + (C <sub>2</sub> H <sub>5</sub> O) <sub>3</sub> Si(CH <sub>2</sub> ) <sub>3</sub> NCO + (CH <sub>3</sub> O) <sub>3</sub> Si(CH <sub>2</sub> ) <sub>2</sub> C <sub>6</sub> F <sub>13</sub>	41.1	17.5	27	17.1	16.8	33.9
NC + (C <sub>2</sub> H <sub>5</sub> O) <sub>3</sub> Si(CH <sub>2</sub> ) <sub>3</sub> NCO + ClSi(CH <sub>3</sub> ) <sub>2</sub> C <sub>18</sub> H <sub>37</sub>	46.7	20.4	31.9	20	23.3	39.9
NC + (C <sub>2</sub> H <sub>5</sub> O) <sub>3</sub> Si(CH <sub>2</sub> ) <sub>3</sub> NCO + Cl <sub>2</sub> Si(CH <sub>3</sub> ) <sub>2</sub>	44.2	19	33.3	19	26	44.7
NC + (C <sub>2</sub> H <sub>5</sub> O) <sub>3</sub> Si(CH <sub>2</sub> ) <sub>3</sub> NCO + Cl <sub>3</sub> SiC <sub>6</sub> H <sub>5</sub>	50.2	23	41.3	22.8	23.3	46.1
NC + (CH <sub>3</sub> O) <sub>4</sub> Si + (CH <sub>3</sub> O) <sub>3</sub> Si(CH <sub>2</sub> ) <sub>2</sub> C <sub>6</sub> F <sub>13</sub>	49	17.8	34.2	17.4	25.7	43.1

## 4.6 Discussion

Within the same fiber we demonstrate two parameters  $\gamma_{LV}$  and  $\gamma_{SV}$  and how these parameters not only influence contact angle but drop morphology. With this knowledge we can control the wettability on NC. Migration, percolation, and wetting of NG can be controlled. On fibers, we have additional parameter which is drop morphology. Figure 4-8 demonstrates the wetting control on NC treated fibers with perfluoroalkyl, octadecyl, and phenyl silanes compared to the complete wetting of bare NC fibers. The decreased linearity of surface energy with increased contact angle and surface tension is evident in figure 4-7. Equilibria of clam shape  $H_2O$  droplets on low surface energy surfaces is predominant on the treated fiber surfaces. Clam shell shape droplets of NG on perfluoroalkyl and octadecylsilane demonstrate the formation of non-axisymmetrical geometry on low surface energy fiber surfaces while phenyl silane treated fibers with higher surface energy demonstrate barrel shape droplets of NG on the fibers surface. This observation describes the ability of the “tuneable” functionality to control the contact angle and the drop morphology at the fiber level.

## 4.7 Conclusions

In this work we explored methodology to characterize the surface chemistry approach of nitrocellulose (NC) to control its wetting and to reduce sweating with energetic plasticizer nitroglycerine (NG). Reactions produced lyophobic surfaces with probe fluids agreed with those reported for the closely-packed monolayers of  $CF_3$ ,  $CH_3$ , and Phenyl-functionalities supported on Si wafers. For NC+NCO reacted with  $C_{18}H_{37}$  and phenyl-silanes,  $H_2O$  contact. Angles were high (85-100°) while the hexadecane contact angles were low (<10°) providing



**Figure 4- 8:** Wetting control on fibers.

examples of hydrophobic yet oleophilic surfaces.

Wettability of functionalized NC fibers was studied by measuring droplets of probe fluids on NC fibers using optical microscopy with water NG, hexadecane, dodecane, undecane, decane, and nonane as probe fluids. Formation of barrel and clam shape fibers were observed on the treated surfaces. Contact angles of fibers resulted in lower measurements compared to the same material in bulk pellet form. The NG contact angles of the treated fibers ranged as follows: fluoroalkyl-NC ( $\theta_{\text{clam}}/\theta_{\text{barrel-shape}} \sim 90^\circ/\sim 50^\circ$ ), alkyl-NC ( $\sim 75^\circ/\sim 35^\circ$ ), oligo (dimethylsiloxyl)-NC ( $\sim 65^\circ/\sim 35^\circ$ ), phenyl-NC ( $\sim 40^\circ/\sim 10^\circ$ ), untreated NC ( $<10^\circ$ ), demonstrating major variations in surface energy in accordance with the nature of surface functionalities.



Critical surface tension  $\gamma_c$  from *n*-alkanes were possible on octadecyl silane (13.96 mJ/m<sup>2</sup>) and silyl-propyl (21.35 mJ/m<sup>2</sup>) treated fibers, unlike bulk surfaces with the same functionality due capillary effect. Surface energies on bulk and treated fibers were in accordance with measured contact angles. Treated fibers demonstrate higher surface energies due to lower lyophobicity of cylindrical fibers.

## **Chapter 5: Porosity and Surface Characterization using Nitrogen Adsorption and Stability of Functionalized Nitrocellulose**

### **5.1 Abstract**

In our previous work nitrocellulose was functionalized by a two-step process using the reaction of 3-(triethoxysilyl-propyl isocyanate followed by reactions with either alkyl-, fluoroalkyl, or phenyl silane producing NC surfaces ranging in lyophobicity.<sup>102</sup> In this work we studied the sorption parameters of nitrogen on untreated NC and surface treated NC. We find the nitrogen adsorption on untreated 12.47% NC demonstrates a Type IV isotherm with narrow hysteresis, evident of secondary porosity<sup>128</sup>. We utilized the BET theory to obtain information about the distribution of nitrogen to include surface area and C constant. C constant values were consistent with the lyophobicity calculated from previous work.<sup>102</sup> The  $\alpha_s$  method showed the nitrogen isotherm for bare NC was comparable with standard data from nonporous solid, and the treatment of NC with silane demonstrated the presence of micropores. We utilized the BJH method to estimate the pore size distribution of the desorption branch of isotherms.

Lower surface energy and increased lyophobicity of modified NC demonstrated increased thermal stability and equivalent energetic properties compared to bare NC in the presence of NG when exposed to increased temperature and humidity. For stability testing at 25°C (10% RH) hydrophobicity remained constant on the fluoro alkyl treated NC surface demonstrates non-wetting at elevated temperatures. In the presence of 80% RH at 25°C, the

homogenous fluoro alkyl surface maintained adequate hydrophobicity ( $\sim 85^\circ$ ). The bare NC exposed to the fluoro-alkyl treated NC demonstrated increased stability in nitrogen content compared to bare NC, an indication of maintaining nitro group stabilization when exposed to extreme environments. Modified NC pellets doped with NG droplets were aged at ambient and elevated temperatures, dry, and in the presence of 80% relative humidity (RH). Samples were characterized and compared with bare NC.

## 5.2 Introduction

It is known that cellulose demonstrates a variety of morphologies resulting from the wide variety of cellulose materials derived from natural products e.g. wood pulp, cotton, bamboo etc.<sup>129</sup> In natural cellulose material, the cellulose polymer chains are arranged in microfibrils with various diameter sizes in the range of 2-25 nm.<sup>129</sup> During the process of nitrating cellulose, swelling of the cellulose fibers from solvent exposure results in the change of fiber volume.<sup>130</sup> It is expected that the nitration of cellulose changes the adsorption properties of all structural elements within the fiber to include the molecular chains and ending with the large polymers.<sup>130</sup> We suggest that within our previous work,<sup>101</sup> it is expected that the NC fiber morphology will change as a result of surface modification. It is also expected that adsorption experiments will verify the wetting studies we performed on the modified NC. We found that fluoroalkylsilane, *n*-octadecylsilane, dimethyldichlorosilane, and phenyltrichlorosilane demonstrate various degrees of hydro/lyophobicity when reacted with 3-(triethoxysilylpropyl) isocyanate or tetramethoxysilane on the surface of NC. In this work, we measure N<sub>2</sub> sorption of military grade NC derived from wood pulp. According to literature, the adsorption properties of the cellulose used for nitration, will depend on the raw

material in which it was derived. In this chapter we discuss adsorption properties of bare NC and treatment of NC with silane. In this chapter, we also utilized several techniques to characterize the surface functionalization of military grade nitrocellulose (NC). Here, we report a rigorous set of characterization parameters to confirm surface modification, fiber lyophobicity, and thermal stability. Apparent contact angle measurements using water as probe fluid, DSC analysis, and elemental composition were used to monitor the thermal stability of conditioned modified NC in the presence of surface NG.

### **5.3 Physical Adsorption of Vapor: Theoretical Overview**

Adsorption is the process in which a solid (adsorbent) can take up a volume of condensable gas (adsorbate) in which the effectiveness of the solid depends on the exposed surface area and is a result of surface energy.<sup>131</sup> Adsorption can occur by either physical (physisorption) or chemical (chemisorption) forces. For this study our materials were exposed to physical sorption, since we did not observe chemical reactions between adsorbant and adsorbate in our studies. We expected the reactions with NC and gases to be reversible and characteristic of van der Waals forces.<sup>126</sup> Gas adsorption for surface area measurements is physisorption at the critical temperature ( $T_c$ ) at which the adsorbate is in equilibrium between the vapor and liquid phase at a particular pressure. A measured amount of adsorbate is released to the adsorbant (previously purged with heat and vacuum to remove surface contaminants) and adsorption onto the sample occurs until equilibrium is reached. The difference between the amount of gas dosed and amount remaining is the quantity adsorbed, which is plotted versus the equilibrium pressure.<sup>126-133</sup>

## 5.4 Adsorption Isotherms

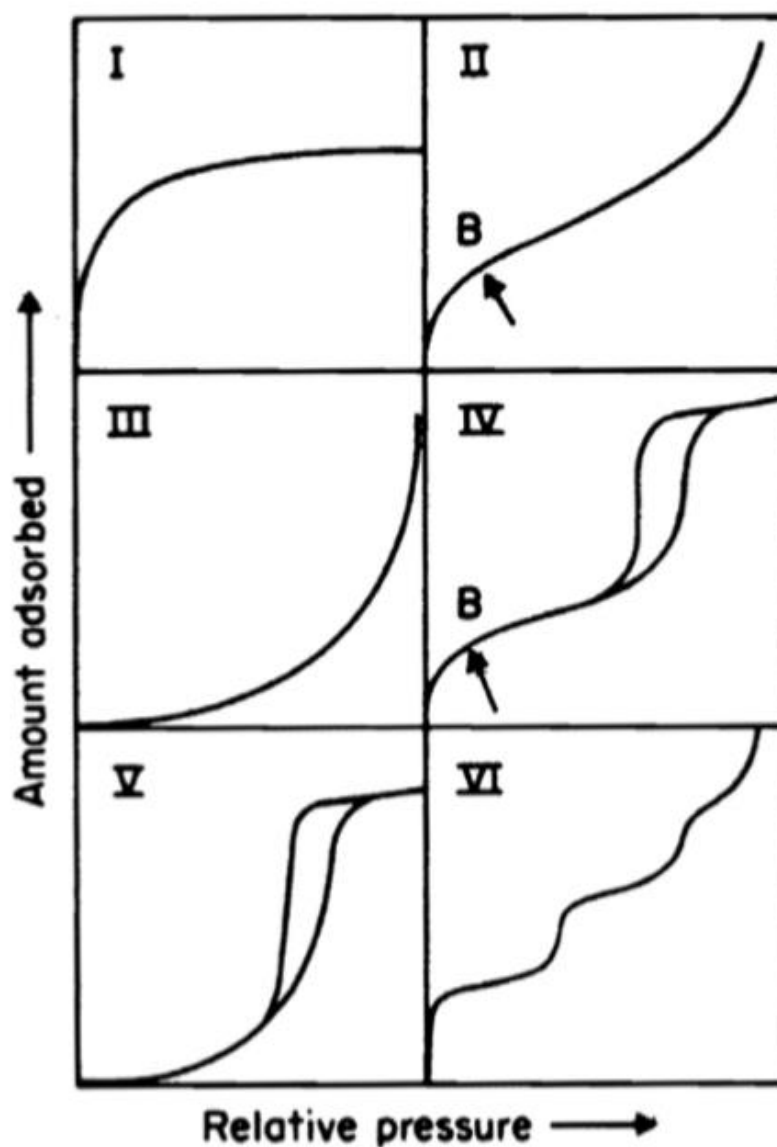
The measurement of sorption enables both adsorption and desorption to be measured and studied. When the term ‘adsorption’ is used discussing adsorption isotherm measurements, it is referring to both adsorption and desorption in which the addition and withdraw of gas may generate a hysteresis loop.<sup>133</sup> The adsorption isotherm is a plot of the quantity of gas adsorbed in moles per gram of adsorbant versus relative pressure ( $p/p_0$ ) in which  $p$  is absolute pressure and  $p_0$  is atmospheric pressure. The relative pressure accounts for the pressure between 0-1 atm. The driving force of adsorption is the minimization of surface energy on a solid.<sup>133-136</sup>

There are two fundamental techniques used to measure adsorption isotherms. The most common technique is volumetric method using nitrogen ( $N_2$ ) adsorption at 77K and standard pressure. Water vapor can also be used as adsorbate in volumetric measurements. In our work we used the conventional procedure for the determination of  $N_2$  adsorption isotherm. This conventional technique makes use of a discontinuous, point-by-point procedure. Successive amounts of the adsorptive are introduced and at each stage the system is allowed sufficient time to attain equilibrium, corresponding to a sequence of points on the adsorption isotherm. This approach is more recent and is dependent on the principle of ‘quasi-equilibrium.’<sup>135</sup>

The second fundamental technique to obtain adsorption isotherms is a gravimetric method using water vapor adsorption at room temperature.<sup>135</sup> Adsorption isotherms resulting from physical adsorption are grouped into five classes (Types I-V) Figure 5-1.

The Type II adsorption isotherm gives evidence of macroporous material (2-50 nm pore width).<sup>133-136</sup> The Type III adsorption isotherm usually represents hydrophobic surfaces

at low water activities and hydrophilic surfaces at high water activities.<sup>133-136</sup> Type IV isotherm is also representative of mesoporous materials and due to capillary condensation, gives a hysteresis loop attributed to the filling and emptying of the pores.<sup>133</sup> Capillary condensation is the occurrence whereby a gas condenses to a liquid phase in a pore at a pressure ( $p$ ) less than the saturation pressure ( $p_0$ ) of the bulk liquid.<sup>133</sup>



**Figure 5- 1:** Types of adsorption isotherms (IUPAC 1985).<sup>139</sup>

*Image reproduced from reference 139, Permission from American Chemical Society, 1993.*

A common feature of Type IV isotherms is a final saturation plateau, of variable length.<sup>133</sup> Type V adsorption isotherm also is representative of adsorption/desorption hysteresis and its initial low uptake due to adsorption onto non-polar surfaces.<sup>133</sup> The Type V isotherm is typically observed with experiments with zeolites.<sup>133</sup> The Type VI adsorption isotherm occurs in a step-wise nature in which each step is allowing monolayer formation on an inhomogeneous surface.<sup>133</sup> The classification of hysteresis loops recommended by IUPAC<sup>137</sup> is displayed by Figure 5-2. This classification is based on experimental observations of classical principles of pore filling, primarily by the use of the Kelvin equation for mesopore analysis.<sup>133-138</sup> Hysteresis loops are typically related with the filling and emptying of mesopores. Type H1 is associated with porous materials consisting of well-defined cylindrical-like pore channels. Type H2 is associated with materials that does not have a well-defined pore shape and pore size distribution. Type H3 is observed in aggregates that have slit-shape pores. Type H4 is associated with narrow slit pores and pores in the micropore region ( $< 2$  nm).<sup>139</sup>

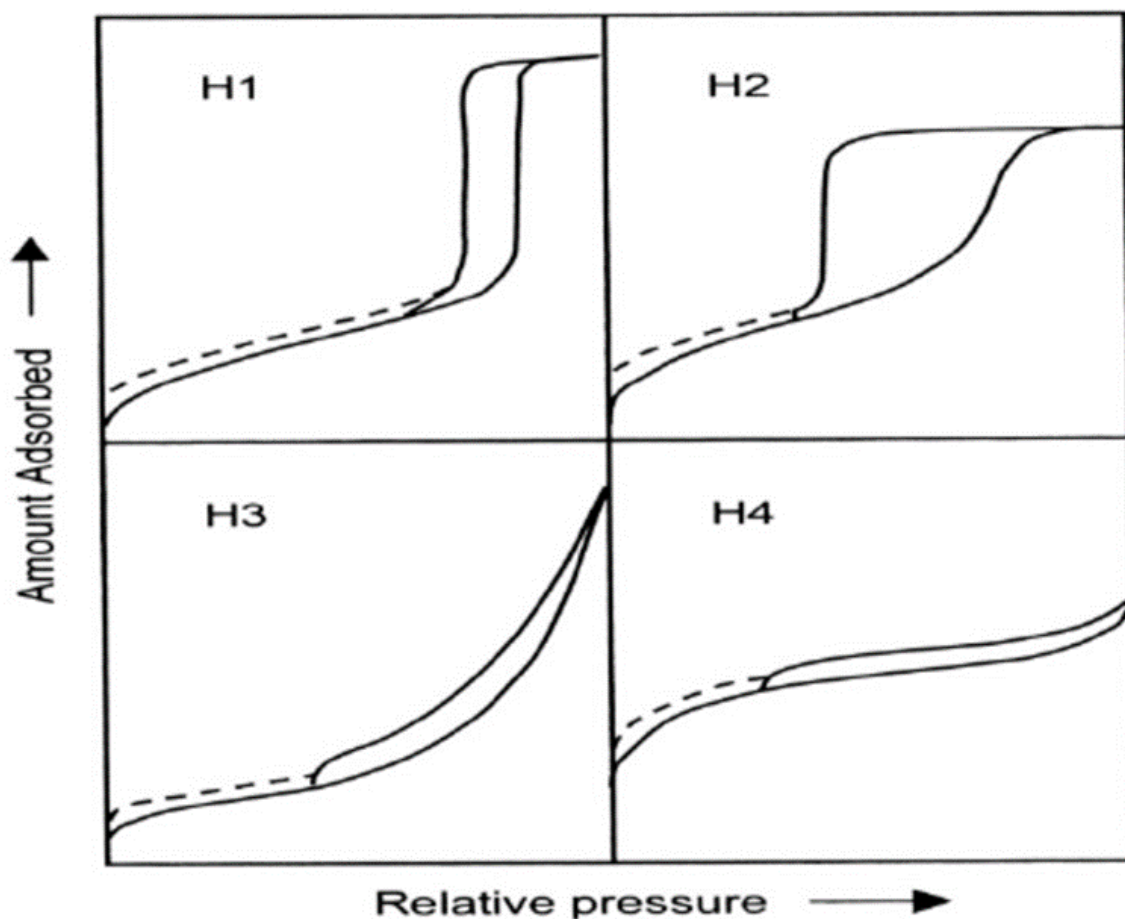
## **5.5 Experimental**

### **5.5.1 General Information**

The nitrocellulose used in this study was a blended military grade cellulose manufactured at Radford AAP, Virginia. Nitroglycerine (NG) was supplied as 5% nitroglycerin in ethanol (SDM 36) by Copperhead Chemical Company. Elemental analysis give a nitrogen content of 12.45%.

### 5.5.2 Nitrogen Adsorption

Nitrogen adsorption isotherms were measured at liquid nitrogen temperature using a Quantachrome iQ sorption analyzer. Samples were purged for eight hours before measurements. The NC was heated 60°C during the degassing process. *Note: Temperatures above 60°C will promote the start of degradation of NC. ~ 1 gram samples were prepared for this experiment.*



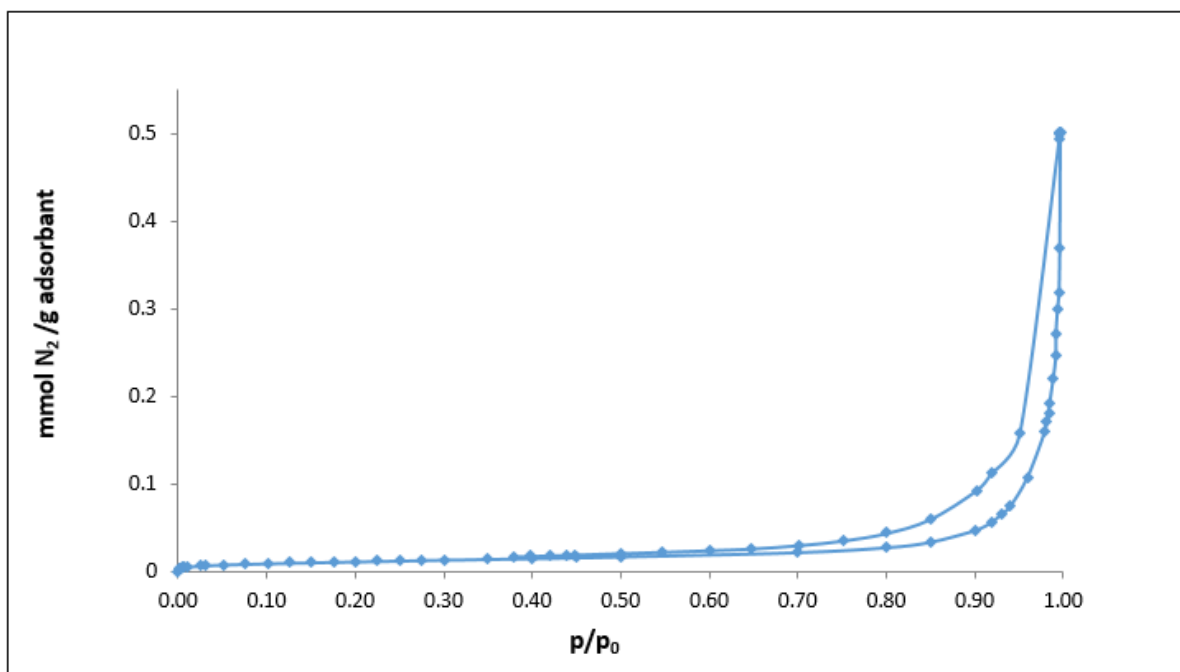
**Figure 5- 2:** Classification of hysteresis loops (IUPAC 1985).<sup>137</sup>

*Image reproduced from reference 137, Permission from American Chemical Society, 1999.*



## 5.6 Nitrogen Adsorption Isotherm on Nitrocellulose

Figure 5-3 shows a nitrogen adsorption isotherm generated from bare military grade nitrocellulose ~12.45%. The experiment was carried out by increasing the pressure up to condensation pressure followed by reduced pressure to observed both the adsorption and desorption branches. The shape of the isotherm and presence of hysteresis could essentially be viewed as Type IV adsorption isotherm. The isotherm presented a narrow hysteresis loop closure at  $\sim .4 p/p_0$  where  $N_2$  can condense as a liquid in pores. This observation is associated with capillary condensation in mesopores. The narrow hysteresis displayed in Figure 5-3, is characteristic of a Type 3 loop, giving evidence of containing slit like pores or perhaps having pores that reside between amorphous particles. According to literature, pore types fall into two categories, either true porosity or secondary porosity.<sup>133,140,141</sup> Previous adsorption studies on cellulose powders designate the material as having a fractal geometry, lacking in uniformity.<sup>131</sup> Therefore, NC may not be porous itself, but may possess pores or aggregates composed of plate-like particles that are behaving similar to mesopores. Although we were dealing with most likely what appears to be secondary porosity,  $N_2$  adsorption allowed for gathering sufficient data for textural characterization of military grade NC, providing results for parameters that have not yet been studied.



**Figure 5- 3:** Nitrogen adsorption isotherm of bare nitrocellulose at 77K.

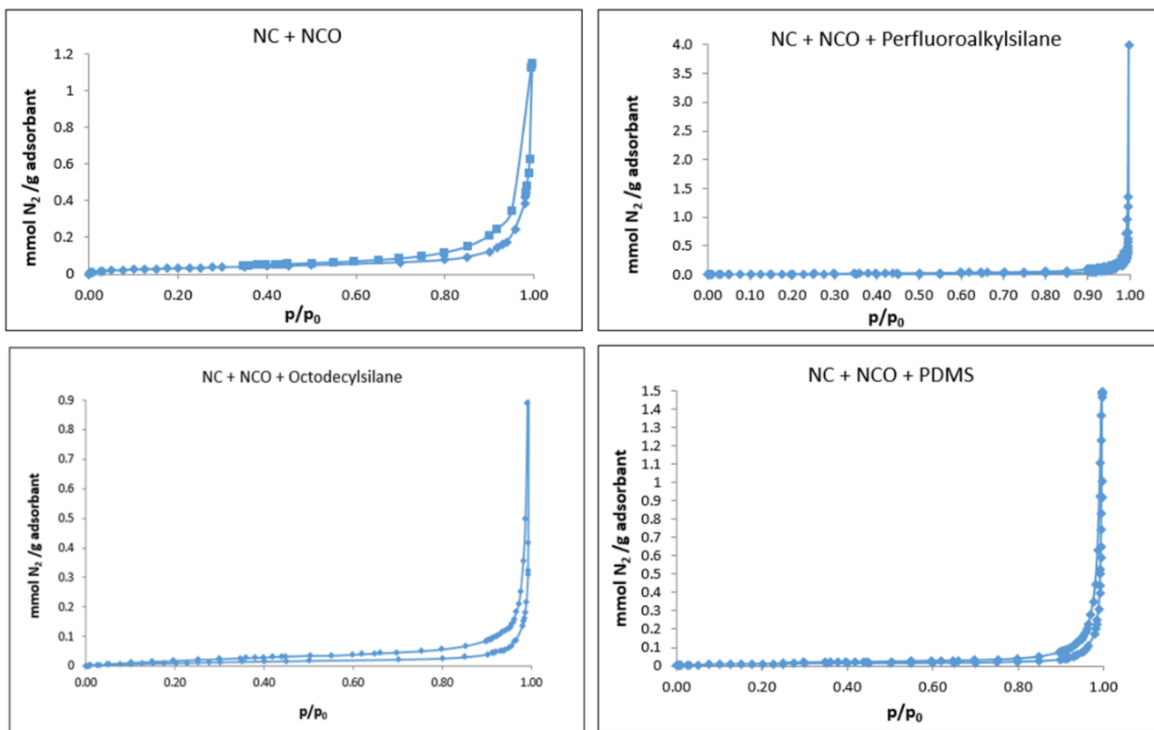
### 5.7 Nitrogen Adsorption Isotherm on Functionalized Nitrocellulose

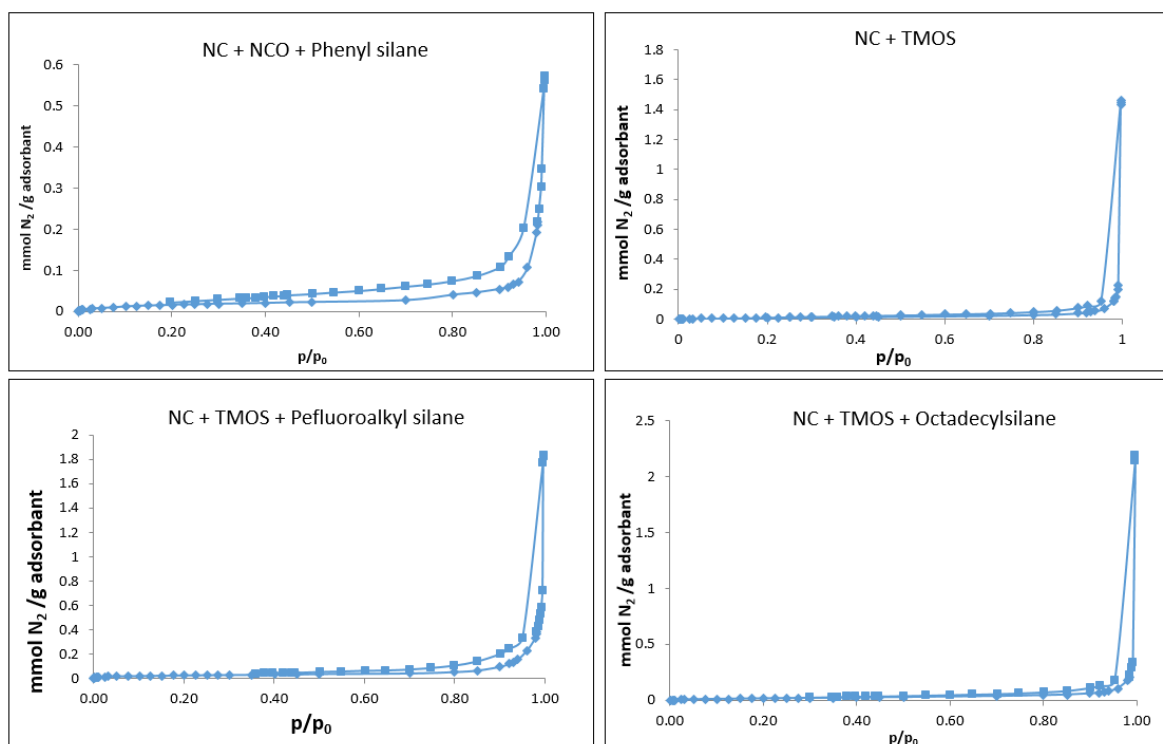
With the functionalization of NC with triethoxysilyl propyl isocyanate (NC+NCO), the formation of carbamate replacing hydroxyl groups on the NC surface demonstrated similar trends regarding isotherm type and narrow hysteresis loop (Figure 5-4). The addition of perfluoralkyl silane resulted in a narrower hysteresis compared to NC or NC+NCO. Perfluoro alkyl, which is characterized by a carbon backbone may have contributed to mesoporous ‘like’ gap closure within the textural make-up of NC, making secondary porosity less noticeable with the addition of perfluoralkyl silane. The significant decrease in surface energy of NC caused by treatment with perfluoralkyl silane is most likely the cause of narrow hysteresis, a result of minimized condensation in the pores. The N<sub>2</sub> adsorption generated from the addition of to the carbamate treated NC slightly lowered the

adsorption pressure but maintained a hysteresis similar to bare NC. The treatment with phenyl silane demonstrated a slightly more open hysteresis loop closing at  $\sim 2$  relative pressure. The direct treatment of tetramethoxysilane (TMOS) with NC showed a drop in mmol of  $N_2$  Per gram of adsorbant compared to bare NC. We will see in the following section that when compared to standard isotherms, adsorption of NC treated with silanes shows trends of micropore formation.

## 5.8 BET Analysis

The BET model developed by Brunauer, Emmett and Teller<sup>131-133</sup> is based on a model of physisorption that is extended from the original Langmuir model that is used for the characterization of porous materials. The Langmuir model takes into consideration the area of adsorption that represents a single monolayer.<sup>133 135</sup> BET is based on an over-simplified





**Figure 5- 4: Nitrogen Adsorption Isotherms of Nitrocellulose**

functionalized with triethoxysilyl propyl isocyanate (NCO), NCO and perfluoroalkylsilane, NCO and octadecylsilane, NCO and phenylsilane, tetramethoxysilane (TMOS), TMOS and perfluoroalkylsilane, TMOS and Octadecylsilane.

assumption that the molecules are formed in layers, in which each layer acts as a bed for the previous layer, and each layer above the latter are assumes liquid-like properties.<sup>131</sup> The best fit for BET is the portion of an isotherm at  $\sim 0.3$   $p/p_0$ , in which this section of the isotherm produces a linear fit of a BET plot that is dependent on the adsorption system and operating temperature. Surface area the  $C$  constant, pore shape, and pore size distribution can be estimated after surface modification. Surface area is obtained using a single point BET method (only one point in the isotherm) or multi point BET method (at least 3 points up to 7 points or 11 points) in this lower  $p/p_0$  region. For our study we used the multi point BET method selecting 10 points for the linear fit. Equation 5-1 gives the BET model where  $n$  is the number of moles of nitrogen adsorbed and  $n_m$  is the monolayer capacity, which is the number of moles of nitrogen that fills a surface of a single monolayer.  $p_0$  is the saturation

vapor pressure and  $c$  is the  $C$  constant given in equation 5-3 where  $(q_1 - q_L)$  is the net heat of adsorption,  $R$  is the constant, and  $T$  is temperature.<sup>133-137</sup> Equation 5-2 is a form of the BET used for plotting.<sup>133-137</sup> Figure 5-5 shows the linearity of BET plot from the  $N_2$  adsorption of bare NC with an  $R^2$  value of .9998 showing defined linearity in BET region. The BET plots shown in Figure 5-5 show that the treatment of NC with triethoxysilyl propyl isocyanate, which forms the carbamate on NC, maintains linearity within the BET portion of the adsorption isotherm compared to bare NC. BET plots of NC treated with additional silanes, slightly dropped in linearity compared to bare NC, although there was not a noticeable scatter of data points away from the linear BET plots (Table 5-1).

$$\frac{n}{n_m} = \frac{c \left( \frac{p}{p^0} \right)}{(1 - p/p^0)(1 + (c - 1) \frac{p}{p^0})} \quad \text{Eq. 5- 1}$$

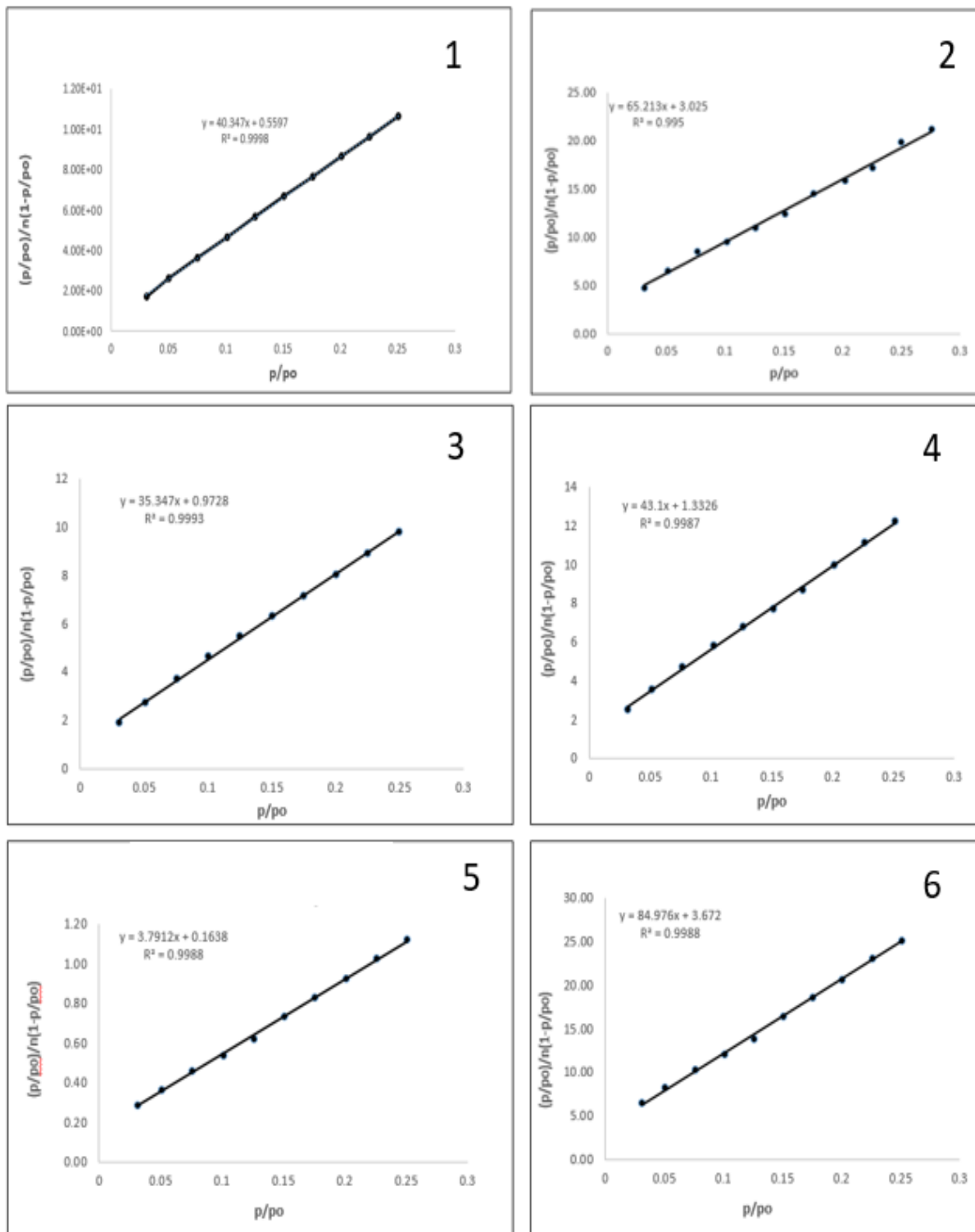
$$\frac{1}{n(p/p^0 - 1)} = \frac{\text{Intercept}}{n_m c} + \frac{\text{Slope}}{n_m c} \frac{p}{p^0} \quad \text{Eq. 5- 2}$$

$$c = e^{(q_1 - q_L)/RT} \quad \text{Eq. 5- 3}$$

In a  $N_2$  isotherm, the interactions are relatively weak and uniform, and the measurement of accumulated nitrogen on the surface of the material provides the surface area. Table 5-1 gives the surface area values ( $S_{BET}$ ) in  $m^2/g$  of bare NC and treated NC. The surface area of

bare NC and its treated surfaces ranged from 1.35-2.70 m<sup>2</sup>/g. These estimate are low based on the nature of the fibrous material. Treated of NC with silane did not significantly change the surface area.

The  $C$ -constant ( $C_{\text{BET}}$ ) is a dimensionless value obtained from equation 5-3 that is related to the heat of adsorption in which it makes no assumptions.<sup>133</sup> It analyzes the true surface energy of the powder. The liquid N<sub>2</sub> gives you the surface phobicity in which there is a uniform surface. The  $C$  constant uses a semi-quantitative scale.<sup>131-133</sup> For our purposes, it relates to the contact angle on a fiber. Typical  $C$  constant values are in the range of 10-150 for nitrogen at 77 K for well-defined monolayers on many non-porous and mesoporous adsorbates. Low  $C$  constants indicate a non-polar surface while high  $C$  constants value indicates strong adsorbent-adsorbate interactions.<sup>133</sup> For surface functionalization it is an important parameter for comparing the untreated surface versus the treated surface.



**Figure 5- 5: BET Plots**

of (1) Bare NC and NC treated with the following: (2) Tri-silyl-propyl-NCO (3)Phenylsilane (4) Octadecylsilane, (5) Perfluoroalkylsilane, (6) Polydimethylsiloxane.

Table 5-1 gives the  $C_{\text{BET}}$  value of 73.00 for bare NC, demonstrating a moderate adsorbent-adsorbate interaction. The addition of the propyl silyl carbamate (NCO) decreases the energetic interaction of the NC fibers with  $\text{N}_2$ . The treatment of NC+NCO with fluoroalkyl gives the lowest  $C_{\text{BET}}$  values at ~14, followed by ~18-19 for octadecyl (C18) and polydimethylsiloxane (PDMS). The addition of phenylsilane to NC+NCO gives a  $C_{\text{BET}}$  value of 22.00 NC treated with tetramethoxysilane (TMOS) gave a  $C_{\text{BET}}$  value of 80.00. This value shows that the addition of TMOS to NC is energetically more reactive with  $\text{N}_2$  than bare NC, This could be in part to the additional formation of silanol on the surface of NC. The treatment of the NC + TMOS surface with fluoroalkyl again reduced the  $C_{\text{BET}}$  value to ~14 and the addition of octadecyl to NC + TMOS to 19.00. These values are consistent with our previous work that demonstrates the addition of fluoroalkyl to NC fibers results in the lowest surface energy values and highest contact angle values for multiple probe fluids.<sup>102</sup> Octadecyl and PDMS treated NC surfaces also present low surface energy followed by phenyl silane, demonstrating the various ranges of lyophobicity that the NC surface can take on especially with the addition of our so-called “primer-layers” of NCO and TMOS based on our previous work.<sup>15,102</sup>

## 5.9 $\alpha_s$ Method for Nitrogen Adsorption

The  $\alpha_s$  method developed by Sing et al.<sup>131-133</sup> compares experimental data with standard data from nonporous solid for the purpose of conformity, specifically porosity.<sup>133</sup> For our experiments we utilized standard data from nonporous hydroxylated silica.<sup>133-135</sup> The  $\alpha_s$  method uses a normalizing factor ( $n_s$ ), which is the amount adsorbed at some fixed relative pressure ( $p/p_0$ ), in practice this is equal to 0.4, therefore normalizing the adsorption



$n/n_{0.4} (= \alpha_s)$  from an isotherm on a reference sample of nonporous hydroxylated silica which is plotted against  $p/p_0$ .<sup>133-135</sup>

**Table 5- 1:** BET Values for Bare and Treated Nitrocellulose.

	$C_{\text{BET}}$	$S_{\text{BET}} \text{ m}^2/\text{g}$	$R^2$
Bare NC	73.00	2.40	0.9998
NC + NCO	37.00	2.70	0.9993
NC + NCO + TDF	14.00	2.30	0.9987
NC + NCO + C18	18.00	1.50	0.9988
NC + NCO + PDMS	18.98	2.00	0.9988
NC + NCO +phenyl silane	22.00	1.40	0.995
NC + TMOS	80.00	2.00	0.9959
NC + TMOS + TDF	14.00	1.50	0.999
NC + TMOS + C18	18.00	1.40	0.9959

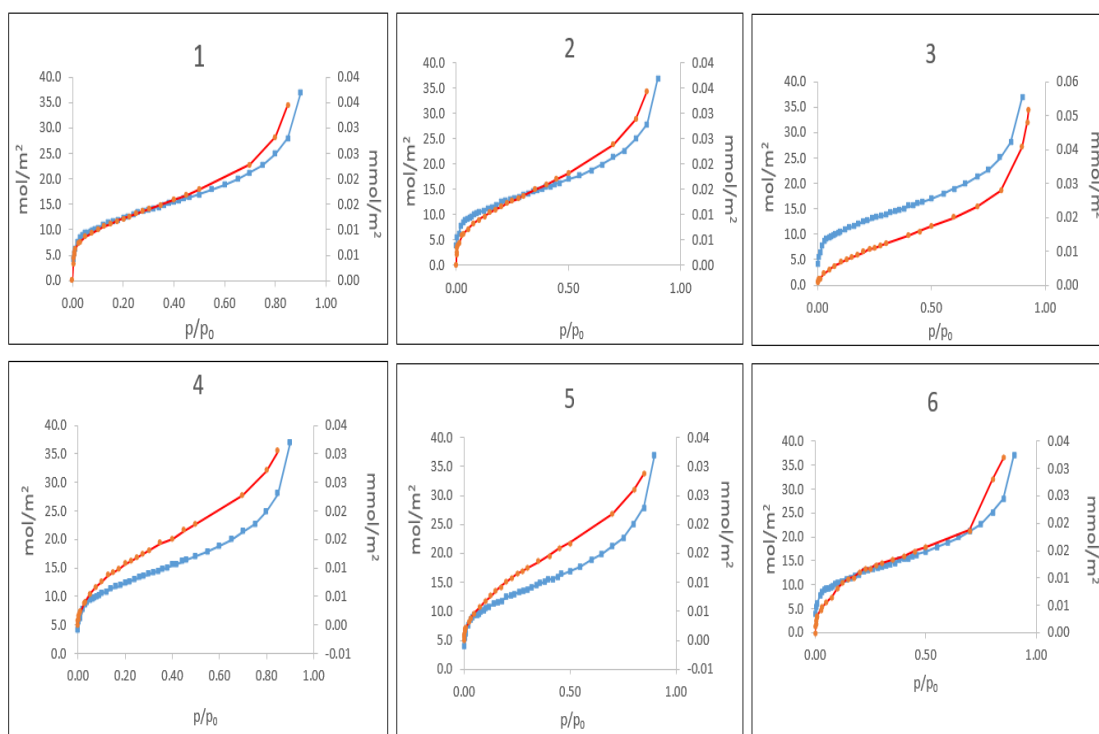
This procedure generates a standard  $\alpha_s$  curve.<sup>133</sup> This curve was then used to construct an  $\alpha_s$  plot of bare and treated nitrocellulose based off of  $\text{N}_2$  isotherms. This comparison of isotherm shape offers a direct means of comparing the shapes of a pair of isotherms.<sup>133</sup> The graphical comparison in the following figures describes the adsorption portion of the isotherm normalized in  $\text{mmol/m}^2$ .

Figure 5-6 compares bare NC with nonporous hydroxylated silica obtained from Gregg and Sing et al.<sup>131-133</sup>, The curve for bare nitrocellulose demonstrates an S-shape similar to that of the standard isotherm. The shape of the adsorption isotherm for bare NC in  $\text{mmol/m}^2$  suggests similar textural properties as nonporous hydroxylated silica. It can be seen that the amount of  $\text{N}_2$  adsorbed per square meter on bare NC is approximately the same as

the amount absorbed on the non-porous geometrical surface of standard silica. This portion of the isotherm generated from bare NC does not take into account the overall Type IV isotherm for NC that demonstrates narrow hysteresis and the presence of capillary condensation due to mesopore filling. Figure 5-6 shows  $\alpha_s$  plots of treated NC compared to nonporous hydroxylated silica. NC treated with triethoxysilylpropyl carbamate (NCO) maintained similar S-shape curve with bare NC but produced a slightly linear upward trend at  $.3 p/p_0$ . The addition of polydimethyl silane (PDMS) to NC+ NCO also demonstrated a sufficient S-shaped curve similar the standard isotherm. The further treatment of NC+NCO with fluoroalkyl and octadecyl ( $C_{18}$ ) silane demonstrated an upward linear trend from  $\sim .2$ -. $7 p/p_0$  eliminating the S-shape curve that represents the standard isotherm. The addition of phenyl silane showed a steep upward linear deviation at  $\sim .7 p/p_0$  from the standard S-shaped curve. The addition of tetramethoxysilane (TMOS) to NC along with fluoroalkyl and octadecyl ( $C_{18}$ ) silane demonstrated deviations in isotherm shape when compared to the standard isotherm and bare NC. These trends resulting in deviation of the standard S-shape curve for Type II and IV isotherms indicates the presence of micropores after treatment.

## 5.10 Pore Size Distribution PSD

Pore size distribution in a porous media controls the transport behavior the fluids through them.<sup>135</sup> For nitrocellulose, the gas may flow through fractured pores or aggregates composed of plate-like particles.<sup>133,136</sup> Pore size analysis using nitrogen adsorption is based on the Kelvin equation with a method devised by Barret, Joyner, and Halenda (BJH method) that assumes cylindrical pore geometry.<sup>133</sup> This approach is a procedure for calculating PSD from experimental adsorption isotherms using the Kelvin model of pore filling.<sup>133-137, 141-142</sup>



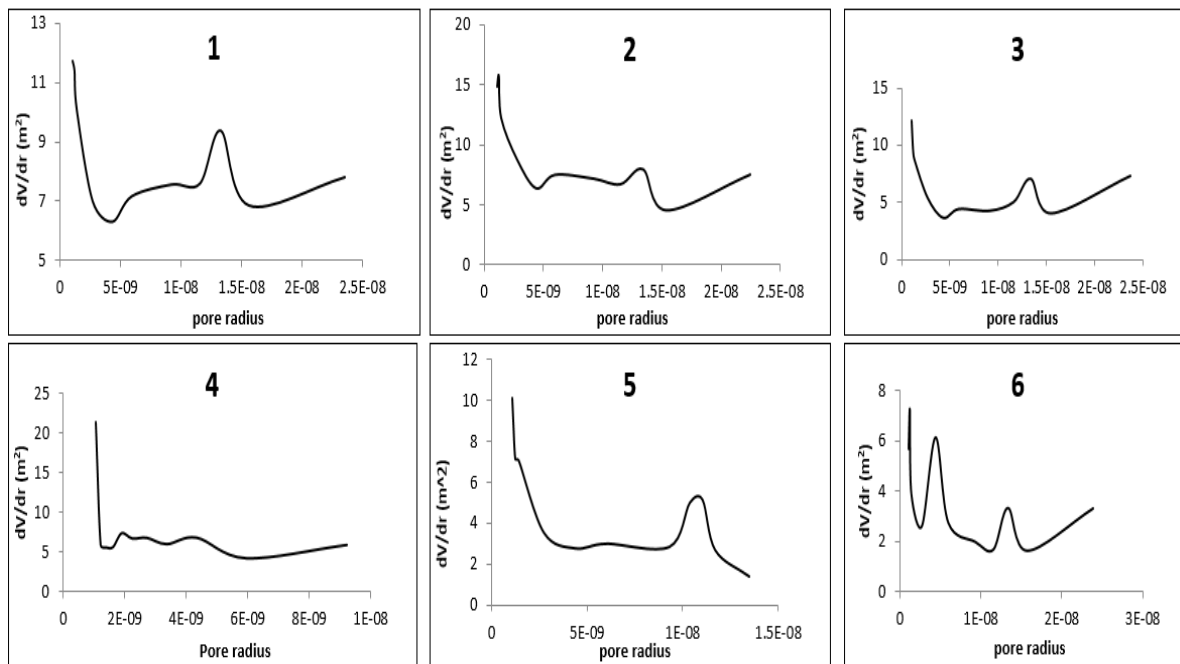
**Figure 5- 6:  $\alpha_s$  Plot**

(1) Bare NC, (2) NC+NCO, (3) NC+PDMS, (4) NC+ Octadecylsilane (5) NC+ C6F13. (6) Phenylsilane.

As described in sections 5-8 and 5-9, our samples produce a low pressure Type IV isotherm with a narrow hysteresis loop, evident of the occurrence of capillary condensation. Figure 5-7 shows the BJH PSD obtained for bare NC by plotting  $dV/dr$  ( $m^2$ ) by pore radius (nm) using the desorption branch of the adsorption isotherm. The distribution for bare NC is bimodal with an initial increase of in the parameter  $dV/dr$  increase at  $\sim 6$  nm and leveling off until the presence of a major peak at  $\sim 13.0$  nm.

NC treated with triethoxy silyl propyl isocyanate (NCO) shares the same distribution with bare NC with the distribution shifting slightly to the left of the curve, but maintaining a major peak at  $\sim 13$  nm. The addition of perfluoroalkyl silane to NC + NCO provides a slight noticeable presence of pore size at  $\sim 5$  nm. The presence of a wide distribution from  $\sim 5$ -15

nm is present and drops off after ~ 15 nm. This data is in align with the low adsorption and narrow hysteresis observed from the isotherms generated from perfluoroalkyl treatment of NC+NCO. The treatment of NC+NCO with octadecylsilane shows a major distribution peak ~11 nm decreasing the overall pore size by ~ 2nm. The treatment of NC+NCO with PDMS remained consistent with the pore size of bare NC and NC+NCO. The treatment of NC+NCO with phenylsilane decreased the major pore size down to ~4.5 nm and presented another major peak at ~13 nm with smaller pores. Treatment of NC with TMOS resulted in a trimodal distribution with a low accumulated pores at ~ 2.7 nm and ~9 nm. A major peak at ~ 13 nm is present but decreased in  $dv/dr$  ( $m^2$ ) compared to bare NC. The addition of perfluoroalkylsilane to NC + TMOS was similar to the addition of perfluoroalkylsilane to NC + NCO. The treatment of NC + TMOS with octadecylsilane resulted in identical PSD to NC + TMOS.



**Figure 5- 7: Pore Size Distribution**

(1) bare NC and NC treated with the (2) NC+NCO (3) Polydimethylsiloxane (4) Perfluoroalkyl (5) Octadecylsilane (6) Phenylsilane.

## 5.11 Conditioning and Thermal Stability

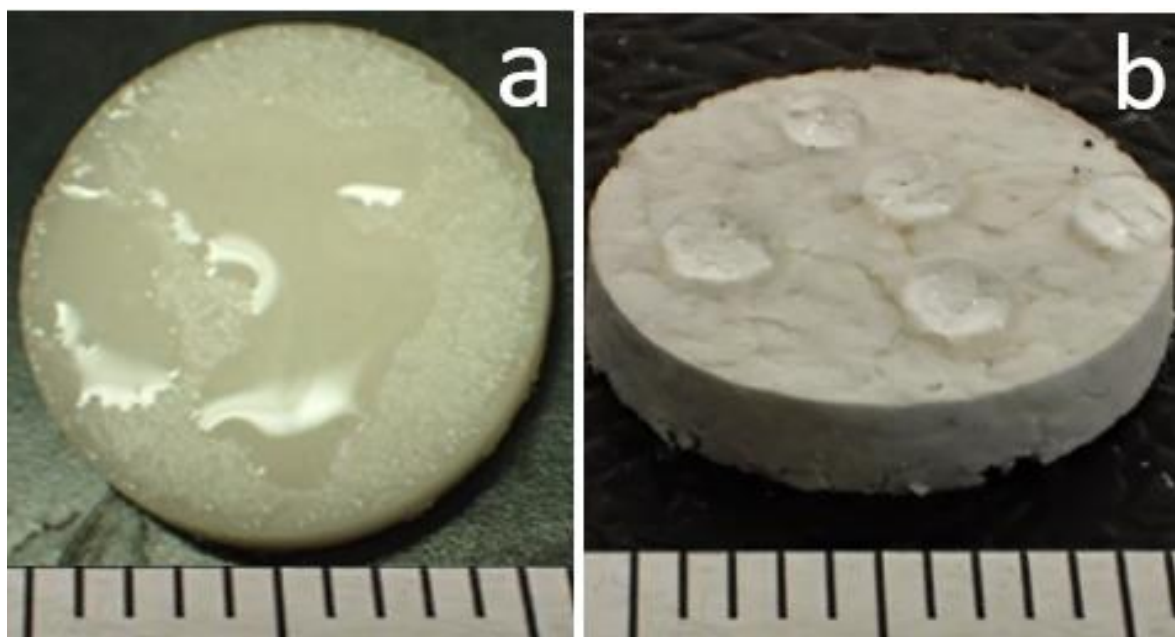
### 5.11.1 General Information

NC samples were pressed into pellets using a Perkin Elmer 13mm IR die under a Carver Laboratory Press at 8 metric tons pressure and held for 1 min to ensure adequate pellet formation. 25  $\mu$ L (5 droplets) of NG were dispensed on appropriate pellets using a Drummond WIRETROL 5ul pipette. The samples were placed in desiccators prepared in dry and 75% humidity. Samples were conditioned at ambient, 50°C, and 65°C up to 3 weeks. Samples were pulled out of the conditioning chambers according to selected timed intervals for chemical characterization.

Pellets of modified NC were conditioned at seven, fourteen, and twenty-one days, exposed to 25°C, 50°C, and 65°C in 10% (dry) and 80% RH Conditions were chosen based on previous propellant aging and shelf-life predictions.<sup>3,5,10</sup> For this experiment, we chose the highly NG phobic fluoro alkyl silane surface determined by previous work.<sup>102</sup> Samples chosen for thermal stability were based on the following reaction parameters:

1. *Homogenous surface*; NC dissolved in THF, followed by addition of 3-(triethoxysilylpropyl) isocyanate and hydrolysis of tridecafluoro 1,1,2,2,-tetrahydrooctyl trimethoxysilane.
2. *Heterogeneous surface*; NC stirred in toluene, followed by addition of 3-(triethoxysilylpropyl) isocyanate and hydrolysis of tridecafluoro 1,1,2,2,-tetrahydrooctyl trimethoxysilane.
3. *Thick primer layer*; tetramethoxy silane vaporized surface followed by addition of tridecafluoro 1,1,2,2,-tetrahydrooctyl trimethoxysilane (stirred in toluene).

NG droplets were applied to selected pellets to study the influence of NG on the surface and chemical stability. NG droplets were applied to the fluoro alkyl treated pellet in a way so that adequate space for H<sub>2</sub>O droplets could be applied for contact angle measurement. NG and water completely wet bare NC, therefore contact angle measurements on the bare NC surface was not feasible, The NG soaked NC pellets were used for nitrogen content. Figure 5-8 show the dispensed droplets on bare NC and fluoro alkyl treated NC. The progress of potential aging effects and NG exposure to surface functionalized NC was evaluated by static water contact angles ( $\theta_{Adv}$ ), and elemental analysis.



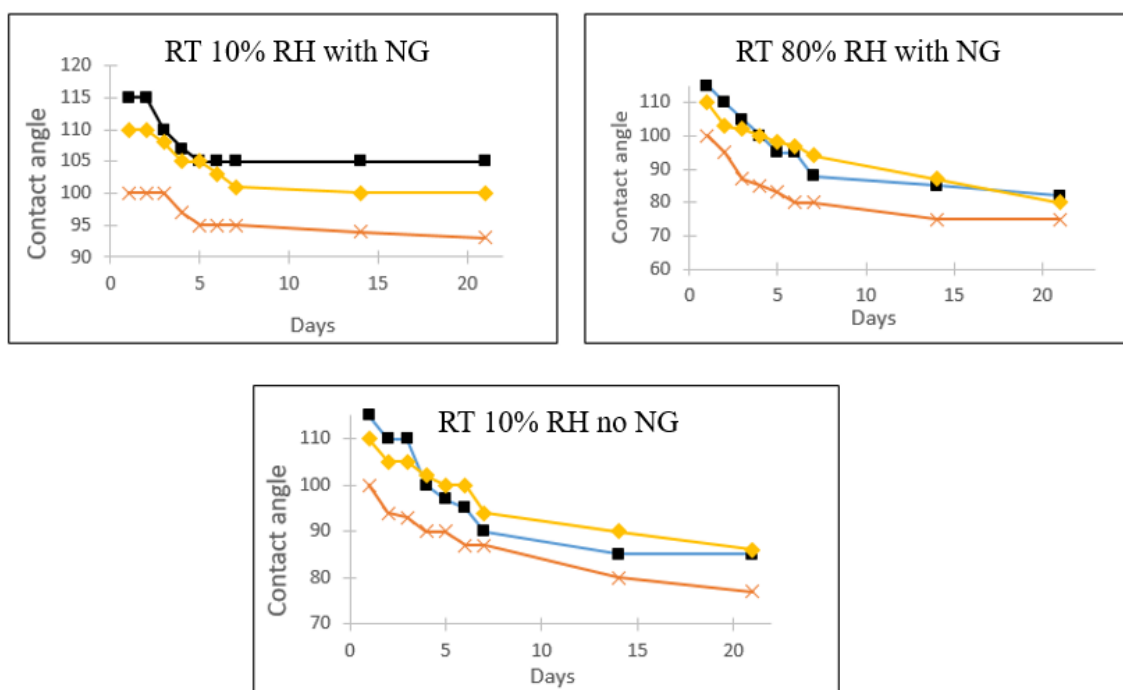
**Figure 5- 8: Dispensed Droplets**

(a) Soaking of nitroglycerin droplets ( $\sim 75\mu\text{L}$ ) on a pellet of bare NC. (b) Droplets of nitroglycerin on a pellet of C<sub>6</sub>F<sub>13</sub>-NC for aging and wetting measurements. Scale bar: one unit is 1 mm.

### 5.11.2 Wetting Measurements

The fluoro alkyl NC homogeneous surface showed optimal hydrophobicity over time and temperature exposure. Fig. 5-9 and 5-10 show the change in water contact angle over time exposed to 21°C, 50°C, and 65°C (10% and 80% RH). At 21°C and NG exposure, the homogenous surface maintained a water  $\theta_{Adv}$  of 115° and slightly decreased to 110° at day three and 107° at day four. The H<sub>2</sub>O  $\theta_{Adv}$  (105°) at twenty-one days, demonstrates constant surface hydrophobicity based on selected conditions. When exposed to 80% RH. for 21 days (25°C) the water contact angles for the homogenous surface decreased ~28° in the presence of extreme humidity. However, the surface maintained a sufficient degree of hydrophobicity (~85°) with and without the presence of surface NG. This is most likely due to formation of a pre-wetted surface at the NC interface in which surface moisture impacts the measurement of the advancing water contact angle. The surface designated ‘thick primer layer’, representing vapor deposition of tetramethoxysilane with the addition of fluoro alkyl, demonstrates a similar trend to the fluoro-alkyl homogeneous layer in regard to hydrophobicity. The thick primer layer was ~5° less hydrophobic than the homogeneous surface. Both surfaces present a decrease in water advancing contact angles at seven days and complete wetting at fourteen days (80% RH 65°C). NC surfaces functionalized with 3-(triethoxysilylpropyl) isocyanate followed by addition of fluoro alkyl prepared in toluene are designated as ‘heterogeneous’ with initial H<sub>2</sub>O advancing contact of 95°. The heterogeneous surface maintained hydrophobicity at 21°C for the duration of the study. At 80% RH (25°C), water advancing contact angles decreased by 25° after twenty-one days. At 50°C and 65°C 10% RH, hydrophobicity decreased ~5°, with and without the presence of NG. When exposed to 50°C (80% RH) the water advancing contact angles decreased by 15° at day two, 8° at day three,

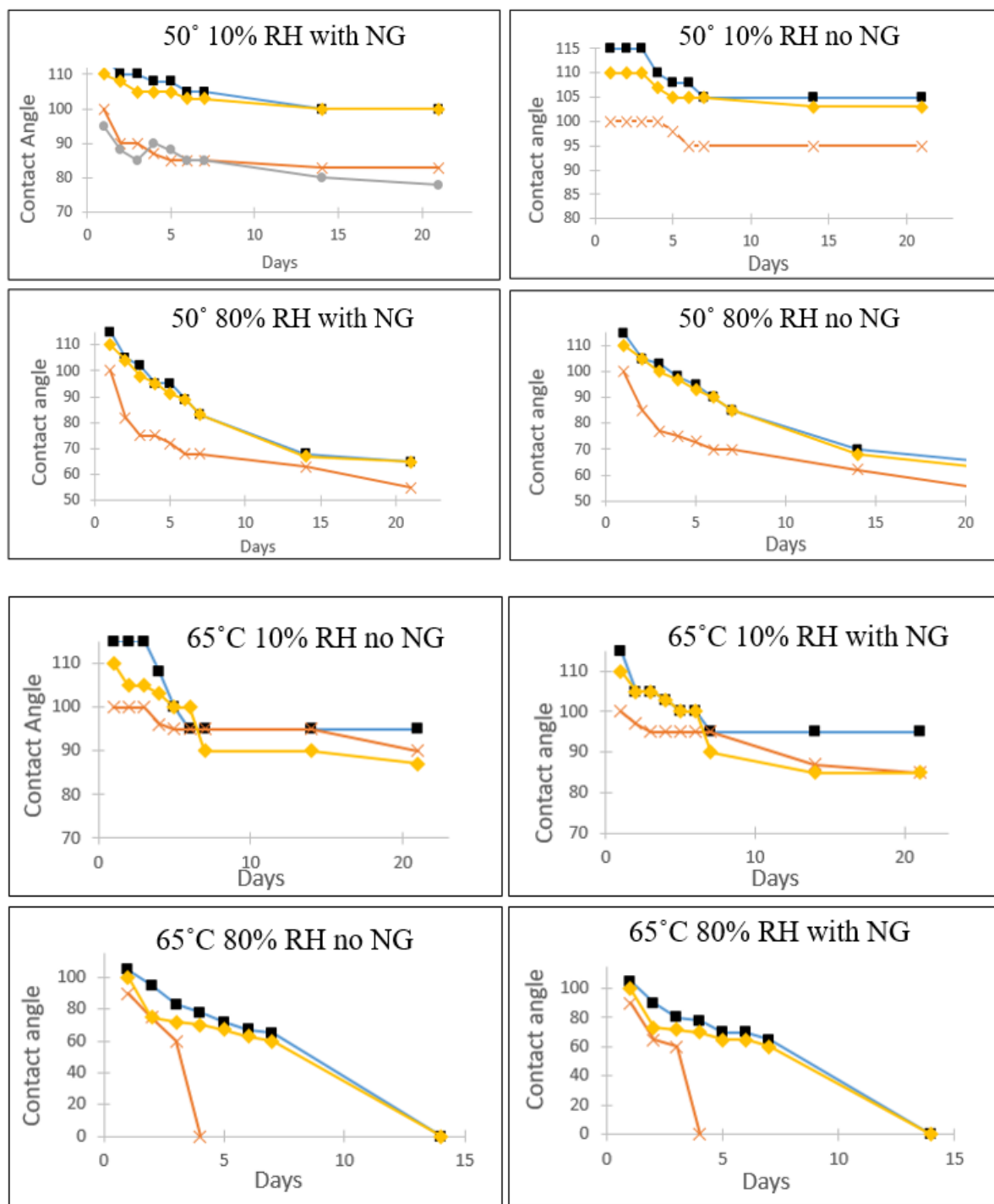
and stabilized at  $\sim 75^\circ$  at seven days. At week two, the water contact angle measurement was  $62^\circ$ . Week three showed a water contact angle measurement of  $55^\circ$ , a  $45^\circ$  difference from day one. When exposed to  $65^\circ\text{C}$  (80% RH), the heterogeneous surface showed water contact angle measurements of  $65^\circ$  at day two and  $60^\circ$  for day three. At day four, complete wetting by water was observed on the heterogeneous surface. Over all, the NG droplets remained visible and intact on the pellet surface exposed to dry conditions at  $25^\circ\text{C}$  and  $50^\circ\text{C}$  up to three weeks. Surface NG remained intact during exposure of 80% humidity at  $25^\circ\text{C}$ . Exposure of 80% humidity at  $50^\circ\text{C}$  resulted in NG to leaving the NC pellet surface within three days. In the presence of  $65^\circ\text{C}$  (10% and 80% RH), the surface NG was no longer visible on the pellet surface.



**Figure 5- 9:** Change of water contact angle of NC- $\text{C}_6\text{F}_{13}$  aged at room temperature over 21 days.

$\text{C}_6\text{F}_{13}$ -NC water  $\theta$  over time (■)  $\text{C}_6\text{F}_{13}$ -NC homogenous surface,  
(▲)  $\text{C}_6\text{F}_{13}$ -NC heterogeneous surface, (x)  $\text{C}_6\text{F}_{13}$ -NC thick-layer.





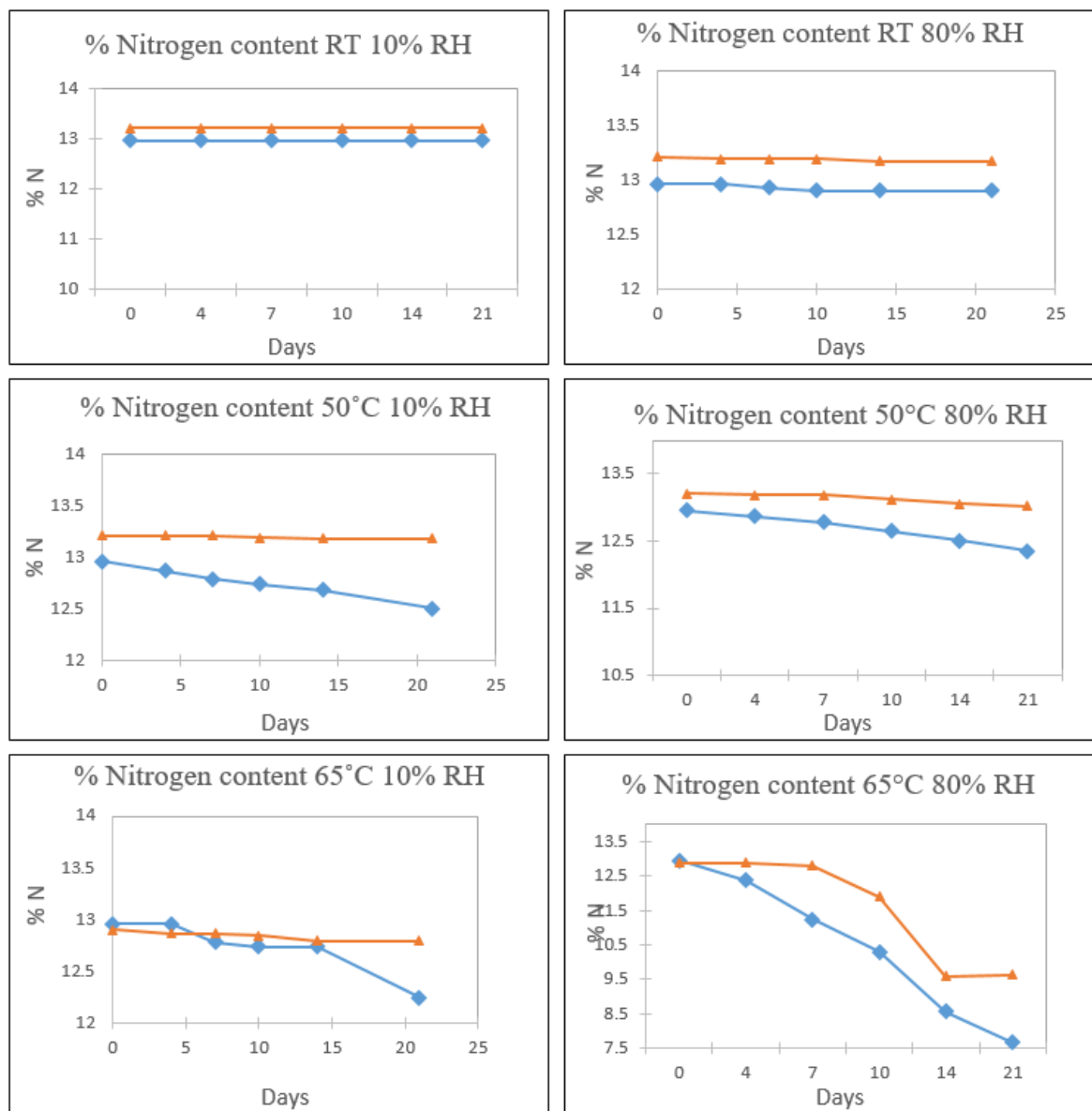
**Figure 5- 10:** Nitrocellulose treated with  $C_6F_{13}$  at 50°C and 65°C for 21 days.

$C_6F_{13}$ -NC water  $\theta$  over time (■)  $C_6F_{13}$ -NC homogenous surface,

(▲)  $C_6F_{13}$ -NC heterogeneous surface, (×)  $C_6F_{13}$ -NC thick-layer.

### 5.11.3 Elemental Nitrogen

Percent nitrogen content was used as a parameter for stability. The homogeneous silane fluoro alkyl NC was chosen for this study because of its optimal performance.<sup>102</sup> Figure 5-11 demonstrates the loss of percent nitrogen over time based on aging temperature. Samples were conditioned at room temperature (RT), 50°C, and 65°C (10% and 80% humidity) up to twenty-one days. Samples exposed to 10% humidity at room temperature maintained baseline % N throughout the testing duration as expected. For RT at 50°C (10% RH). Bare NC had a slight decrease in %N while the C<sub>6</sub>F<sub>13</sub> treated NC maintained %N continuity. At 65°C (10% RH), the nitrogen content of bare NC dropped from 13.0 to 12.0% nitrogen content. When exposed to 80% RH at room temperature, the %N remained stabilized for both the bare and treated NC. The fluoro alkyl treated surface initially decreased and stabilized at day four, maintaining stability up to twenty-one days. At 50°C (80% RH) bare NC showed a slight decrease in %N. For samples exposed to 80% RH; 65°C, the results were more dramatic. Bare NC progressively decreased in nitrogen content down to ~7.5% nitrogen at twenty-one days while perfluoralkyl treated NC decreased down to ~9.5% at 14 days and stabilized to 21 days. Overall, the NC treated with perfluoralkyl demonstrated a steady %N compared to bare NC demonstrating increased stability to humidity exposure overtime. The fluoro alkyl treated NC with the addition of 80% RH, maintained nitrogen content stability up to seven days (12.8% without NG, 12.66% with NG), and decreasing to 9.64% (without NG) and 10.32% (with NG) at twenty-one days. The increased nitrogen content of fluoroalkyl treated NC compared to bare NC, demonstrates the effectiveness of the treated surface.



**Figure 5- 11:** Change of nitrogen content over time of bare NC and NC-C<sub>6</sub>F<sub>13</sub> aged at 50°C and 65°C 10% and 80% relative humidity (RH).

C6F13 —▲—  
 Bare NC —◆—

The increased stabilization of percent nitrogen for the fluoro alkyl treated surface is an indication of two likely scenarios. The first being stabilization of nitro groups due to minimizing surface energy of NC with fluoro alkyl functionality. Moreover, the ability of the

modified NC to inhibit NG from soaking through fluoro alkyl treated fibers.

## 5.12 Conclusions

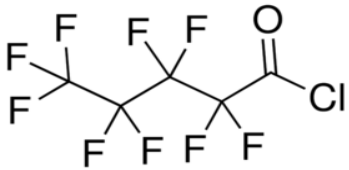
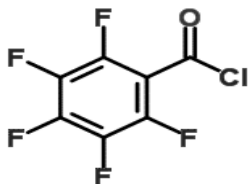
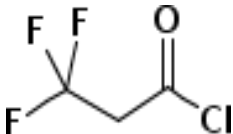
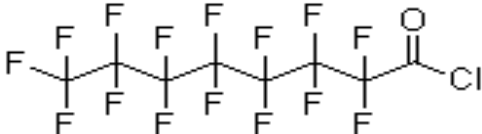
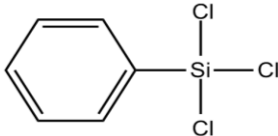
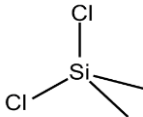
In this work we explored the sorption parameters of untreated NC and NC modified with different groups ranged as follows: fluoroalkyl, alkyl, oligo(dimethylsiloxyl), phenylsilane. The surface chemistry of NC can be modified to exhibit hydro/lyophobic properties. The nitrogen adsorption isotherm of bare NC takes the shape of Type IV adsorption isotherm. The isotherm presented a narrow hysteresis loop closure at  $\sim .4$   $p/p_0$  where  $N_2$  can condense as a liquid in pores. The addition of the aforementioned functional groups lowered the adsorption and resulted in an increased narrow hysteresis.  $\alpha_s$  plots were constructed to compare bare and treated NC to a standard isotherm. Bare NC demonstrated similar trends to the standard isotherm while the treated NC suggested a presence of micropores. BET analysis demonstrated low surface area on bare and treated NC. The  $C_{BET}$  value of 73.0 for bare NC demonstrated moderate adsorbent-adsorbate interaction. The addition of the propyl silyl carbamate (NCO) decreased the energetic interaction of the NC fibers with  $N_2$ . The treatment of NC+NCO with fluoroalkyl demonstrated the lowest  $C_{BET}$  values at  $\sim 14.0$ , followed by  $\sim 19.0$  for octadecyl ( $C_{18}$ ) and polydimethylsilane (PDMS), with the addition of phenyl silane to NC+NCO gives a  $C_{BET}$  value of 22.0, demonstrating surface interactions similar to our previous work. NC treated with tetramethoxysilane (TMOS) gave a  $C_{BET}$  value of  $\sim 80.0$  demonstrating the addition of TMOS to NC is energetically more reactive with  $N_2$  than bare NC. The pore size distribution was determined by the BJH method using the desorption method. Bare NC demonstrated a bimodal PSD with an initial with a major peak at  $\sim 13.0$  nm. NC treated with triethoxy silyl propyl isocyanate (NCO) shared the

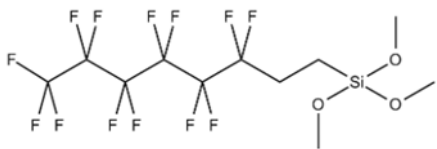
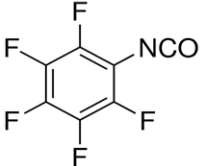
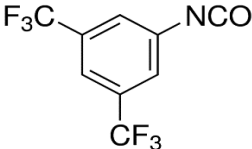
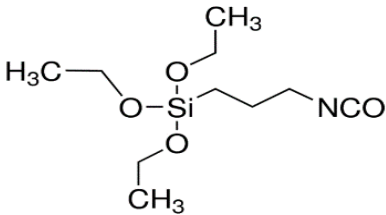
same distribution with bare NC. The addition of perfluoroalkyl silane to NC + NCO showed a wide distribution from ~5.0-15.0 nm. The treatment of NC+NCO with octadecylsilane shows a major ~11.0 nm. The treatment of NC+NCO with phenylsilane decreased the major pore size down to ~4.5 nm and presented another major peak at ~13.0 nm. The treatment of NC with TMOS resulted in a triple mode distribution.

For stability testing at 25°C (10% RH) hydrophobicity remained constant on the fluoro alkyl treated NC surface demonstrates non-wetting at elevated temperatures. In the presence of 80% RH at 25°C, the homogenous fluoro alkyl surface maintained adequate hydrophobicity (~85°). The bare NC exposed to 65°C, 80% RH demonstrated a faster rate of percent nitrogen loss. The addition of NG initially increased the nitrogen content with decreasing amounts during the conditioning process. Bare NC and the fluoro alkyl treated surface demonstrated significant nitrogen loss in the presence of 80% RH after fourteen days, although the fluoro-alkyl treated surface maintained a higher percent nitrogen content over time. The bare NC and fluoro-alkyl treated surface demonstrates lyophobic properties, based on the initial percent nitrogen loss and therefore stabilizing until seven days, where a slow decrease was observed up to twenty-one days. The fluor-alkyl treated NC demonstrated increased stability in nitrogen content compared to bare NC, an indication of maintaining nitro group stabilization when exposed to extreme environments.

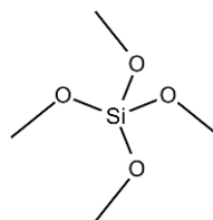
## APPENDIX A

### Molecules used in NC Surface Modifications

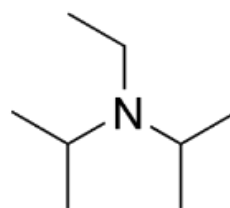
<b>Figure A- 1: Nonafluoropentanoyl Acyl chloride</b>	
<b>Figure A- 2: Pentafluorobenzoyl Acyl chloride</b>	
<b>Figure A- 3: 3,3,3,-trifluoropropanionyl Acyl chloride</b>	
<b>Figure A- 4: Pentadecafluorooctanoyl Acyl chloride</b>	
<b>Figure A- 5: Phenyltrichlorosilane</b>	
<b>Figure A- 6: Dimethyldichlorosilane</b>	

<p><b>Figure A- 7: n-octadecyldimethyl chlorosilane</b></p>	$\text{CH}_3(\text{CH}_2)_{16}\text{CH}_2-\text{Si}(\text{CH}_3)_2\text{Cl}$
<p><b>Figure A- 8:</b></p> <p><b>Tridecafluorotetramethoxyhydrooctyl trimethoxysilane</b></p>	
<p><b>Figure A- 9: Pentafluorophenyl isocyanate</b></p>	
<p><b>Figure A- 10: 3-5 bis(trifluoromethyl)phenyl Isocyanate</b></p>	
<p><b>Figure A- 11: Trimethylsilyl isocyanate</b></p>	$\text{H}_3\text{C}-\text{Si}(\text{CH}_3)_2-\text{NCO}$
<p><b>Figure A- 12: 3-(Triethoxysilyl)propyl isocyanate</b></p>	

**Figure A- 13: Tetramethoxysilane**



**Figure A- 14: Hunig's Base**

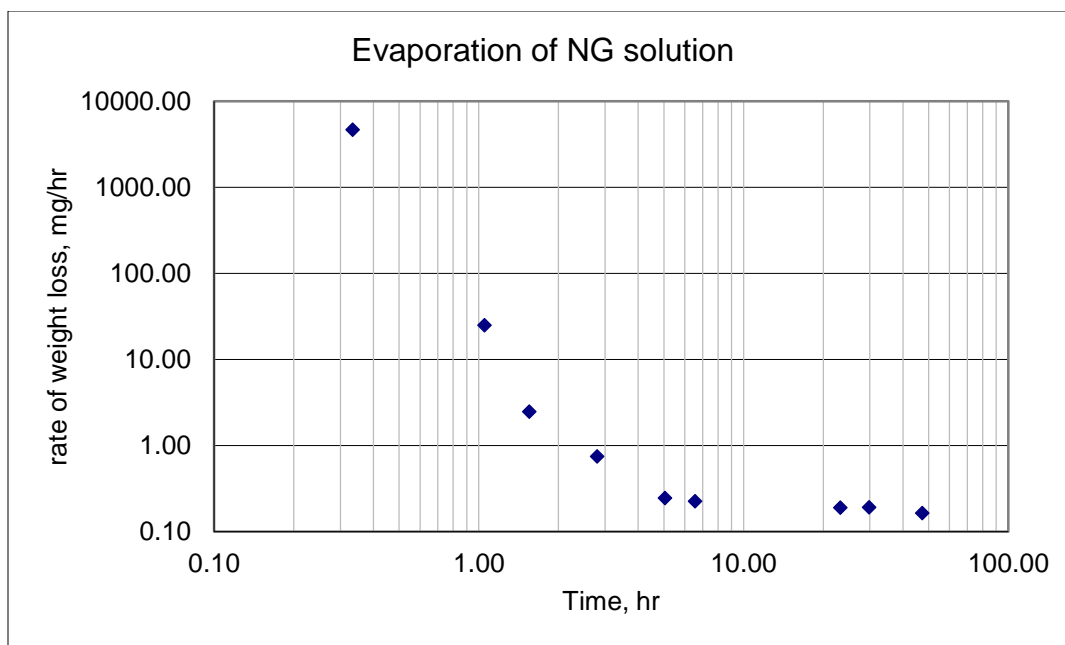




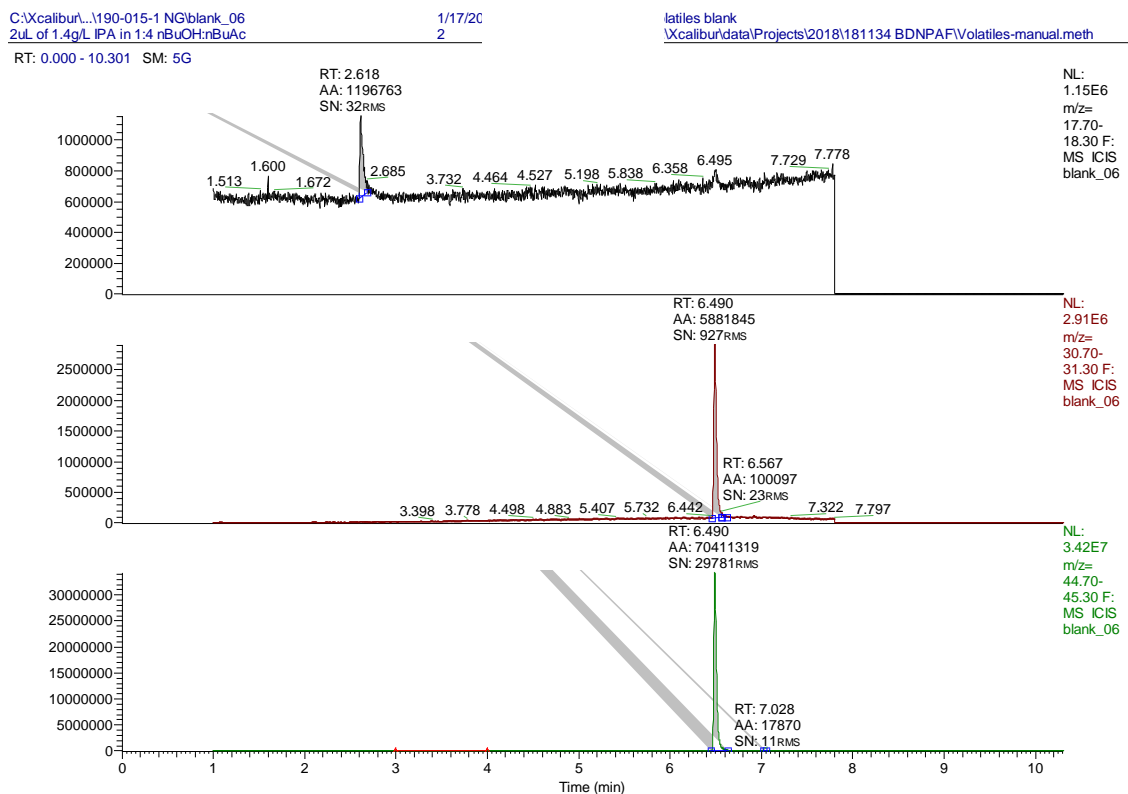
## APPENDIX B

**Table B- 1:** Solvent Loss Over Time to Monitor Remaining Nitroglycerin for Purity Conformation.

Sample Runs	elapsed time, hr	wt (g), tin + NG (ethanol solution)	wt (g), NG residue	loss rate, mg/hr
2019.01.15 0:00		1.262803		
2019.01.15 9:21	0.00	2.923803	1.661000	
2019.01.15 9:41	0.33	1.367800	0.104997	4668.01
2019.01.15 10:24	1.05	1.349900	0.087097	24.98
2019.01.15 10:54	1.55	1.348660	0.085857	2.48
2019.01.15 12:09	2.80	1.347730	0.084927	0.74
2019.01.15 14:24	5.05	1.347179	0.084376	0.24
2019.01.15 15:54	6.55	1.346841	0.084038	0.23
2019.01.16 8:33	23.20	1.343698	0.080895	0.19
2019.01.16 15:08	29.78	1.342437	0.079634	0.19
2019.01.16 15:38	30.28	1.332760	0.069957	
2019.01.17 8:37	47.27	1.329983	0.067180	0.16
2019.01.17 11:08	49.78	1.310281	0.047478	



**Figure B- 1:** Solvent loss of ethanol/NG stock solution for purity.



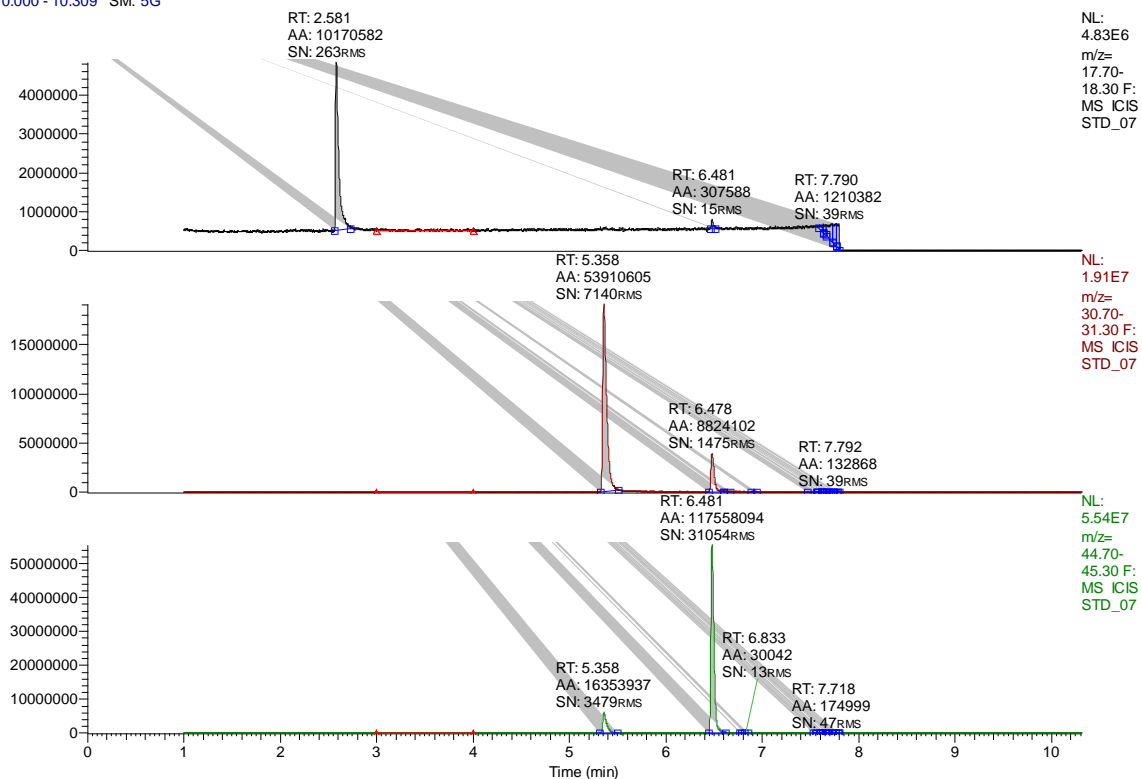
**Figure B- 2: GC-MS Chromatogram.**

Solvent blank: 4:1 (v:v) n-BuAc : n-BuOH w/ 1.4mg/mL isopropanol internal std; extracted at m/z 18, 31, 45 (top, middle, bottom) for water, ethanol, isopropanol.

C:\Xcalibur\190-015-1 NG\STD\_07  
 2uL of solvents in 1:4 nBuOH:nBuAc w/ 1.4g/L IPA  
 RT: 0.000 - 10.309 SM: 5G

1/17/20  
 3

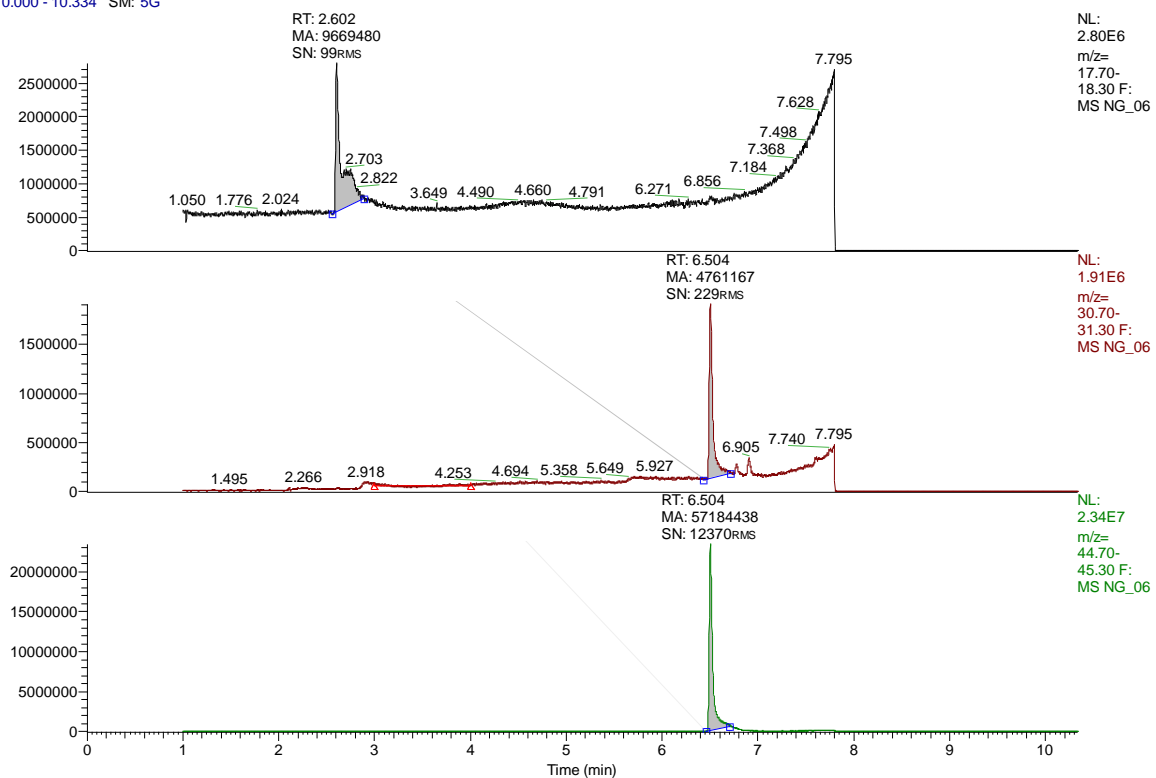
latiles standard b16-4 p93  
 \Xcalibur\data\Projects\2018\181134 BDNPAF\Volatiles-manual.meth



**Figure B- 3: GC-MS Chromatograms**

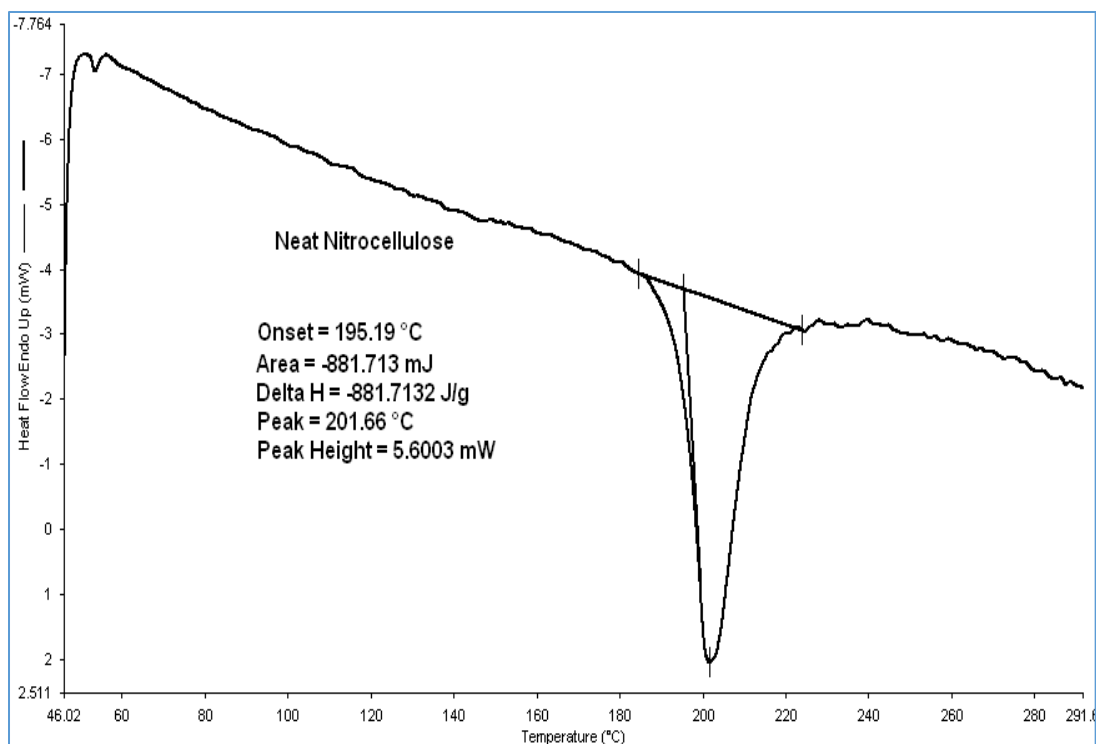
water and ethanol standard in 4:1 (v:v) n-BuAc : n-BuOH w/ 1.4mg/mL isopropanol internal std; extracted at m/z 18, 31, 45 (top, middle, bottom) for water, ethanol, isopropanol.

RT: 0.000 - 10.334 SM: 5G

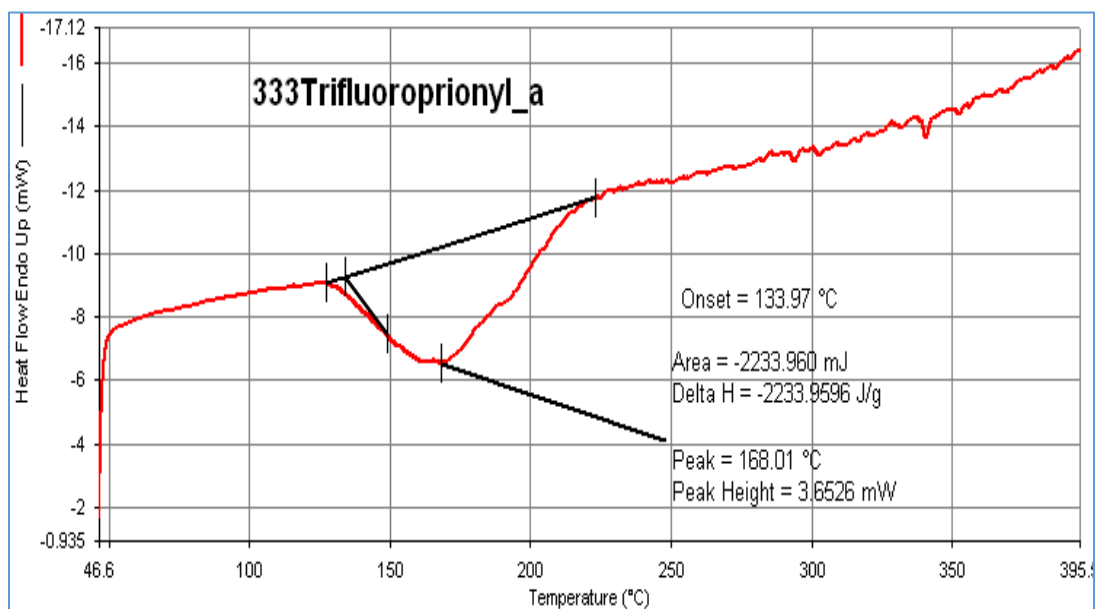


**Figure B- 4: GC-MS Chromatogram**

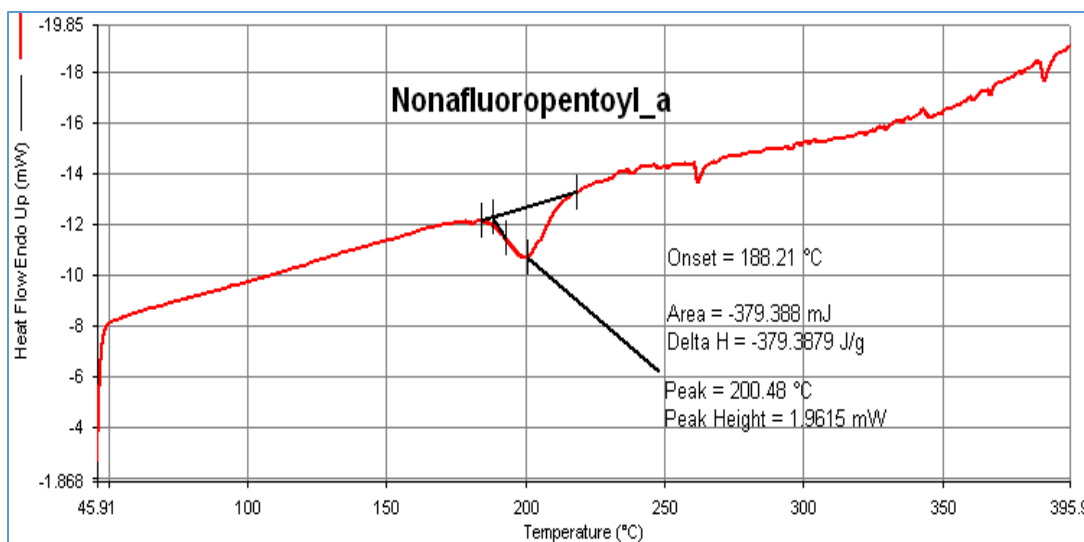
5uL nitroglycerin + 20uL solvent 4:1 (v:v) n-BuAc : n-BuOH w/ 1.4mg/mL isopropanol internal std; extracted at m/z 18, 31, 45 (top, middle, bottom) for water, ethanol, isopropanol.



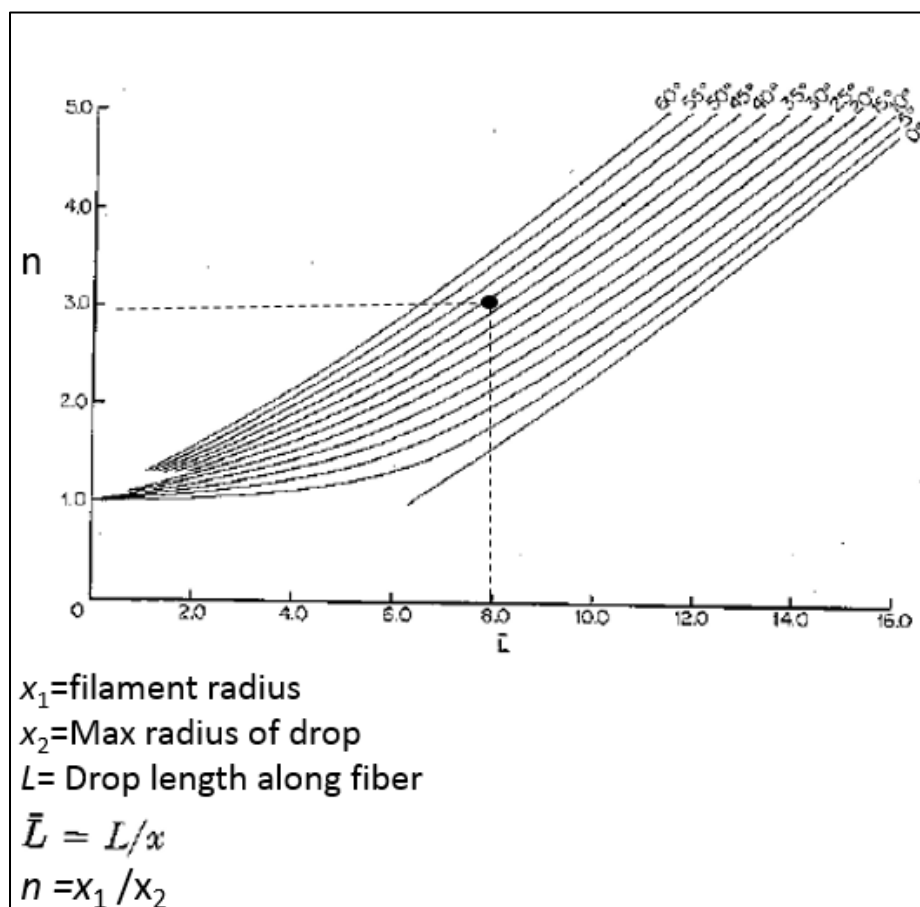
**Figure B- 5:** DSC thermogram of neat NC decomposition (exotherm down).



**Figure B- 6:** DSC thermogram of 3,3,3-trifluoropropanionyl acyl chloride treated NC showing decomposition. (Exotherm down)



**Figure B- 7:** DSC thermogram of nonafluoropentanoyl acyl chloride treated NC showing decomposition. (Exotherm down)



**Figure B- 8:** Measured parameters for estimating dimensionless symmetric contact angles of NG droplet on a functionalized NC surface.

**Table B- 2:** Standard Data for Adsorption of N<sub>2</sub> at 77K On nonporous hydroxylated silica. <sup>133</sup>

p/po	mol/m2	a <sub>s</sub> , (=n/n <sub>0.4</sub> )
0.00	4.0	0.26
0.01	5.4	0.35
0.01	6.2	0.40
0.02	7.7	0.50
0.03	8.5	0.55
0.04	9.0	0.58
0.05	9.3	0.60
0.06	9.4	0.61
0.07	9.7	0.63
0.08	10.0	0.65
0.09	10.2	0.66
0.10	10.5	0.68
0.12	10.8	0.70
0.14	11.3	0.73
0.16	11.6	0.75
0.18	11.9	0.77
0.20	12.4	0.80
0.22	12.7	0.82
0.24	13.0	0.84
0.26	13.3	0.86
0.28	13.6	0.88
0.30	13.9	0.90
0.32	14.2	0.92
0.34	14.5	0.94
0.36	14.8	0.96
0.38	15.1	0.98
0.40	15.5	1.00
0.42	15.6	1.01
0.44	16.1	1.04
0.46	16.4	1.06
0.50	17.0	1.10
0.55	17.8	1.14
0.60	18.9	1.22
0.65	19.9	1.29
0.70	21.3	1.38
0.75	22.7	1.47
0.80	25.0	1.62
0.85	28.0	1.81
0.90	37.0	2.40

## References

1. Huang, Z.P.; Nie, H.Y.; Zhang, Y.; Tan, H.Y.; Ma, X.g. *J. of Hazardous Mat.* **2012**, 229-300. 251-257.
2. Angeles, M.; de la Ossa, F.; Torre, Mercedes, T.; Riuz-Garcia, C. *Advances in Materials Science Research.* **2012**, 7, 201-220.
3. Kohler, J., Meyer, R. *Explosives*. 4<sup>th</sup>, revised and extended edition. **1993**, ISBN-3-527-28506.
4. Hercules. *Nitrocellulose Chemical and Physical Properties*. **1979**, Hercules Incorporated, Hercules Plaza, Wilmington, DE, 19894.
5. Maag, H.J.; Klingenberg, G. *Propellants, Explosives, Pyrotechnic*. **1996**, 21, 1-7.
6. Venkatesan, D.; Srinivasn, M.; Audisesha, R.; Pendse, V.V. *Polym. Int.* **1993**, 32, 395-399.
7. Eyley, S.; Thielemans, Wim. *Nanoscale*. **2014**, 6, 7764-7779.
8. Reid, E.E. *Industrial and Engineering Chemistry*. **1954**, 46, 9, 1802-1806.
9. Fernandez de la Ossa, A.; Lopez-Lopez, M.; Torre, Mercedes, T.; Ruiz-Garcia, C. *Trends in Analytical Chemistry*. **2011**, 30, No. 11.
10. Department of the Army United States. *Military Explosive Technical Manual*. **September, 1984**, TM-9-1300-214, Headquarters Washington D.C., 9-1.
11. Peterson, M.L.; Way, J.W. *I/EC Chemical Engineering Reviews*. **1959**, 51, 9, 1081-1085.
12. Gottlieb, L.; Bar, S. *Propellants, Explosives, Pyrotechnics*. **2003**, 28, 1, 12-27.
13. Heng, S.Y.; Pan, T.X.; Kong, Y.H.; Liu, Z.R. *Propellants, Explosives, Pyrotechnics*. **1991**, 16, 31-35.



14. Vogelsanger, B.; Ossola, B.; Bronnimann, E. *Propellants, Explosives, Pyrotechnics*. **1996**, 21, 330-336.
15. Grau, H.A.; Fadeev, A.Y. *Methods for Modifying Nitrocellulose Having Lyophobic Properties*. US Patent 9,856,328 January 2, **2018**.
16. Dionisio, M.; Sotomayor, J. *Journal of Chemical Education*. **2000**, 77, 1.
17. Gao, L.; McCarthy, T.J. *Langmuir*. **2006**, 22, 6234-6237.
18. Kalantarian, A.; David, R.; Neumann, A.W. *Langmuir*. **2009**, 25, 14146-14154.
19. Fadeev, A. Y. Hydrophobic Monolayer Surfaces: Synthesis and Wettability. *In: Encyclopedia for Surface and Colloid Science*, 2nd Ed.; Somasundaran, P., Ed.; Taylor & Francis: New York, **2006**, Vol. 4, 2854-2875.
20. Fadeev, F.Y.; McCarthy, T.J. *Langmuir*. **1999**, 15, 3759-3766.
21. Despa, F.; Berry, S.R. *Biophysical Journal*. **2007**, 92, 373-378.
22. Korhonen, J.T.; Huhtamaki, T.; Ikkala, O.; Ras, R.H.A. *Langmuir*. **2013**, 29, 3858-3863.
23. Zdziennicka, A.; Szymczyk, Katarzyna.; Krawczyk, J.; Janczuk, B. *Applied Surface Science*. **2017**, 405, 88-101.
24. Sutton, T.C.; Harden, H.L. *J. of Phys Chem*. **1933**, 38(6), 779-781.
25. Korosi, G.; Kovats, E. *J. Chem Eng Data*. **1981**, 26, 3.
26. Zisman, W.A. *Adv. Chem. Ser.*, **1964**, 43, 1-51.
27. Abe, H.; Kiyokaw, S.; Yoshimura, Y. *Chemical Physics Letters*. **2018**, 699, 275-278.
28. Sugden, S. *Journal of American Chemical Society*. **1925**, 47, 1, 60-64.
29. App.Knovel.com/web.ThermoData Engine (TDE) Version 10: NIST Standard Reference Database 103b, **2015**.

30. Cellulose Chemistry and Properties: Fibers, Nanocelluloses and Advanced Materials.  
Edited by Rojas, O.J. Springer Int. Publishing, **2016**.
31. Klemm, D.; Heublin, B.; Fink, H.P.; Bohn, A. *Angew. Chem. Int. Ed.* **44**, **2005**. 3358-3393.
32. Edgar, K.J.; Buchanan, C.M.; Debenham, J.S.; Rundquist, P.A.; Seiler, B.D.; Shelton, M.C.; Tindall, D. *Progress in Polymer Science.* **2001**, *26*, 1605-1688.
33. Rongwie, W.; Boron. G.; Wunder, S.L. *Langmuir.* **2000**. *16*(15). 6298-6305.
34. Li, S.; Zhang, S.; Wang, X. *Langmuir.***2008**, *24*, 5585-5590.
35. Achoundong, C.S.K.; Bhuwania, N.; Burgess, S.K.; Karvin, O.; Johnson, J.R.; Koros, W.J. *Macromolecules.***2013**, *46*, 5584-5594.
36. Tang, J.; Sisler, J.; Grishkewich, K.C. *J. Colloid Interface Science.* **2017**, *494*, 397-409.
37. Cunha, A.G.; Gandini, A. *Cellulose.* **2010**. *17*, 875-889.
38. Edgar, K.J.; Buchanan, C.M.; Debenham, J.S.; Rundquist, P.A.; Seiler, B.D.; Shelton, M.C.; Tindall, D. *Progress in Polymer Science.* **2001**, *26*, 1605-1688.
39. Cunha, A.G.; Freire, C.S.R, Silvestre, A.; Neto, P.C.; Gandini, A, Orblin, E.; Fardim, P. *Biomocromolecules.* **2007**, *8*, 1347-1352.
40. Cunha, A.G.; Freire, C.; Silvestre, A.; Neto, C.; Gandini, A.; Orblin, E.; Fardim, P. *Langmiur.* **2007**, *23*, 10801-10806.
41. Achoundong, C.S.K.; Bhuwania, N.; Burgess, S.K.; Karvin, O.; Johnson, J.R.; Koros, W.J. *Macromolecules.***2013**, *46*, 5584-5594.
42. Khan, Z.F.; Sakaguchi, T.; Shiotsuki, M., Nishio, Y.; Masuda, T. *Macromolecules.* **2006**, *39*, 6025- 6030.
43. Khan, Z.F.; Sakaguchi, T.; Shiotsuki, M., Nishio, Y.; Masuda, T. *Macromolecules.* **2006**, *39*, 9208- 9214.

44. Chen, X.; Liu, Y.; Qin, F.; Kong, L.; Zou, H. *Journal of Chromatography A*. **2003**, 1010, 185-194.
45. Bantz, M.R.; Brantley, E.L.; Weinstein, R.D.; Moriarty, J.; Jennings, K.G. *Journal of Physical Chemistry B*. **2004**, 108, 9787-9794.
46. Vilar, M.R.; Boufi, S.; Ferraria, A.N.; Botelho do Rego, A.N. *Journal of Physical Chemistry*. **2007**, 111, 12792-12803.
47. Thakur, M.K.; Gupta, K.R.; Thakur, V.K. *Carbohydrate Polymers*. **2014**, 111, 849-855.
48. Belgacem, M.N.; Gandini, A. *Monomers, Polymers and Composites from Renewable Resources*. **2008**, Chapter 18, 385-400.
49. Tehrani, A.D.; Neysi, E. *Carbohydrate Polymers*. **2013**, 97, 98-104.
50. Avila-Ramirez, J.A.; Fortunati, E.; Kenny, M.J.; Torre, L. *Carbohydrate Polymers*. **2017**, 157, 1358-1364.
51. Hatton, F.L.; Malmstrom, E.; Carlmark, A. *European Polymer Journal*. **2015**, 65, 325-339.
52. Pasquini, D.; Belgacem, M.N.; Gandini, A.; Curvelo-da Silva, A.A. *J. of Colloid and Interface Sci*. **2006**, 295, 79-83.
53. Mischnick, P.; Momcilovic, D. *Advances in Carbohydrate Chemistry and Biochemistry*. **2010**, 64, 117-210.
54. Iler, R.K. *The Chemistry of Silica*. **1979**, Wiley & Sons: New York, 108-160.
55. Brinker, C.J. *Journal of Non-Crystalline Solids*. **1988**, 100, (1-3), 31-50.
56. Reid, E.E. *Industrial and Engineering Chemistry*. **1954**, 46, (9), 1801-1808.
57. Peterson, M.; Way, I. *Ind.eng.Chem*. **1957**, 49, (9), 1485-1488.

58. Krassig, H.; Schurz, J.; Steadman, R.G.; Schliefor, K.; Albrecht, W. *Ind. Polym. Handbook*. **2001**, 3, 1423-1500.
59. Teng, Y.; Yu, G.; Fu, Y.; Yin, C. *Int J. of Bio Macromolecules*. **2018**, 107, 383-392.
60. Amaraseker, A.S.; Hasan, H.A.; Ha, Uyen. *Carbohydrate Polymers*. **2016**, 154, 8-12.
61. Gilberto, S.; Bras, J.; Dufresne, A. *Langmuir*. **2010**, 26, 402-411.
62. Niyogi, S.; Sarkar, S.; Adhikari, B. *Indian Journal of Chemical Technology*. **2002**, 9, 330-333.
63. Mormann, W.; Michel, U. *Carbohydrate Polymers*. **2002**, 2, 201-208.
64. Sjöholm, E.; Gustafsson, K.; Eriksson, B.; Brown, W.; Colsjö, A. *Carbohydrate Polymers*. **2000**, 41, 153-161.
65. Alvarez, A.; Yanez, J.; Contreras, D.; Saavedra, R.; Saez, P. *Forensic Science International* 280. **2017**, 169-175
66. Hayashi, T.; Mukamel, S. *Journal of Physical Chemistry B*. **2007**, 111, 11032-11046.
67. N. Koji. *Infrared Absorption Spectroscopy*. Holden-Day Inc. San Fransisco, **1962**.
68. Liebert, T. *ACS Symposium Series*. **2010**, Vol. 1033. **SBN13**: 9780841200067.
69. Hillman, D.E.; J.I., Paul. Materials Quality Assurance Directorate Royal Arsenal East Woolrich London SE18 6TD Procurement Ministry of Defence. **Nov. 1977**, Report NO. 262.
70. Hunig, S.; Kiessel, M. *Chemische Berichte*. **1958**, 91, (2), 380-392.
71. Silane Coupling Agents: Connecting Across Boundries, Gelest, Inc. ([www.gelest.com](http://www.gelest.com)). **2006**.
72. Qiu, X.; Tao, S.; Ren, X.; Hu, S. *Carbohydrate Polymers*. **2012**, 88, 1272-1280.
73. Gilberto, S.; Bras, J.; Dufresne, A. *Langmuir*. **2010**, 26, 402-411.

74. Hozumi, A.; Kim, B.; McCarthy, T.J. *Langmuir*. **2009**, 25, 6834-6840.
75. Girouard, N.M.; Xu, S.; Schueneman, G.T.; Shafner, M.L. *Applied Materials and Interfaces*. **2016**, 8, 1458-1467.
76. Lu, Jue.; Askeland, Per.; Drzal, T. *Polymer*. **2008**, 49, 1285-1296.
77. Hadjadj, A.; Jbara, O.; Tara, A.; Gilliot, M.; Malek.; Maffi, E.M.; Tighzert, L. *Composite Structures*. **2016**, 135, 217-223.
78. Siqueira, G.; Bras, J.; Dufresne, A. *Langmuir*. **2010**, 26, 402-411.
79. Hair, M.L. *Infrared Spectroscopy in Surface Chemistry*, Marcel Dekker N.Y. **1967**.
80. Grdadolnik. J. *Vibrational Spectroscopy*. **2003**, 31, 279-288.
81. Grdadolnik. J.; Mare'chal, Y. *Vibrational Spectroscopy*. **2003**, 31, 289-294.
82. House, J.E.; Flentge, P.; Zack, P.J. *Thermochimica Acta*. **1978**, 24, 133-138.
83. Kono, H.; Fujita, S. *Carbohydrate Polymers*. **2012**, 87, 2582-2588.
84. Plueddemann, E.W., *Silane Coupling Agents*, 2<sup>nd</sup> edition. Plenum, N.Y. **1991**.
85. Colleoni, C.; Donelli, I.; Freddi, G.; Migani, V.; Rosace, G. *Surface & Coatings Technology*. **2013**, 235, 192-203.
86. Fadeev, A.Y.; McCarthy, T.J. *Langmuir*. **2000**, 16, 7268-7274.
87. Masson, M.; Lauritzen, E.; Holm, A. *Electrophoresis*. **1993**, 14, (9), 860-865.
88. Puig, H.; Bosch, I.; Gehrke, L.; Schifferli-Hamad, K. *Trends Biotechnol.* **2017**, 35(12), 1169-1180.
89. Holstein, C.A.; Chevalier, A.; Bennet, S.; Anderson, C.E.; Keniston, K.; Olsen, C.; Li, B.; Bales, B.; Moore, D.R.; Fu, E.; Baker, D.; Yager, P. *Anal. Bioanal. Chem.* **2016**, 408, (5), 1335-1346.
90. Katada, N.; Toyama, T.; Niwa, M. *Journal of Physical Chemistry*. **1994**, 9, 7647-765

91. Colleoni, C.; Donelli, I.; Freddi, G.; Migani, V.; Rosace, G. *Surface & Coatings Technology*. **2013**, 235, 192-203.
92. Fadeev, A.Y.; Kazakevich, Y.V. *Langmuir*. **2002**, 18, 2665-2672.
93. Zheng, P.; McCarthy, T.J. *Langmuir*. **2010**, 26, 18585-18590.
94. Ross, S.; Nguyen, N. *Langmuir*. **1988**, 4, 1188-1193.
95. Haitami, A.E.; Goldmann, M.; Cousin, F.; Dosseh, Gilberte.; Cantin, S. *Langmuir*. **2015**, 31, 6395-6403.
96. Isrealachvilli, J.N.; Gee, M.L. **1989**, *Langmuir*, 5, 288-289.
97. CRC Book of Chemistry and Physics. Ed. By David Lide. 89<sup>th</sup> ed., **2008-2009**.
98. Haul, R.; Mittag, R. *Zeitschrift für Elektrochemie und Angewandte Physikalische Chemie*. **1949**, 53, 380-383.
99. Carroll, B.J. *J. of Colloid and Interface Sci.* **1976**, 57, 3, 488-495.
100. Song, B.; Bismarck, A.; Tahhan, R.; Springer, J. *J. of Colloid and Interface Sci.* **1988**, 197, 68-77.
101. Grau, H.A.; Fadeev, A.Y. *J. of Colloid and Interface Sci.* **2018**, 547, 145-152.
102. Lorenceau, E.; Clanet, C.; Quere, D. *J. of Colloid and Interface Sci.* **2004**, 279, 192-197.
103. McHale, G.; Newton, M.I.; Carrol, B.J. *Oil & Gas Science and Technology*. **2001**, 56, 47-54.
104. McHale, G.; Kab, N.A.; Newton, M.I.; Rowan, S.M. *J. of Colloid and Interface Sci.* **1997**, 186, 453-461.
105. Berim, O.B.; Ruckenstein, E. *Journal of Physical Chemistry B*. **2005**, 109, 12515-12524.

106. Lu, Z.; Ng, T.W.; Yu, Yang. *International Journal of Heat and Mass Transfer*. **2016**, 93, 1132-1136.
107. Davoudi, M. Amrei,, M.M.; Tafreshi, H.V.; Chase, G.G. *Separation and Purification Technology*. **2018**, . 204, 127-132.
108. Jenkins, L.M.; Donald, A.M. *Langmuir*. **1999**, 15, 7829-7835.
109. Freire, C.S.R.; Silvestre, A.J.D.; Neto C.P.; Gandini, A.; Fardim, P.; Holmbom, B. *J. of Colloid and Interface Sci*. **2006**, 301 1, 205-209.
110. Hale, M.I., Newton G.M.; *Colloids and Surfaces*. **2002**, 103, 79-86.
111. Chou, T.H.; Hong, S.J.; Liang, Y.E.; Tsao, H.K.; Sheng, Y.J. *Langmuir*. **2011**, 27, 3685-3692.
112. Schellbach, S.L.; Monteiro, S.N.; Drelich, J.W. *Materials Letters*. **2016**, 164, 599-604.
113. Mead-Hunter, R. Mullins, B.J.; Becker, T. Braddock, R.D. *Langmuir*. **2010**, 17, 1, 227-232.
114. Hale, G.M.; Newton, M.I. *Colloids and Surfaces*. **2002**, 103, 79-86.
115. Berim, G.O.; Ruckenstein, E. *Journal of Colloid and Interface Science*. **2005**, 286, 681-695.
116. de Ruiter, R.; de Ruiter, J.; Eral, H.B.; Semprebon, C.; Brinkmann, M.; Mugele, *Langmuir*. **2018**, 28, 13300-13306.
117. Korosi, G.; Kovats, E. *Journal of Chemical Engineering Data*. **1981**, 26, (3).
118. Li, D.; Neumann, A.W. *Advances in Colloid and Interface Science*. **1992**, 39, 299-345.
119. Van Oss, C.J.; Good, M.K.; Chaudhury, J. *Protein Chem*.**1986**, 5, 385-402.
120. Van Oss, C.J.; Good, M.K.; Chaudhury, *Advanced Coll. Interf. Science*.**1987**, 28, 35-60.
121. Van Oss, C.J.; Good, M.K.; Chaudhury, *Langmuir*.**1988**, 4, 884-891.

122. Pothan, L.A.; Simon, F.; Spange, S.; Thomas, S. *Biomacromolecules*. **2006**, 7, 3, 892-898.
123. Crist, B.V. *J. of Electron Spectroscopy and Related Phenomena*. **2019**, 231, 75-87.
124. Moulder, J.F.; Stickle, W.F.; Sobol, P.E.; Bomben, K.D. *Handbook of X-Ray Photoelectron Spectroscopy*. **1995**, Physical Electronics, Inc, Perkin-Elmer Corp.
125. Andrade, J.D. *Surface and Interfacial Aspects of Biomedical Polymers, Surface Chemistry and Physics* (Plenum Press, N.Y.) **1985**, Vol. 1, 120-125.
126. Nilsson, M.; Mihranyan, A.; Valizadeh, S.; Stromme, M. *J. Phys. Chem. B*. **2006**, 110, 15776-15781.
127. Stromme, M.; Mihranyan, A.; Ek, R.; Niklasson, G.A. *J. Phys. Chem. B*. **2003**, 107, 14378-14382.
128. Gunko, V.M.; Tomaszewski, W.; Krupaska, V.T.; Turov, K.V.; Leboda, R.; Turov, V.V. *Central European Journal of Chemistry*. **2014**, 12(4), 509-518.
129. Sing, K. *Colloids and Surfaces A; Physicochemical and Engineering Aspects*. **2001**, 187-188, 3-9.
130. Sing, K. *Pure and Applied Chemistry*. **1982**, 54, No. 11 2201-2218.
131. Gregg, S.J.; Sing, K.S.W. *Adsorption, Surface Area and Porosity 2<sup>nd</sup> Edition*. **1982**, Academic Press INC.
132. El-Naggar, A.Y. *Journal of Emerging Trends in Engineering and Applied Sciences*. **2013**, 4, (2). 281-286.
133. Zhao, X.S.; Lu, G.Q. *J. Phys. Chem. B*. **1998**, 102, 1556-1561.
134. Thode, E.F.; Swanson, J.W.; Becher, J.J. *The institute of Paper Chemistry*. **1957**, Appleton, Wisconsin.



135. Lowell, S.; Shields, J. E.; Thomas, M. A.; Thommes, M., *Characterization of Porous Solids and Powders: Surface Area, Pore Size and Density*. **2006**, Springer Netherlands.
136. Thommes, M.; Morell, J.; Cychosz, K. A.; Fröba, M. *Langmuir*. **2013**, 29 (48), 14893-14902.
137. Murray, K.L.; Seaton, N.A.; Day, M.A. *Langmuir*. **1999**, 15, 6728-6737.
138. Kruk, M.; Antochuk, V.; Jaroniec, M. *J. Phys.Chem.B*. **1999**, 103, 48, 10670-10678.
139. Denoyel, R.; Colinas-Fernandez, J.; Grillet, Y; Rouquerol, J. *Langmuir*. **1993**, 9, 515-518.
140. Storck, S.; Bretinger, H.; Maier, W.F. *Applied Catalysis A: General*. **1998**, 174, 1,137-146.
141. Zebregs, M.; van Driel. Co-extrusion of Gun Propellant. IM/EM Symposium, Tucson, AZ, May 2009.
142. [www.chm.bris.ac.uk](http://www.chm.bris.ac.uk)



## A Surface Chemistry Experiment Using an Inexpensive Contact Angle Goniometer

**Author:** Madalena Dionísio, João Sotomayor

**Publication:** Journal of Chemical Education

**Publisher:** American Chemical Society

**Date:** Jan 1, 2000

Copyright © 2000, American Chemical Society

### PERMISSION/LICENSE IS GRANTED FOR YOUR ORDER AT NO CHARGE

This type of permission/license, instead of the standard Terms & Conditions, is sent to you because no fee is being charged for your order. Please note the following:

- Permission is granted for your request in both print and electronic formats, and translations.
  - If figures and/or tables were requested, they may be adapted or used in part.
  - Please print this page for your records and send a copy of it to your publisher/graduate school.
  - Appropriate credit for the requested material should be given as follows: "Reprinted (adapted) with permission from (COMPLETE REFERENCE CITATION). Copyright (YEAR) American Chemical Society." Insert appropriate information in place of the capitalized words.
  - One-time permission is granted only for the use specified in your request. No additional uses are granted (such as derivative works or other editions). For any other uses, please submit a new request.
- If credit is given to another source for the material you requested, permission must be obtained from that source.

[BACK](#)

[CLOSE WINDOW](#)

## PENDING ORDER CONFIRMATION

Confirmation Number: Pending

[Print Friendly Format](#)

Order Date: 03-May-2020

Includes Publisher Terms and Conditions

### 1. Encyclopedia of surface and colloid science

0.00 USD

Order license ID  
ISBN-13  
Type of Use

Pending  
9780849396076  
Republish in a  
thesis/dissertation

Publisher  
Portion

TAYLOR & FRANCIS GROUP  
LLC  
Image/photo/illustration

[Publisher Terms and Conditions](#)

[View Details](#)

[Print License](#)

Total Items: 1

Total Due: 0.00 USD

Accepted: All Publisher and [CCC Terms and Conditions](#)

[Continue Shopping](#)

## Taylor & Francis Group LLC - Books Terms and Conditions

Taylor and Francis Group and Informa healthcare are division of Informa plc. Permission will be void if material exceeds 10% of all the total pages in your publication and over 20% of the original publication. This includes permission granted by Informa plc and all of its subsidiaries.

**Cellulose: Fascinating Biopolymer and Sustainable Raw Material**

Author: Andreas Bohn, Hans-Peter Fink, Brigitte Heublein, et al

Publication: Angewandte Chemie International Edition

Publisher: John Wiley and Sons

Date: May 24, 2005

Copyright © 2005 WILEY-VCH Verlag GmbH &amp; Co. KGaA, Weinheim

**Order Completed**

Thank you for your order.

This Agreement between Henry Grau ("You") and John Wiley and Sons ("John Wiley and Sons") consists of your license details and the terms and conditions provided by John Wiley and Sons and Copyright Clearance Center.

Your confirmation email will contain your order number for future reference.

License Number 4821050454567

[Printable Details](#)

License date May 02, 2020

☒ **Licensed Content****Order Details**

Licensed Content Publisher	John Wiley and Sons
Licensed Content Publication	Angewandte Chemie International Edition
Licensed Content Title	Cellulose: Fascinating Biopolymer and Sustainable Raw Material

Type of use	Dissertation/Thesis
Requestor type	University/Academic
Format	Print and electronic
Portion	Figure/table

License date May 02, 2020

☒ **Licensed Content****Order Details**

Licensed Content Publisher	John Wiley and Sons
Licensed Content Publication	Angewandte Chemie International Edition
Licensed Content Title	Cellulose: Fascinating Biopolymer and Sustainable Raw Material
Licensed Content Author	Andreas Bohn, Hans-Peter Fink, Brigitte Heublein, et al
Licensed Content Date	May 24, 2005
Licensed Content Volume	44
Licensed Content Issue	22
Licensed Content Pages	36

Type of use	Dissertation/Thesis
Requestor type	University/Academic
Format	Print and electronic
Portion	Figure/table
Number of figures/tables	1
Will you be translating?	No

**About Your Work****Additional Data**

Title	Surface Functionalization and Characterization of Energetic Nitrocellulose
Institution name	Seton Hall University
Expected presentation date	May 2020

Portions	figure 1
----------	----------

**Requestor Location****Tax Details**

Requestor Location	Henry Grau 89 Layton Rd
--------------------	----------------------------

Publisher Tax ID	EU826007151
------------------	-------------

Requestor Location	SUSSEX, NJ 07461 United States Attn: Henry Grau
--------------------	---



### Perfluoroacylated Ethyl Cellulose: Synthesis, Characterization, and Gas Permeation Properties

**Author:** Fareha Zafar Khan, Toshikazu Sakaguchi, Masashi Shiotsuki, et al

**Publication:** Macromolecules

**Publisher:** American Chemical Society

**Date:** Dec 1, 2006

*Copyright © 2006, American Chemical Society*

#### PERMISSION/LICENSE IS GRANTED FOR YOUR ORDER AT NO CHARGE

This type of permission/license, instead of the standard Terms & Conditions, is sent to you because no fee is being charged for your order. Please note the following:

- Permission is granted for your request in both print and electronic formats, and translations.
  - If figures and/or tables were requested, they may be adapted or used in part.
  - Please print this page for your records and send a copy of it to your publisher/graduate school.
  - Appropriate credit for the requested material should be given as follows: "Reprinted (adapted) with permission from (COMPLETE REFERENCE CITATION). Copyright (YEAR) American Chemical Society." Insert appropriate information in place of the capitalized words.
  - One-time permission is granted only for the use specified in your request. No additional uses are granted (such as derivative works or other editions). For any other uses, please submit a new request.
- If credit is given to another source for the material you requested, permission must be obtained from that source.

BACK

CLOSE WINDOW



### Assessment of the surface area and microporosity of activated charcoals from immersion calorimetry and nitrogen adsorption data

**Author:** R. Denoyel, J. Fernandez-Colinas, Y. Grillet, et al

**Publication:** Langmuir

**Publisher:** American Chemical Society

**Date:** Feb 1, 1993

*Copyright © 1993, American Chemical Society*

#### PERMISSION/LICENSE IS GRANTED FOR YOUR ORDER AT NO CHARGE

This type of permission/license, instead of the standard Terms & Conditions, is sent to you because no fee is being charged for your order. Please note the following:

- Permission is granted for your request in both print and electronic formats, and translations.
  - If figures and/or tables were requested, they may be adapted or used in part.
  - Please print this page for your records and send a copy of it to your publisher/graduate school.
  - Appropriate credit for the requested material should be given as follows: "Reprinted (adapted) with permission from (COMPLETE REFERENCE CITATION). Copyright (YEAR) American Chemical Society." Insert appropriate information in place of the capitalized words.
  - One-time permission is granted only for the use specified in your request. No additional uses are granted (such as derivative works or other editions). For any other uses, please submit a new request.
- If credit is given to another source for the material you requested, permission must be obtained from that source.

BACK

CLOSE WINDOW

## An Adsorption-Based Method for the Characterization of Pore Networks Containing Both Mesopores and Macropores



**Author:** K. L. Murray, N. A. Seaton, M. A. Day

**Publication:** Langmuir

**Publisher:** American Chemical Society

**Date:** Sep 1, 1999

*Copyright © 1999, American Chemical Society*

### PERMISSION/LICENSE IS GRANTED FOR YOUR ORDER AT NO CHARGE

This type of permission/license, instead of the standard Terms & Conditions, is sent to you because no fee is being charged for your order. Please note the following:

- Permission is granted for your request in both print and electronic formats, and translations.
- If figures and/or tables were requested, they may be adapted or used in part.
- Please print this page for your records and send a copy of it to your publisher/graduate school.
- Appropriate credit for the requested material should be given as follows: "Reprinted (adapted) with permission from (COMPLETE REFERENCE CITATION). Copyright (YEAR) American Chemical Society." Insert appropriate information in place of the capitalized words.
- One-time permission is granted only for the use specified in your request. No additional uses are granted (such as derivative works or other editions). For any other uses, please submit a new request.

If credit is given to another source for the material you requested, permission must be obtained from that source.

BACK

CLOSE WINDOW